

University of Alberta

Probing the Molecular Interactions of an Asphaltene Model Compound in
Organic Solvents and Aqueous Solutions Using a Surface Forces Apparatus
(SFA)

by

Jing Wang

A thesis submitted to the Faculty of Graduate Studies and Research
in partial fulfillment of the requirements for the degree of

Master of Science

in

Chemical Engineering

Department of Chemical and Materials Engineering

©Jing Wang

Spring 2012

Edmonton, Alberta

Permission is hereby granted to the University of Alberta Libraries to reproduce single copies of this thesis and to lend or sell such copies for private, scholarly or scientific research purposes only. Where the thesis is converted to, or otherwise made available in digital form, the University of Alberta will advise potential users of the thesis of these terms.

The author reserves all other publication and other rights in association with the copyright in the thesis and, except as herein before provided, neither the thesis nor any substantial portion thereof may be printed or otherwise reproduced in any material form whatsoever without the author's prior written permission.

ABSTRACT

ABSTRACT

A fundamental understanding of the molecular interactions between asphaltene molecules in bulk and at oil-water interface is of great value in crude oil production. Yet, the chemical composition and molecular structures of asphaltenes are not fully understood. The objective of this study is to investigate the similarity and disparity between an asphaltene model compound C5Pe and real asphaltene molecules in the context of interaction force profiles, molecular aggregation/adsorption at clay-solvent interfaces. The intermolecular and surface forces of C5Pe in organic solvents and aqueous solutions were directly measured by a Surface Forces Apparatus (SFA). Repulsive forces were observed between asphaltene (and C5Pe) surfaces in pure toluene, and strong adhesion were measured in heptane. pH, salt concentration and Ca^{2+} showed strong impact on the interaction of two C5Pe surfaces. Our results provide an important insight into basic interaction mechanism of asphaltene-type molecules and their interfacial activities in O/W and W/O emulsions.

ACKNOWLEDGEMENTS

ACKNOWLEDGEMENT

I would like to express my deepest gratitude to Professor Zhenghe Xu and Professor Hongbo Zeng, for their guidance in the planning and execution of this research. Without their encouragement and support, this research would not have been completed. I have learned a lot from the valuable guidance and challenging discussions with them. It has been my honour and a privilege to be their student.

The financial support from Discovery Grant Award and an NSERC RTI Grant Award (H. Zeng) and NSERC Industrial Research Chair Program in Oil Sands Engineering (Z. Xu) is acknowledged.

I am very indebted to Professor Johan Sjöblom and his student Nils van der Tuuk Opedal for providing the asphaltene model compounds, joining me with the experiment, discussions and revising the papers.

I would like to thank all the colleagues from Oil Sands Extraction Group for all the support and discussions and I enjoyed working in this group.

I appreciate the help from Ms. Jie Ru, Ms. Lisa Carreiro and Mr. Jim Skwarok in training me with the instrument operation, providing technical help and materials purchase.

My thanks are also extended to my friend and fellow Dr. Qingye Lu and all the other fellows in Surface Force Group for creating a pleasant working environment, for their friendship and support.

Finally, I would like to thank my boyfriend Peng Huang for his unwavering support in the past two years. Without the support, this work would not have been possible.

TABLE OF CONTENTS

TABLE OF CONTENTS

CHAPTER 1 INTRODUCTION	1
1.1 Asphaltenes and asphaltene model compounds	1
1.2 Objectives	3
1.3 Organization of thesis.....	3
CHAPTER 2 LITERATURE REVIEW	5
2.1 Characteristics of asphaltenes	5
2.1.1 <i>Elemental composition of asphaltenes</i>	5
2.1.2 <i>Molecular weight</i>	7
2.1.3 <i>Fractions of asphaltenes</i>	9
2.1.4 <i>Precipitation of asphaltenes</i>	11
2.1.5 <i>Film properties</i>	13
2.1.6 <i>Molecular interactions of asphaltenes</i>	15
2.2 Asphaltene model compounds	17
2.2.1 <i>Model compounds focusing on molecular weight or aggregation</i>	18
2.2.2 <i>Model compounds focusing on the physicochemical properties</i>	19
CHAPTER 3 SURFACE FORCE REVIEW	22
3.1 DLVO theory.....	23
3.1.1 <i>Van de Waals forces</i>	23
3.1.2 <i>Electrostatic double layer force</i>	25
3.2 Extended DLVO theory	32

TABLE OF CONTENTS

3.2.1 <i>Hydrophobic force</i>	33
3.2.2 <i>Steric force</i>	34
3.2.3 <i>Hydration force and bridging force</i>	36
CHAPTER 4 MATERIALS AND EXPERIMENTAL TECHNIQUES	38
4.1 Materials	38
4.2 Surface forces apparatus (SFA) technique	38
4.2.1 <i>Multiple beam interference (MBI)</i>	38
4.2.2 <i>Film thickness studies using MBI</i>	40
4.2.3 <i>Force measurement</i>	42
4.2.4 <i>Other unique functions of SFA 2000</i>	45
4.2.5 <i>C5Pe film preparation</i>	46
4.2.6 <i>Operation procedure</i>	47
4.2.7 <i>Experiment configurations</i>	49
4.3 Langmuir trough and LB film deposition	51
4.3.1 <i>Principles of Langmuir trough and LB film deposition</i>	51
4.3.2 <i>Technique of Langmuir trough and LB film deposition</i>	53
4.3.3 <i>Silicon wafer cleaning (Piranha cleaning)</i>	55
4.4 Atomic force microscope (AFM) imaging	55
4.4.1 <i>Fundamental principle of AFM imaging</i>	55
4.4.2 <i>AFM imaging</i>	56
4.5 Other techniques	57

TABLE OF CONTENTS

4.5.1 Contact angle measurement	57
4.5.2 Ellipsometer	57
CHAPTER 5 INTERACTIONS OF C5Pe IN ORGANIC SOLVENTS	58
5.1 Introduction	58
5.2 Characterization of C5Pe film.....	60
5.2.1 AFM imaging	60
5.2.2 Langmuir trough, LB film deposition and contact angle measurement	61
5.3 Adsorption kinetics	64
5.3.1 High concentration adsorption.....	64
5.3.2 Adhesion	66
5.3.3 Data fitting and nature of the interaction forces	66
5.3.4 Low concentration adsorption	69
5.3.5 Comparison with real asphaltenes	71
5.4 Interactions in toluene and heptane	72
5.4.1 In toluene	72
5.4.2 In heptane	72
5.6 Summary of chapter	73
CHAPTER 6 INTERACTIONS OF C5Pe IN AQUEOUS SOLUTIONS.....	76
6.1 Introduction	76
6.2 Characterization of C5Pe film.....	77
6.3 Surface force analysis.....	80

TABLE OF CONTENTS

6.3.1 A typical force measurement	80
6.3.2 Adhesion	80
6.3.3 Data fitting and nature of the interaction forces	82
6.4 Effect of pH.....	84
6.5 Effect of salinity	88
6.5.1 At pH above pKa.....	88
6.5.2 At pH below pKa	89
6.6 Effect of Ca ²⁺	91
6.5 Summary of chapter	94
CHAPTER 7 SUMMARY	96
7.1 General conclusions	96
7.2 Suggestions for future work	97
REFERENCES	99

LIST OF TABLES

LIST OF TABLES

Table 2.1	Chemical composition of West Texas and Louisiana Asphaltene samples.	6
Table 5.1	Fitting parameters using Alexander-de Gennes theory.....	68
Table 5.2	Film thickness (nm) obtained by different methods.	69
Table 5.3	Fitting parameters using Alexander-de Gennes theory at high and low compression regimes.	69

LIST OF FIGURES

LIST OF FIGURES

Figure 1.1	Structure of an asphaltene model compound C5Pe (MW=689).....	2
Figure 2.1	A typical scheme for SARA separation.....	5
Figure 2.2	Examples of the two possible models for the asphaltene structures.....	8
Figure 2.3	Air-water interface: pressure-area isotherms of mixed monolayer of asphaltenes and demulsifiers at various molar ratios of asphaltene to demulsifier.	14
Figure 2.4	Structure and molecular weight of the asphaltene model compounds synthesized and characterized.	20
Figure 3.1	An example of atom arrangement at the surface.	22
Figure 3.2	Phase 1 and phase 2 interact through media 3.....	25
Figure 3.3	Schematic of Stern-Grahame electric double layer model.	26
Figure 3.4	Potential distribution in the double layer.....	28
Figure 3.5	A schematic showing the relation between surface energy and decay length.	30
Figure 3.6	An example showing the influence of Stern potential on the total energy of interaction of two spherical particles	31
Figure 3.7	A schematic show of EDLVO forces.	33
Figure 4.1	A basic light reflectance and transmittance.	39
Figure 4.2	Transmission and reflection fringes at different transmission or reflection index.....	40
Figure 4.3	A schematic diagram of a FECO interferometer.	41
Figure 4.4	An example of thickness difference calculation.	41
Figure 4.5	The sectional view of SFA 2000.	43

LIST OF FIGURES

Figure 4.6 Configuration of the two discs loaded in SFA chamber.....	44
Figure 4.7 Schematic of drop-coating method.....	47
Figure 4.8 Schematic of experimental setup for measuring the molecular interactions of asphaltene model compound C5Pe..	48
Figure 4.9 FECO fringes of two bare mica surfaces in contact and in separation	49
Figure 4.10 Geometry of the experiments in organic solvents.	50
Figure 4.11 Geometry of the experiments in aqueous solutions.....	50
Figure 4.12 Schematic view of Langmuir technique.	52
Figure 4.13 Deposition of a monolayer onto a substrate.	53
Figure 4.14 A SP - area isotherm including different phase and phase transitions.	54
Figure 5.1 AFM images of (a) bare mica surface; (b) C5Pe adsorbed on mica surface; (c) C5Pe adsorbed on mica surface after immersion in toluene for 0.5 hour; (d) C5Pe adsorbed on mica surface after immersion in heptane for 0.5 hour.	61
Figure 5.2 (a) Interfacial pressure-area isotherms of C5Pe film at toluene-water interface obtained with an interfacial Langmuir trough. (b) AFM image of the C5Pe film deposited with LB method	63
Figure 5.3 Force-distance profiles of two mica surfaces interacting in 0.02 wt% C5Pe-toluene solution at different time intervals: (a) approaching plots and fitting curves by Alexander-de Gennes (AdG) theory; (b) retracting plots following the approaching in (a)	65
Figure 5.4 AFM images of C5Pe surfaces prepared by immersing the mica surface for 20 hours in a C5Pe-toluene solution of (a) 0.02 wt% and (b) 0.002 wt%.....	66

LIST OF FIGURES

- Figure 5.5 Experimentally measured repulsion forces and best fitted curves using the Alexander-de Gennes (AdG) theory.....68
- Figure 5.6 Force-distance profiles of two mica surfaces interacting in 0.002 wt% C5Pe-toluene solution at different time intervals during (a) approaching and (b) retracting following the approaching in (a).70
- Figure 5.7 Force-distance profiles of two mica surfaces interacting in 0.01 wt% asphaltene-toluene solution at different time intervals during (a) approaching and (b) retracting following the approaching in (a).71
- Figure 5.8 Force-distance profiles between two C5Pe films (symmetric configuration) and between a C5Pe film and a bare mica surface (asymmetric configuration) in (a) toluene and (b) heptane.....73
- Figure 6.1 AFM images of (a) bare mica surface, (b) C5Pe adsorbed on mica, and (c) C5Pe adsorbed on mica after immersing in pH 2, 10 mM KCl solution for 10 min.79
- Figure 6.2 Proposed schematic of C5Pe aggregates on mica surface: (a) micelle-like aggregates, (b) an ordered bilayer structure and (c) complex aggregates combining micelle-like and “multi-layer” aggregation.79
- Figure 6.3 Force-distance profiles of two C5Pe surfaces interacting in 0.1 mM KCl solution at pH 2: (a) approaching force curve; (b) retracting force curve following the approaching in (a).....81
- Figure 6.4 Force-distance profiles of two C5Pe surfaces interacting in 0.1 mM KCl solution at different pH during approaching. Solid lines are fitted curves using the AdG model. Inset is the adhesion measured during the separation.87
- Figure 6.5 Force-distance profiles of two C5Pe surfaces interacting in 0.1 mM KCl solution at pH 4 and pH 6. solid lines are the fitted curves by AdG equation at short separation distance and high compression regime, and dash lines are the fitted curves using the DLVO theory at long separation distance and low compression regime87

LIST OF FIGURES

- Figure 6.6 Force-distance profiles of two C5Pe surfaces interacting in pH 6 of different KCl concentrations during approaching. Solid lines are fitted curves using AdG equation; dash lines are the fitted curves using DLVO theory.....89
- Figure 6.7 (a) Force-distance profiles of two C5Pe surfaces interacting in aqueous solutions of pH 2 of different KCl concentrations during approaching. (b) Proposed conformation change of C5Pe molecules and aggregates under low and high KCl concentrations.91
- Figure 6.8 (a) Force-distance profiles of two C5Pe surfaces interacting in 10 mM KCl solutions at pH 2 in the presence of different amount of Ca^{2+} ions. Solid lines are fitted curves using the AdG equation93
- Figure 6.9 Force-distance profiles of two C5Pe surfaces interacting in 100 mM KCl solutions at pH 6 in the presence of different amount of Ca^{2+} ...93
- Figure 6.10 AFM images of a C5Pe film coated mica after immersing in aqueous solution of pH 2 with 10 mM KCl + 0.1 mM CaCl_2 for 10 min: (a) topography and (b) phase images.94

NOMENCLATURE

NOMENCLATURE

F_{DLVO}	Derjaguin-Landau-Verwey-Overbeek forces, N
F_{VDW}	van der Waals force, N
F_E	electrostatic force, N
A	Harmaker constant, J
A_{ii}	Harmaker constant of material i , J
A_{132}	Harmaker constant of phase 1 and phase 2 through media 3, J
z	center-to-center distance between two molecules, m
R, R_1, R_2	radii of spherical bodies, m
U	energy, J
D	separation distance between two surfaces, m
ρ_1, ρ_2	numbers of atoms per unit volume in two interaction bodies, mol^{-1}
C	coefficient in the particle-particle pair interaction, J
n_i	number density of ion i , mol^{-1}
n_{i0}	number density of ion i in the bulk, mol^{-1}
ψ	potential in the electric double layer, V
e	electron charge, $1.602 \times 10^{-19} \text{ C}$
k	Boltzmann constant, $1.381 \times 10^{-23} \text{ J K}^{-1}$
z_i	valence of ion i
T	absolute temperature, T
κ	inverse Debye length, m^{-1}

NOMENCLATURE

ϵ_r, ϵ_0	relative permeability of the medium (dimensionless) and vacuum, $C V^{-1} m$
ψ_d	surface potential of a particle, V
C_e	capacity of a capacitor, $C V^{-1}$
σ_d	total charge at the stern layer, $C m^2$
F_{HB}	hydrophobic force, N
F_S	steric force, N
F_{HD}	hydration force, N
F_B	bridging force, N
F_{total}	extended DLVO force, N
H	curvature of the mica surface, m
C1, C2	parameters characterizing the magnitudes of the short and long range hydrophobic force respectively, m
A_s	amplitude setpoint
A_0	free amplitude
K	hydrophobic force constant, J
Γ	number of the grafted chains per unit area
R_g	radii of the particle, m
P(D)	repulsive pressure between two brush-bearing surfaces, $N m^{-2}$
L	length of the polymer brushes, m
s	average distance between two grafting points, m

NOMENCLATURE

A_a	area of arbitrary surface, m^2
F_{s-s}	surface force between two spheres, m
F_{s-p}	surface force between a sphere and a plane, m
F_{c-c}	surface force between two cylindrical surfaces, m
U_{p-p}	interaction energy for two parallel plates, J
N_0	Avogadro number, 6.02×10^{23} , mol^{-1}
N_B	number of monomer units per chain, mol^{-1}
E_i, E_r, E_t	energy of incident light, reflected light and transmitted light respectively, J
$r(r'), t(t')$	reflected index and transmitted index from one material to another respectively
δ	phase due to optical path difference
p	transmitted times
T', R'	relative transmitted and reflective light energy
ϕ	phase change on the reflection at each surface
K_s	spring stiffness, $N m^{-1}$
ΔD_0	piezoelectric tube expanded distance, m
$W(D)$	energy per unit area between two flat surface, J
$\Delta\lambda_n, \Delta\lambda_{n-1}$	wavelength move of the n th and $(n-1)$ th fringe, m
F_A	force applied by the measured system during LB trough measurement, N
m_w	mass of the wilhelmy plate, kg

NOMENCLATURE

t_p, w_p	thickness and width of the plate respectively, m
Υ	surface tension of the liquid or interface, N m^{-1}
Υ_0	surface tension of a pure subphase
V_p	volume of the proportion of plate immersed in liquid, m^3

CHAPTER 1 INTRODUCTION**1.1 Asphaltenes and Asphaltene model compounds**

In a Hot Water Extraction (HWE) process for bitumen extraction from oil sands¹, water-in-oil (W/O) or oil-in-water (O/W) emulsions are present in the system of bitumen flotation in oil sands and wastewater treatment. The water droplets in W/O emulsions contain dissolved salts that can lead to equipment corrosion in bitumen upgrading process. The oil droplets in O/W emulsions reduce the recovery of bitumen and cause many difficulties in dealing with wastewater. In these cases, the coalescence of water/oil droplets is mandatory. However, the emulsions are believed to be stabilized by asphaltene macromolecules or aggregates²⁻⁴, and it is really hard to make the water/oil droplets coalesce. Asphaltenes are one class of compounds present in crude oil defined not by their structure but as a solubility class. They are commonly defined as soluble in toluene but insoluble in short-chained hydrocarbons such as heptane or hexane.⁵⁻⁸ The knowledge of asphaltenes has increased a lot and analysis has shown asphaltenes to be sheet-like, polyaromatic hydrocarbons built up from carbons and hydrogen, together with varying amount of heteroatoms (nitrogen, oxygen and sulfur, etc), as well as traces of metals like nickel and vanadium.⁹ However, what the results gave is the average over the whole distribution, yet the exact fraction structure, chemical composition and the polar groups are still unobtainable. In addition, these parameters may vary from wellbore to wellbore. Chemical composition is not the only unanswered question of asphaltenes. The molecular weight is also controversial after several decades research and discussion.¹⁰ Asphaltenes are of amphiphilic nature, and they can absorb in water-oil interface like surfactants, with the polar groups residing in aqueous phase and non-polar group in oil phase. The stability of W/O emulsion is determined by the interaction of the droplet and the droplets are covered by asphaltenes, therefore the interactions between asphaltenes become important in understanding the mechanism of emulsification and water coagulation. Although intensive study has

been carried out on the mechanism of emulsion stabilization by asphaltenes, no widely acceptable conclusion has been reached.

It could be anticipated that the traditional way of studying extracted asphaltenes over their average properties will never be able to end the controversies. There seems to exist two ways to terminate this situation. One is to continue trying to divide the whole asphaltenes into numerous subfractions and study each subfraction to determine which are responsible for the undesired properties.¹¹⁻¹² Another way is to use model compounds with defined molecular structure and similar physiochemical properties as those asphaltenes. Asphaltene model compounds are synthesized and investigated in many studies, but these studies mainly focused on the problem of molecular weight or aggregation and did not pay attention to the interfacial tension, emulsion stabilization and film properties.¹³⁻¹⁶ Several asphaltene model compounds were synthesized by modifying a polyaromatic compound and their interfacial properties and emulsion stability were studied by Nordgard and his colleagues using varying techniques.^{9,17-18} Among the polar compounds, C5Pe with its structure shown in Figure 1.1 was received as a gift from their group as an example to be studied here.

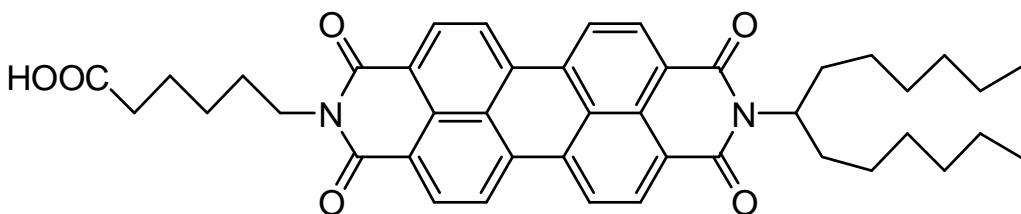


Figure 1.1 Structure of an asphaltene model compound C5Pe (MW=689) with nomenclature N-(1-hexylheptyl)-N'-(5-carboxylicpentyl) perylene-3,4,9,10-tetracarboxylic bisimide.

1.2 Objectives

The objective of this thesis is to focus on the interaction forces of an asphaltene model compound C5Pe in organic solvents and aqueous solutions to help elucidate the molecular interaction mechanism and interfacial activities of asphaltene type molecules in W/O and O/W emulsions, and to investigate the similarity and disparity between C5Pe and real asphaltene molecules in the context of interaction forces and molecular aggregation/adsorption at clay-solvents interface. More specific objectives are:

- To measure directly the interaction forces between C5Pe using a surface forces apparatus (SFA) in attempt to predict the C5Pe, thus asphaltene, interaction behaviours and deduce the emulsion stabilization mechanism.
- To investigate the dynamic adsorption behaviour at clay-solvent interface and the interaction forces of C5Pe in organic solvents.
- To study the effect of industrial operation parameters such as solution pH, salinity, and divalent ions on the interaction forces between C5Pe in aqueous solutions.
- To determine the origin of the interaction forces between C5Pe in both aqueous solutions and organic solvents and provide guidance to control the interactions of C5Pe.
- To compare the interaction forces and aggregation/adsorption behaviour of C5Pe and real asphaltenes to determine their similarity and disparity.

The information obtained from asphaltene model compounds system is of great importance for elucidating the mechanism of asphaltene-caused problems in petroleum industry

1.3 Organization of thesis

The thesis is a summary of the results collected during the MS.c program regarding the molecular interactions of an asphaltene model compound C5Pe.

Chapter 5 has been published in Energy & Fuel and Chapter 6 is going to be submitted to Journal of Physical Chemistry C.

Chapter 1 gives a brief introduction to asphaltenes, asphaltene related issues, asphaltene controversies and asphaltene model compounds.

Chapter 2 reviews the literature on the characterization of asphaltenes, asphaltene model compounds, fundamental studies on the interaction of asphaltenes and interfacial properties of asphaltene model compounds.

In chapter 3, the literatures related to the surface force are reviewed. This includes the general review of surface force, the classic DLVO and extended DLVO theories. Derjaguin approximation is also discussed considering the geometry of the two surfaces in the experiment.

Chapter 4 concerns the experimental techniques used in this thesis. The principle and setup of SFA technique, the AFM imaging technique, Langmuir Trough experiment and LB film deposition and other supporting techniques are introduced.

Chapter 5 presents the molecular interactions of C5Pe in organic solvents. The comparison of the molecular aggregation/adsorption behaviour between C5Pe and real asphaltenes are also mentioned.

Chapter 6 focuses on the molecular interactions of C5Pe in aqueous solutions. The effect of industrial operation conditions such as pH, salinity and divalent ions are discussed.

The general conclusions and suggestions for future work are given in chapter 7.

CHAPTER 2 LITERATURE REVIEW

2.1 Characteristics of asphaltenes

As described in the INTRODUCTION section, asphaltenes are defined based on solubility as a fraction of crude oil that is soluble in toluene but insoluble in short-chained hydrocarbons such as heptane and hexane.¹⁹ A typical separation of asphaltenes and other crude oil fractions is shown schematically in Figure 2.1.

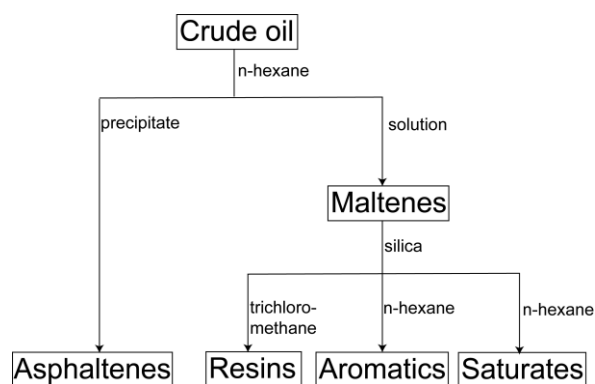


Figure 2.1 A typical scheme for SARA separation.

Asphaltenes adsorb at oil/water interface to stabilize oil-in-water (O/W) or water-in-oil (W/O) emulsions, adsorb at solid surface²⁰ influencing the wettability in, for example, reservoir rocks, and precipitate to cause the wellbore or pipeline plugging²¹. The detailed characterization of asphaltenes is introduced in the following.

2.1.1 Elemental composition of asphaltenes

The amount of carbon and hydrogen in asphaltenes vary usually over a narrow range, corresponding to a hydrogen-to-carbon ratio of $1.15 \pm 0.5\%$.¹⁹ It is the heteroatom content that the asphaltenes differ significantly from the crude oil source. Asphaltenes contain amounts of nitrogen, oxygen, sulphur and trace amounts of nickel and vanadium.²² The crude oil composition varies from field to field, sometimes even from wellbore to wellbore, and this will be reflected in the

asphaltene fractions as well. But usually the amount of oxygen and sulphur can vary from 0.3 to 4.9% and 0.3 to 10.3%, respectively.¹⁹ For example, a chemical composition study of two American asphaltenes from West Texas and Louisiana is shown in Table 2.1.

Table 2.1 Chemical composition of West Texas and Louisiana Asphaltene samples.²³

Parameters	West Texas	Louisiana
Elemental		
Carbon	85.78	86.24
Hydrogen	7.16	6.78
Nitrogen	1.19	1.23
Sulphur	2.71	0.65
Oxygen	1.34	3.19
Metal content		
Vanadium	190	13
Nickel	266	63
Iron	178	526

In asphaltene compositions, heteroatoms play important roles in determining asphaltene properties, such as interfacial properties, aggregation and precipitations. The nitrogen can give asphaltene molecules both basic and neutral behavior, depending on whether the nitrogen is a part of a quinolines or a carbazole moiety.²⁴ Oxygen atoms are believed to originate mainly from phenolic, hydroxylic or carboxylic functionalities.²⁴ Sulphur can be a part of both the aromatic core as thiophenes and the aliphatic chains as sulphide derivatives,²⁴ or in other cases as sulphur bridges²². Transition metals as vanadium and nickel are believed to be an element of porphyrin structures in asphaltenes²⁵.

2.1.2 Molecular weight

The molecular weight of asphaltenes has always been under debate through many years. The reason behind the controversies is that asphaltenes have strong trend to self-associate, even at very low concentrations (0.1g/L in toluene).²⁶ In the study of Mullins *et al.*²⁶, the researchers investigated asphaltenes using high-Q, ultrasonic spectroscopy in both aqueous and organic solvents. They brought up the idea of asphaltene nanoaggregate and found that unlike the high concentrations for asphaltene critical micelle concentrations (CMC), the critical nanoaggregate concentration (CNAC) of asphaltene was actually very low. Thus, when people try to analyze the asphaltene samples, they typically measured the size of aggregates not monomeric asphaltenes. Years ago, the researchers studied the molecular weight to be in the range of 1,000-100,000amu^{4,8,27-28}. Yarranton *et al.* did many studies on determining the molecular weight of asphaltenes^{4,27-28}. In their study, they employed a vapour pressure osmometer (VPO) to measure the molar mass of asphaltenes with an increasing asphaltene concentration until a limiting value is reached. The limiting value ranges from 4000 to 10 000 g/mol and depends on the solvent, temperature, and asphaltene fraction. By measuring the interfacial tension, they found that the interfacial tension of water-toluene interface decrease linearly with asphaltene concentration, thus considering the asphaltene did not form aggregate but in the form of single molecules. Other techniques such as Size Exclusion Chromatography (SEC) gave the similar results on asphaltene molecular weight. Currently, researchers have used different techniques to measure the molecular weight. Pomerantz *et al.*²⁹ used the two-step laser mass spectrometry (L2MS), in which desorption and ionization are decoupled and no plasma is produced, to get the asphaltene molecular weight distribution. In their study, the asphaltene sample showed a peak at 600 Da. In 2007, Schneider⁷ and his colleagues determined the asphaltene molecular size by Fluorescence Correlation Spectroscopy to be in the 750 Da range. Other techniques such as depolarization spectroscopy¹⁰ are also widely used in determining asphaltene molecular weight. Right now, the more acceptable

molecular value of asphaltenes might vary from 500 to 1000 amu, with an average of 750 amu.¹⁰ The number of aromatic rings in each molecule is estimated to be in the range of 4 to 10 fused aromatic rings.¹⁰

In addition to the controversies of molecular weight, there has been another debate going on if asphaltenes are composed of only one fused, aromatic core surrounded by aliphatic chains or they are composed of many aromatic cores and these cores are interconnected by aliphatic chains³⁰. The two kinds of models respond to continental and archipelago model shown in Figure 2.2, respectively.



Figure 2.2 Examples of the two possible models for the asphaltene structures. Shown on the left is the continental structure, and on the right is the corresponding archipelago model.³⁰

Both models have supporters. Rogel³¹ theoretically calculated the asphaltene aggregation by assuming asphaltene molecular to be continental and matched the qualitatively prediction with the experimental trend. Other researchers³²⁻³³ built their experimental setup based on the archipelago model.

2.1.3 Fractions of asphaltenes

A standard method to get asphaltene precipitates from crude oil is to use a mixed solvent with short-chained hydrocarbon (heptane) and crude oil at a ratio of 40:1³⁴⁻³⁵ and collect the whole polydisperse asphaltene fractions. It is expected that there is a high degree of dispersity in aromaticity and polarity over the asphaltene samples, which will be reflected in the solubility in the short-chained hydrocarbon. Some studies use asphaltene precipitates in a range of hydrocarbon-to-toluene ratio, so the researchers will get the subfractions with different solubility. In the study of Fossen *et al.*¹¹, the asphaltenes were collected using a three-step precipitation procedure. The first fraction was obtained by mixing 3:1 volume of n-pentane-to-crude oil followed by filtration. The second fraction was precipitated out from an 18:1 n-pentane-to-crude oil solvent. For the third fraction, the sample was collected from asphaltene precipitates from a 40:1 n-pentane-to-crude oil mixture. They tested the three samples regard to the onset of precipitation, interfacial tension and radius of gyration and found that the second fraction was more soluble with increasing heptane-to-crude oil ratios, and more interfacially active and showed different organization properties at the oil-water interface. Their results proved that asphaltenes consist of fractions with different solvent properties. In their later studies¹², they developed a new procedure to get even more asphaltene fractions and suggested the first fractions obtained at low hydrocarbon-to-toluene ratio have the highest degree of polarity, aromaticity and average molecular size. Other researchers also separated the asphaltene fractions based on the polarity differences. Using a fractionation technique that divides the asphaltenes into different subfractions based on polarity, Wattana *et al.*²³ employed three crude oils to get the asphaltene samples with different polarity. From the dielectric constant, solubility and flocculation experiments, they found that the higher polarity fractions had a greater tendency to aggregate and more difficult to remediate, suggesting that the high-polarity asphaltene fractions played an important role in the asphaltene stability in crude oil.

It has been widely accepted that the asphaltene subfractions behave differently in many properties, but people were never able to separate all the fractions of asphaltenes into single molecules. On one hand asphaltenes have very strong diversity, as stated before. On the other hand, asphaltenes get too easy to aggregate. The stabilized water-in-crude oil emulsions have always been a problem bothering the people in oil sands industry. The remained water in crude oil, which is ready for the bitumen upgrading, contains plenty of salt which could cause severe equipment corrosion in the upgrader. So it is required to get rid of the water. However, the emulsions are believed to be stabilized mainly by asphaltenes, either molecules or aggregates. And now more and more people believe the stable interfacial film at oil-water interface are composed of asphaltene aggregates.³¹ And then this is correlated to the critical concentrations for asphaltene in eg. toluene to aggregate. Nevertheless, there has been significant uncertainty regarding the critical micelle concentration (CMC) of asphaltenes and even whether the micelle concept is appropriate for asphaltenes. Surface tension measurement was employed to measure the CMC of asphaltenes in pyridine.³⁶ A clear break in the surface tension occurred at ~400 mg/L. Other surface tension studies reported the CMCs of asphaltene to be much higher, in a concentration of 10 g/L in one study³⁷ and 1.7 g/L in another study³⁸. There are kinetic issues associated with surface tension measurements that might explain the large range difference of values reported for the asphaltene CMC. Thermo-optical techniques revealed a possible CMC in toluene at ~50 mg/L³⁷. Microcalorimetry was also applied to asphaltenes and reported the CMC of asphaltenes to be in a range of several grams per liter³⁹. A report⁴⁰ using microcalorimetry indicated the effects from water on the aggregation and labels the observed transitions at ~3 g/L asphaltene in toluene as CMC and also stated they did not detect a CMC without water being present. Instead of struggling on the CMC of asphaltenes, some researchers²⁶ introduced the terminology of critical nanoaggregate concentration (CNAC) for asphaltenes and finally tested the CNAC to be roughly at 0.1 g/L. Although much effort has been put on determining the critical concentrations of

asphaltene aggregate, there is no unique conclusion accepted yet. A report also showed that the aggregation was influenced by the resin fraction. The asphaltenes showed to be even more prone to stabilize emulsions by removing this fraction and this was explained in a way that the polar groups in the resins can stabilize asphaltene aggregates and disperse the aggregates into oil bulk phase⁴¹.

Even though most people believe the W/O emulsion is stabilized by asphaltene aggregates, some recent studies of interfacial activity of fraction proposed another mechanism behind the interfacial behaviour of asphaltenes.¹¹⁻¹² The researchers fractioned asphaltene samples into both two and four subfractions depending on pentane-to-crude oil ratio and measured the interfacial tension at toluene-water interface for each fraction. The studies showed that the intermediate fraction was the most active one because it has more hydrogen bonding groups such as –OH and –COOH, as indicted. In contrast, the first fraction, which is most polar and aromatic and with the highest average weight, did not show significant interfacial activity, indicating asphaltenes could be divided into non-surface active and surface active fractions. Many other studies support the terminology of (non)surface active as well.^{4,42-44} Yarranton *et al.* studied the emulsion stability by measuring the surface area of water-in-toulene/hexane emulsions and found that only the surface active asphaltenes, that were still soluble and that were present in monomeric state not as aggregates, were able to stabilize emulsions⁴. A similar model was proposed by Czarnecki *et al.*

2.1.4 Precipitation of asphaltenes

The formation and deposition of asphaltene-rich, solid like material during oil recovery have been well documented in the literature⁴⁵⁻⁴⁷. The growing market of crude oil production in deep-water environments and the operations of enhanced oil recovery by miscible displacement are sensitive to the complex phase behaviour of crude oil, especially given that the costs of remediation and lost production resulting from organic deposition in these operations increase almost exponentially. The precipitation of asphaltenes is a complex phenomenon

involving asphaltenes and resins. Hence, many efforts have been poured into getting a better understanding of the precipitation phenomena and forecasting the problems. The precipitation onset, that is the vol% of hydrocarbon in toluene where the asphaltenes start to precipitate, can easily be found by titration and detected by Near-Infrared Spectroscopy (NIR). PTL refers to the amount of light that passes through the sample and is received by the detector. PTL is inversely proportional to the particle size, density of the sampled fluid and number of the particles per volume of the fluid, which means if the pressure drops, the PTL increases; however if the number of asphaltene aggregates increases, the increasing trend of PTL decreases, until the number and size of the suspended aggregates is so large that the incident light is almost totally scattered, which dramatically decreases PTL. The point where PTL stops increasing continually corresponds to the precipitation onset pressure point in a phase diagram. Theoretical calculation can also predict the onset of asphaltene precipitation. Buenrostro-Gonzalez *et al.*⁴⁸ studied the asphaltene precipitation in crude oils both experimentally and theoretically. They used the statistical association fluid theory for potentials of variable range (SAFT-VR) equation of state (EOS) in the framework of a mature theory. A good prediction of asphaltene precipitation over wide temperature, pressure, and composition intervals was obtained by matching a single titration curve or two precipitation onset points with this EOS.

Asphaltene precipitation has usually two steps. The aggregation of asphaltenes is formed first followed by asphaltene flocculation as the second step. With regard to the mechanism of asphaltene flocculation, the researchers have reached a relatively uniform statement that the flocculation is formed due to van der Waals force between the “primary” asphaltene aggregates⁴⁹ or between asphaltene side chains and n-alkanes⁵⁰. Stachowiak *et al.*⁵⁰ studied the interactions between asphaltenes and short-to-medium-chain n-alkanes using titration microcalorimetry and inverse chromatography and showed that the energy of the interactions between n-alkanes and the asphaltene hydrocarbon chains is similar to the energy of the interactions between asphaltene chains. They proposed that the interaction

between asphaltene chains is the driving force of the asphaltene aggregate assembly into asphaltene precipitates. Such conclusion was also reached from the results by Takanohashi *et al.*⁵¹. In their study, simulations on two model compounds were carried out to investigate the effects of aliphatic chains and polar groups. Finally, the aliphatic chains and polar functional groups were found to contribute to the stability of the aggregates, and van der Waals interactions between aliphatic chains acted cooperatively to stabilize the asphaltene aggregates.

2.1.5 Film properties

The film properties of asphaltenes are usually studied by means of Langmuir technique (Langmuir trough and LB film deposition) and sometimes characterized by Atomic Force Microscopy (AFM). Zhang *et al.*^{8,52-55} did a lot of good job in characterizing the properties of asphaltene films. Various asphaltene films between water/toluene^{8,53}, water/air⁵², water/xylene⁵⁶, water/heptane⁵⁷ and water/solvent⁵⁵ have all been thoroughly studied by researchers these years. In general, LB films prepared with asphaltenes display low compressibility and high surface collapse pressure, indicating a strong film^{41,52}. The addition of resins or demulsifiers affects the asphaltene films by rendering the films more compressible, concerning both air/water and oil/water films^{41,54}. An example of the effect of demulsifiers is shown in Figure 2.3. In the pressure-area (π -A) isotherms curve, it is obvious that the demulsifier renders the asphaltene film more compressible. In addition, the critical pressure decreases when X_d increases from 0 to 0.43. The monolayer behaviour is dominated by asphaltenes. But when X_d is bigger than 0.60, the critical surface pressure is dominated by demulsifier instead. The compressibility has strong influence on the coalescence of water droplets in emulsions.

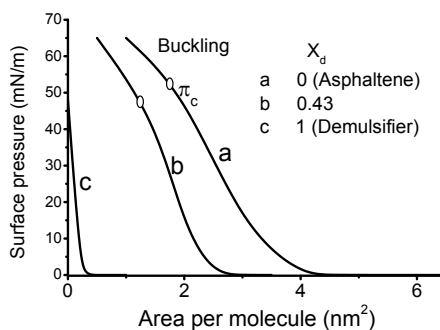


Figure 2.3 Air-water interface: pressure-area isotherms of mixed monolayer of asphaltene and demulsifiers at various molar ratios of asphaltene to demulsifier. The curves of mixed monolayers are plotted against area per molecule of the mixture. X_d is the mole fraction of demulsifier in the initial mixture.⁵⁴

Asphaltene films can be studied both as a monolayer⁵³ or as multilayers⁸. In the study of asphaltene monolayer at toluene/water interface⁵³, the monolayer was found to remain at the toluene/water interface and asphaltene did not migrate from the monolayer to the bulk toluene or water phase. If the hydrocarbon phase was replaced by a fresh toluene phase, the pressure-area isotherm was almost identical to that from the original asphaltene monolayer at the interface. In addition, 2-propanol did not solubilise asphaltene but render the monolayer more flexible. Bonding between the adsorbed monolayer with water molecules could be one of the explanations for the irreversible nature of the asphaltene films. A multilayer of asphaltene film will form by spreading an excess amount of asphaltene on a water subphase.⁸ In the study of asphaltene multilayers, it was found that once the top phase was replaced to fresh toluene, some of the asphaltene would migrate to the bulk toluene phase from the interface, leading to the formation of an asphaltene monolayer at the toluene/water interface. In the study of Zhang *et al.*⁵⁴, it was also shown that the composition of the oil phase affected the films of asphaltene. The interfacial films were shown to be more stable, which corresponds to the highest attainable interfacial pressure, at increasing demulsifier ratios, indicating an increased affinity for the interface

when the aromaticity of the solvent is low. Ese *et al.*⁵⁸ studied the water/air films of asphaltenes from different origins and illustrated that the asphaltenes adsorbed as aggregates when solubilised in a solvent of low aromatic character. Asphaltene films are rigid enough to prevent the water droplets from coalescence due to the strong intermolecular interactions between the molecules, which will be discussed later. These interactions give a viscoelastic network of the asphaltene molecules in a film. Recently, a small-angle neutron scattering (SANC) was used in the asphaltene film study and have shown that the structure of the interfacial layer is a monolayer of the asphaltene aggregates, and the size of the aggregates was correlated the size of the aggregate in the bulk phase.⁵⁹⁻⁶⁰ Nevertheless, this conventional, widely-accepted paradigm of asphaltene structure was denied by the study of Czarnecki⁶¹. The high-resolution Fourier transform ion cyclotron resonance (FT-ICR) mass spectrometry was employed in his study and the data showed that the composition of the surface material collected from the emulsified water droplets was different from asphaltenes, resins, and the parent oil. The material formed at the oil-water interface exhibits optical anisotropy, based on which the molecular organization of the surface phase was proposed. The arrangement of the asphaltene molecules at the aqueous phase was also commonly discussed. There were mainly two configurations suggested. One was that asphaltenes stay on the aqueous surface with their aromatic core lying flat on the aqueous surface.⁶² Another configuration was described as a more tilted geometry of the aromatic core with respect to the surface plane⁶³. It has also been suggested that both configurations exist simultaneously, depending on if the interface is relaxed or compressed.⁴

2.1.6 Molecular interactions of asphaltenes

Many industrial problems such as formation of stable water-in-oil emulsions, wellbore or pipeline plugging, sedimentation during crude blending and alteration of wettability of solids are all attributed to the aggregation of asphaltenes. In order to solve such problems, the interactions between asphaltene molecules have been

intensively studied during the past years. However, the mechanism of asphaltene aggregation is still under investigation. No uniform conclusion has been accepted, neither in organic solvents nor in aqueous solutions.

Asphaltenes are of amphiphilic nature, so some researchers suggested that asphaltene molecules would aggregate like surfactants and form micelles above a certain concentration, which is referred as critical micelle concentration (CMC), in toluene.^{39,64-65} For example, Rogel *et al.* estimated the CMC of asphaltenes through the surface tension measurement and found that the self-aggregation of asphaltenes was affected by their chemical characteristics and structures.⁶⁶ In 1999, Andersen *et al.*³⁹ measured the micellization of asphaltenes using a micro calorimetric titration procedure. The method used the analysis of heat of the dissociation and dilution of the asphaltene micelles when a pure solvent (or solvent mixture) was titrated with an asphaltene solution in the same solvent. The CMC's of asphaltenes in different solvents were obtained and it was found that the CMC decreased upon heptane addition, which is predictable.

However, in other studies, the CMC was not observed in organic solutions.⁶⁷ Instead, a polymeric association was suggested for the aggregation of asphaltenes to account for the polymeric properties observed in asphaltene solutions. For example, Mitchell *et al.*⁶⁸ showed that the asphaltene subfractions with higher molecular weight were polymeric analogues of the subfractions with lower molecular weight. Besides the different suggestions on the aggregation model, the nature of the molecular interactions involved in asphaltene aggregation was also under debate. Some researchers⁶⁹ believe it was due to the strong specific interaction sites located at the periphery of the asphaltene molecules. The specific sites drive the reversible association in two-dimensional sheets, corresponding to morphology consistent with the reported scattering and viscosity data. Buckley *et al.*⁷⁰ disagreed on the specific strong interaction and attributed to van der Waals attraction. The molecular force between asphaltene surfaces in organic solvents were directly measured by Wang *et al.*^{21,71} using AFM. In their study, mixture

solvents of toluene and heptane, which were named heptol, were applied as medium between two asphaltene surfaces. In pure toluene, a strong repulsive force was detected while the repulsive force was decreased with increasing amount of heptane. Adhesive force was increased moronically with increasing amount of heptane. The approaching force curves were well fitted with scaling theory, and the force curve in pure heptanes was fitted by van der Waals force, indicating the attractive force between asphaltenes in toluene was of van der Waals origin. Surface forces apparatus (SFA) was also employed in measuring the interaction force between asphaltene surfaces⁷², and the measured adhesive force was also attributed to van der Waal force.

In bitumen aeration, the small bitumen droplets are required to coalesce in order to be floated. Yet, the small bitumen droplets are usually stabilized by the asphaltenes in the form of bitumen-in-water emulsions. To understand the mechanism of emulsion stabilizaiton in such case, it is extremely important to understand the interactions between asphaltenes in aqueous solutions. The molecular force between asphaltnes are usually directly measured by AFM or SFA. Liu *et al.*⁷³⁻⁷⁵ did a lot of work, trying to figure out the mechanism of emulsion stabilization and the effect of industrial operation conditions on the interactions between asphaltenes. The interactions between asphaltenes and clay and between two asphaltene surfaces were shown to be strongly affected by solution pH, salt concentration and divalent ions due to the charged properties of asphaltene surfaces.

2.2 Asphaltene model compounds

The sections about the characteristics of asphaltenes demonstrate that the knowledge of asphaltenes is limited due to the high polydispersity of this class. There seems to exist two ways to terminate this situation. One is to continue trying to divide the whole asphaltenes into numerous subfractions and study each subfraction to determine which is responsible for the undesired properties¹¹⁻¹². Another way is to use model compound with defined molecular structure and

similar physiochemical properties as those asphaltenes. Model compounds create an easier system because they have known composition, molecular weight and facile characterization by, for example, UV or fluorescence. So from decades year ago, the researchers have been trying to solve the asphaltene or bitumen related issues by means of model compounds. It was reported in 1996, Mulvaney *et al.* carried out a study of interaction force between a solid. From then on, studies on the model compounds have attracted more and more attention. The development of model compounds will be introduced in the following in two sections: the model compounds mainly focusing on the molecular weight issue and model compounds focusing on the interfacial activity issue.

2.2.1 Model compounds focusing on molecular weight or aggregation

As discussed in the asphaltene characteristics section, molecular weight and the mechanism of aggregation of asphaltenes have always been under debate. So many researchers tried to solve the issues by synthesizing model compounds. *Mullins et al.* have in several studies used, for example, perylene and porphyrine dyes together with the fluorescence techniques^{7,10} to study the molecular weight of natural asphaltens and compounds. Fluorescence is a highly sensitive technique enabling the probe to be studied at very low concentrations. Therefore, experiments could be carried out well under the CNAC of the asphaltenes, which avoids the pitfall of measuring the aggregate size. The data from the fluorescence for model compounds with known structure and size could be used to estimate the size of the actual asphaltenes. Under this technique, the nowadays accepted molecular weight of asphaltenes in the range of 500 – 1000 amu was reached. Synthetically made hexabenzocoronene derivatives were also used as model compounds for asphaltenes to approach the self-association behaviour of bitumen fraction, and the association behaviour measurement was carried out using pyrene compounds with both aromatic and polar character.⁷⁶ Very recently, Gray and his co-workers⁷⁷ published a paper related to a supermolecular assembly model. In their article, they brought up that none of the properties of asphaltene components

such as aggregating in crude oil and toluene over a very wide range of concentrations and temperatures, exhibiting strong adhesion to a wide range of surfaces, elastic under tension and porous to solvents is consistent with the architecture that the components were dominated by aromatic stacking caused from electrostatic or van der Waals force (or π - π stacking). So they proposed a new paradigm—combining cooperative binding from acid-base interactions, hydrogen bonding, complexes, metal coordination and interactions between alkyl and cycloalkyl to form the hydrophobic pockets and aromatic π - π stacking. In this way, the aggregation behaviours of asphaltenes in organic solvents and in the presence of water are simulated by the supermolecular model.

2.2.2 Model compounds focusing on the physicochemical properties

In the previous section, the model compounds have been used to address the molecular weight and aggregation issues. No information regarding the use of model compounds on the physicochemical properties was found. However, characterization of the interfacial behaviour is an important way to find the mechanism behind the interfacial activity and emulsion stabilization.¹¹⁻¹² Based on the need for such studies and knowledge about the functionalities of asphaltenes, several asphaltene model compounds (Figure 2.4) were synthesized by modifying a polyaromatic compound and their interfacial properties and emulsion stability were studied by Nordgard and his colleagues using varying techniques.^{9,17-18} The solubility behaviour of the model compounds was studied by means of titration with n-heptane and precipitation onset estimation by NIR spectroscopy, and it turned out that the precipitation behaviour was influenced by both aromatic and polar interactions. And the behaviour that asphaltene model compounds became precipitated upon addition of n-hexane showed similar solubility behaviour of real asphaltenes.⁹ The interfacial behaviour was characterized by measuring the interfacial tension.⁹ The model compounds displayed an interfacial tension between toluene and pH 9 water of around 5 mN/m in the amount of 12.5-35 μ M, indicating a high interfacial activity and

resembling the interfacial activity of real asphaltenes. Besides these three acidic model compounds, another non-acidic model compound was also synthesized and its interfacial behaviour was investigated by use of Langmuir trough together with the other three acidic model compounds.¹⁷ The surface pressure-area isotherms and area loss measurement obtained from Langmuir trough indicated stable films for the acidic compounds, and the pressure-area isotherms were comparable to real asphaltene isotherms. However, the non-acidic model compound failed to form a stable film, indicating a profound impact of acidic functional groups in such model compound molecules. This suggested that the acidic subfractions of asphaltenes could be problematic subfractions for the emulsion stabilization.

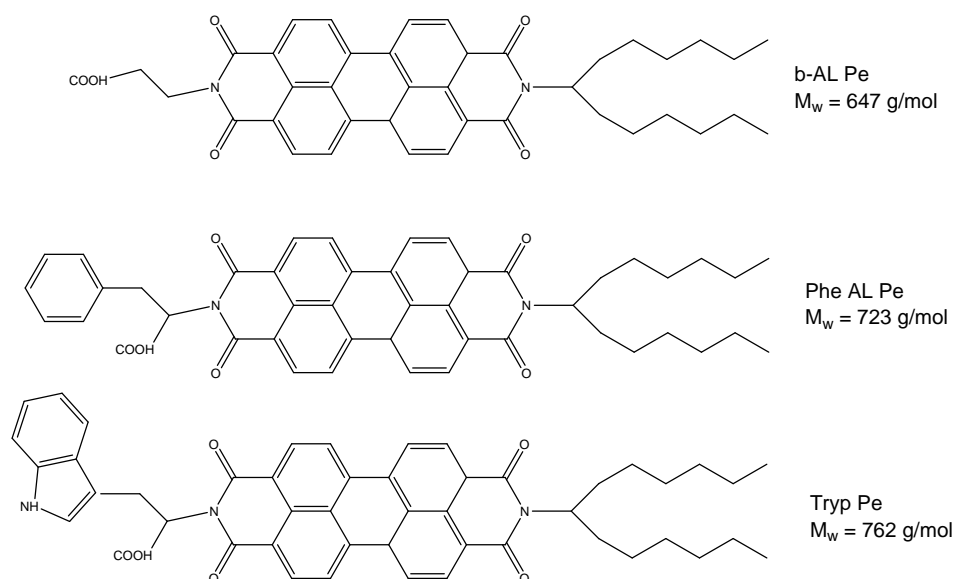


Figure 2.4 Structure and molecular weight of the asphaltene model compounds synthesized and characterized.

The properties of the films deposited with LB technique were investigated with SS fluorescence¹⁷. From the spectra of the model compounds together with the mean molecular area obtained in surface pressure – area isotherms, a head on arrangement for the acidic model compounds was proposed. This arrangement gave the proof for the favourable $\pi - \pi$ interaction between the aromatic cores, which yields an extra stabilization in the surface plane.

The emulsions and adsorption behaviour of the model compounds were also studied.¹⁸ We all know that the emulsion behaviour stabilized by crude oil fraction has been a challenge for all the researchers, so it is easy to investigate the emulsion behaviour using single molecular systems as a function of true concentrations. Hopefully, the emulsion stabilization study for model compounds will open up a new sight for the real asphaltene study. In Nordgard's study, the emulsions were prepared with the model compounds in xylene and pH 8 water. The surfactant concentration was kept constant with varying amount of water cut (WC). The mean volumetric diameter of the emulsions was determined by a modified PFG NMR method. The results showed that the size and stability of the emulsions depends on the WC, time and model compound type. However, the emulsions did be stabilized by the model compounds just like real asphaltenes. The adsorption behaviour of the model compounds onto hydrophilic silica was carried out as a way to model the adsorption onto the water surface.¹⁸ The results showed that the acidic model compounds would adsorb onto the surface while the non-acidic model compounds would not. By calculating the mean molecular area of the compounds from adsorption data, the results were similar to the molecular area data collected from Langmuir trough, and the same head-on arrangement was suggested. The study showed that the acidic or similar hydrogen bonding groups, present in an asphaltene structure greatly increased the power of model compounds to stabilize emulsions.

CHAPTER 3 SURFACE FORCE REVIEW

Surface force is the force that acts across an internal or external surface element in a material body. The surface force originates from the unbalanced forces of the surface atoms in a material. An example is shown in Figure 3.1. Assuming this material is a complete crystal material and all the atoms are arranged in order, in which case the atoms inside the bulk is balanced from the force balance point of view because all the atoms around it are the same and symmetrically arranged. However, for the atoms at the surface, only one direction could be balanced while the other direction is not. So the surface of the material is unstable, it would like to react with other surfaces or materials to get its balance. Like the atom A in Figure 3.1, the force in the horizontal direction is balanced, but in the vertical direction, it bears a down-to-the-bulk total force. Surface force is omnipresent and it is important in also every field, no matter microworld or the macroworld. In this thesis, we are studying the surface force of C5Pe, trying to find the emulsion stabilization mechanism. Actually, understanding the surface forces not only helps us to get better understanding of emulsions, but also contributes in any surfactant related issues. The related theories or descriptions of surface forces are summarized in the following.

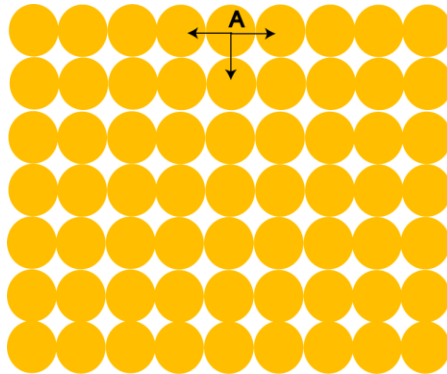


Figure 3.1 An example of atom arrangement at the surface.

3.1 DLVO theory

The DLVO theory is named after Derjaguin, Landau, Verwey and Overbeek. This theory describes the long-range force between charged surfaces interacting through a liquid medium. It combines the effect of electrostatic force and van der Waals force. It is usually expressed as:

$F_{DLVO} = F_{VDW} + F_E$, where F_{DLVO} is the DLVO force, F_{VDW} is van der Waals force and F_E is electrostatic force.

3.1.1 Van de Waals forces

Van der Waals forces are omnipresent between any surfaces in any medium. They are sum of the attractive or repulsive forces between molecules or between parts of the same molecule.⁷⁸ The van der Waals forces have three distinct origins: 1) Keesom force between two permanent dipoles; 2) Debye force between a permanent dipole and a corresponding induced dipole and 3) London dispersion force between two instantaneously induced dipoles. The van der Waals forces are relatively weak comparing to normal chemical bonds but play a fundamental role in many fields. It should be noted that van der Waals forces differ from covalent and ionic bonding in that they are caused by correlations in the fluctuation polarizations of nearby particles and that they are dependent on the relative orientation of the molecules and less sensitive to environmental changes. The detailed description of van de Waals forces can be found in the textbook of Israelachvili⁷⁹. As an example, the van der Waals energy between spherical bodies of radii R_1 and R_2 was approximated by Hamaker⁸⁰ by

$$U(z; R_1, R_2) = -\frac{A}{6} \left[\frac{2R_1 R_2}{z^2 - (R_1 + R_2)^2} + \frac{2R_1 R_2}{z^2 - (R_1 - R_2)^2} + \ln \frac{z^2 - (R_1 + R_2)^2}{z^2 - (R_1 - R_2)^2} \right] \quad (3-1)$$

where A is Hamaker constant which depends on the material properties, z is the center – to – center distance, so $z = R_1 + R_2 + r$, where r is the distance between

the surfaces. When the two surfaces are close to each other, that is r is far less than R_1 or R_2 ,

$$U(r; R_1, R_2) = -\frac{AR_1R_2}{(R_1+R_2)6r} \quad (3-2)$$

The van der Waals force

$$F_{VDW}(r) = -\frac{dU(r)}{dr} \quad (3-3)$$

By doing the derivation, the van der Waals force between two spheres with radii R_1 and R_2 is

$$F_{VDW}(r) = -\frac{AR_1R_2}{(R_1+R_2)6r^2} \quad (3-4)$$

If $R_1 = R_2$,

$$\frac{F_{VDW}}{R} = -\frac{A}{6D^2} \quad (3-5)$$

The Harmaker constant in this equation depends on the material's own properties. In 1956, the Harmaker constant was calculated based on Lifshitz approach with consideration of the dielectric properties of the intervening medium as $A = \pi^2 \times C \times \rho_1 \times \rho_2$, where ρ_1 and ρ_2 are the numbers of atoms per unit volume in two interacting bodies and C is the coefficient in the particle-particle pair interaction.⁸¹

For the interaction of phase 1 and phase 2 through media 3 (Figure 3.2), the combined Harmaker constant A_{132} can be calculated in equation 3-6:

$$A_{132} = (\sqrt{A_{11}} - \sqrt{A_{33}})(\sqrt{A_{22}} - \sqrt{A_{33}}) \quad (3-6),$$

where A_{ij} is the Harmaker constant of the material i .

Harmaker constant could be positive or negative. When it is positive, van der Waals force is negative, which mean van der Waals forces are attractive, and when Harmaker constant is negative, van der Waals forces are repulsive. For two

identical particles interacting through media 2, $A_{11} = A_{22}$, $A_{132} = A_{131} = (\sqrt{A_{11}} - \sqrt{A_{33}})^2$ is always non-negative. So the van der Waals force between two identical phases is always attractive.

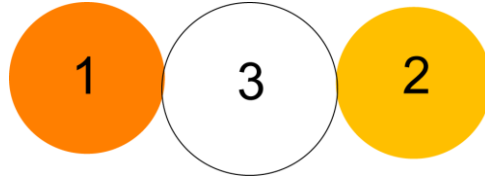


Figure 3.2 Phase 1 and phase 2 interact through media 3.

3.1.2 Electrostatic double layer force

When a surface is immersed in an electrolyte solution, it could be charged by the dissociation of surface groups or by adsorption of charged molecules or by crystal lattice defects, etc. The charged surface results in the development of a wall surface potential which will attract counterions from the bulk solution and repel co-ions. In equilibrium, the surface charge is balanced by oppositely charged counterions in the bulk solution. The region near the surface of enhanced counterions is called the electric double layer. The structure of the electric double layer was first described as parallel plate capacitor⁸², which has its reasonability as we can see in the following. But the most acceptable model is proposed by Stern and Grahame (Figure 3.3). In the Stern-Graham model, counterions bound to the surface form the stern layer and remaining counterions form a cloud in rapid thermal motion. There is another layer called shear layer, inside which the ions don't move with the bulk solution and beyond which the ions move with the bulk solution. So in practical, the deepest surface potential that can be measured is from this layer, and the measured potential is called zeta potential. There are many instruments measuring the zeta potential of a particle, all based on the electrophoresis or electrical osmosis measurement. The detailed zeta potential measurement and instrument introduction could be found elsewhere.⁷³⁻⁷⁵

It is known that the concentration of the electrolyte ions in the diffuse layer obeying the Boltzmann distribution⁸³:

$$n_i = n_{i0} \exp\left(-\frac{z_i e \psi}{kT}\right) \quad (3-7)$$

Where n_i is the number density of ion i , n_{i0} is the number density of ion i in the bulk, ψ is the potential in the electric double layer, e is the electron charge, k is Boltzmann constant, z_i is the valence of ion i and T is the absolute temperature.

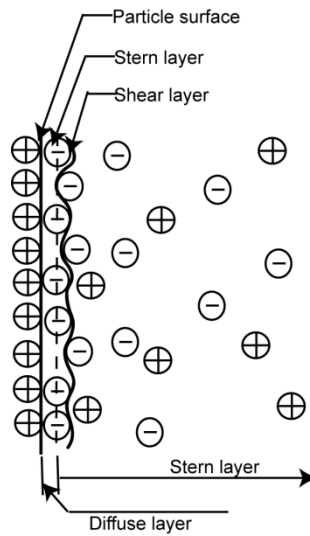


Figure 3.3 Schematic of Stern-Grahame electric double layer model.

The Poisson equation is written as:

$$\frac{d^2 \psi}{dx^2} = -\frac{\rho^*}{\epsilon_r \epsilon_0} \quad (3-8)$$

where ϵ_r and ϵ_0 is the relative permeability of the medium and permeability of vacuum,

$$\rho^* = \sum_{i=1}^n z_i e n_i = \sum_{i=1}^n z_i e n_{i0} \exp\left(-\frac{z_i e \psi}{kT}\right) \quad (3-9)$$

By substituting equation 3-9 into 3-8, the Poisson equation is written as:

$$\frac{d^2\psi}{dx^2} = -\frac{1}{\varepsilon_r\varepsilon_0} \sum_{i=1}^n z_i e n_{i0} \exp\left(-\frac{z_i e \psi}{kT}\right) \quad (3-8a)$$

Recall Taylor expansion when $-\frac{z_i e \psi}{kT} < 1$,

$$\exp\left(-\frac{z_i e \psi}{kT}\right) = 1 - \frac{z_i e \psi}{kT} \quad (3-10)$$

Substituting 3-10 into 3-8a and noting that $\sum_{i=1}^n (z_i e n_{i0}) = 0$, we can get the equation:

$$\frac{d^2\psi}{dx^2} = \frac{1}{\varepsilon_r\varepsilon_0} \sum \frac{z_i^2 e^2 n_{i0}}{kT} \psi \quad (3-8b)$$

Define

$$\frac{1}{\varepsilon_r\varepsilon_0} \sum \frac{z_i^2 e^2 n_{i0}}{kT} = \kappa^2 \quad (3-11)$$

Equation 3-8b becomes

$$\frac{d^2\psi}{dx^2} = \kappa^2 \psi \quad (3-8c)$$

From the definition of κ , we know that it is independent of surface charge but depend on the solution conditions. Higher ion valence and higher ion concentration induce higher κ value. Assuming the surface potential of a particle is ψ_d , the boundary condition should be: at $x = 0$, $\psi = \psi_d$; at $x = \infty$, $\psi = 0$. At this boundary condition, the equation is solved as:

$$\psi = \psi_d \exp(-\kappa x) \quad (3-8d)$$

So it is known that the surface potential in the stern layer decreases exponentially. According to the Stern-Graham theory, the potential in the diffuse layer decreases linearly. The potential distribution schematic is drawn in Figure 3.4. If you draw a tangent line at $x = 0$ (stern plane), the crossover point with x axis is κ^{-1} , which is called the decay length.

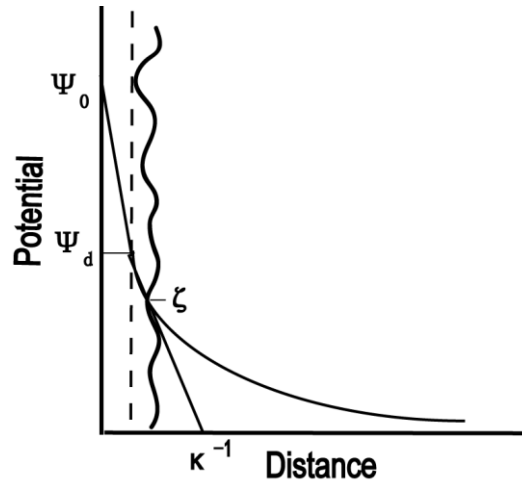


Figure 3.4 Potential distribution in the double layer.

The total charge σ_d at the stern layer could be written as:

$$\sigma_d = - \int_0^{\infty} \rho^* dx = - \int_0^{\infty} -\epsilon_r \epsilon_0 \frac{d^2 \psi}{dx^2} dx = \kappa \epsilon_r \epsilon_0 \psi_d \quad (3-12)$$

Then

$$\frac{\sigma_d}{\psi_d} = \frac{\epsilon_r \epsilon_0}{\kappa^{-1}} = C_e \quad (3-13)$$

C_e is the capacity of a capacitor. That is the reason for the reasonability to describe the structure of the electric double layer as parallel plate capacitor. The κ^{-1} describes the double layer thickness or the decay of the electric potential and therefore the interaction between the two neighboring surfaces.

When two charged particles approach, the electric double layer surrounding the particles starts to overlap, resulting in the repulsion or attraction in the osmotic pressure, which is produced by the difference of concentrations between inside the gap and the bulk solution. The interaction force $F_E(D)$ and energy $U_E(D)$ between two parallel planes can be expressed in Equation 3-14 and 3-15.

$$F_E(D) = kT \sum_{n=1}^{\infty} (n_i - n_{i\infty}) - \frac{\epsilon_r \epsilon_0^2}{2} \left(\frac{d\psi}{dx} \right)^2 \quad (3-14)$$

$$U_E(D) = - \int_{\infty}^D F_E(h) dh \quad (3-15)$$

Only with some approximations and boundary conditions (B.C.) can the interaction force and energy be algebraically solved.⁸³ For the B.C., if the surface charge arises from lattice imperfections or irreversible adsorption of charged species or dissociation of surface strong acid/base groups, the surface charge is independent of surface potential and the separation between the two surfaces. Therefore, the surface charge is constant, in which case the constant surface charge density boundary conditions can be used since the potential determining ions have insufficient time to re-arrange during the approach of the two surfaces during force measurement. For example, the basal plane of the clay minerals is charged due to the lattice imperfections of the surface itself, the surface charge won't be changed with surface potential or separation distance. The constant surface charge boundary condition could be written as:

$$\text{At } x = 0, \frac{d\psi}{dx} \Big|_{x=0} = \text{constant}, \text{ and at } x = \infty, \psi = 0.$$

In other cases, if the surface charge arises from reversible ion adsorption, the potential determining ions can rearrange quickly to suit every configuration of the interacting surfaces to keep the surface potential constant when the two surfaces approach or separate from each other at a slow rate. For example, the metal oxides and semi-soluble minerals can keep the surface potential at constant since they are charged from reversible ion adsorption. The constant surface potential boundary condition could be written as:

$$\text{At } x = 0, \psi = \psi_d \text{ and at } x = \infty, \psi = 0.$$

For a symmetric system (cations and anions carry the same valence charges), such as NaCl, CaSO₄, the surface potential could be calculated at constant surface charge density B.C. as:

$$U_E(D) = \frac{64n_0kTY^2}{\kappa} \exp(-\kappa D) \quad (3-16)$$

where n_0 is the number density of ions in bulk solution, and $Y = \tanh \frac{ze\psi_d}{4kT}$.

At low ψ_d , $\frac{ze\psi_d}{4kT} < 1$, $Y = \tanh \frac{ze\psi_d}{4kT} \cong \frac{ze\psi_d}{4kT}$, in this case

$$U_E(D) = 2\varepsilon_r\varepsilon_0^2k\psi_d \exp(-\kappa D) \quad (3-16a)$$

which tells us that at higher salt concentration (higher κ), the double layer energy decreases, which corresponds to a case shown in Figure 3.5.

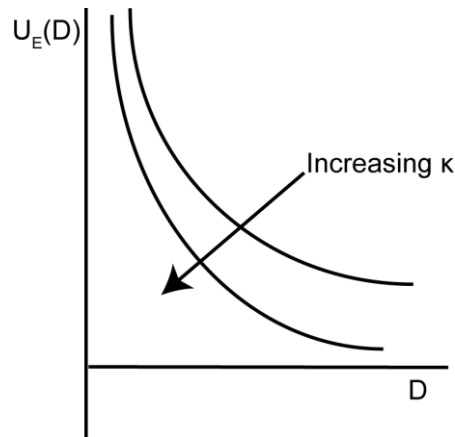


Figure 3.5 A schematic showing the relation between surface energy and decay length.

In DLVO theory, the total force is the sum of van der Waals force and electrostatic force. So

$$U_{total} = U_E(D) + U_{VDW}(D) = \frac{64n_0kTY^2}{\kappa} \exp(-\kappa D) - \frac{A}{12\pi D^2} \quad (3-17)$$

This equation clearly shows that the total interaction energy strongly depends on the stern potential ψ_d (i.e. Y), and κ . As the stern potential decreases, the repulsive electrostatic force decreases, and the total force will become attractive along all

the separation distance. Figure 3.6 shows an example of the effect of stern potential on the interaction energy of two spherical particles.

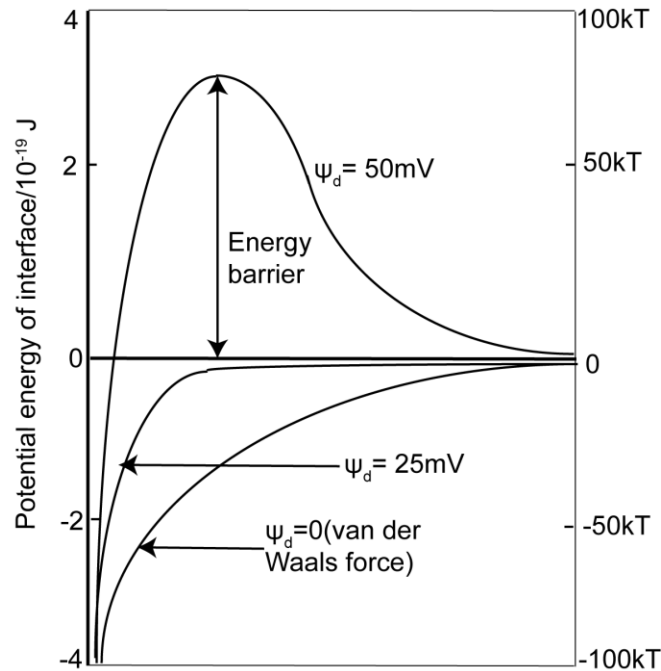


Figure 3.6 An example showing the influence of Stern potential on the total energy of interaction of two spherical particles: $a = 200 \text{ nm}$; $T = 298 \text{ K}$; $z = 1$; $A_{11} = 2 \times 10^{-19} \text{ J}$; $A_{33} = 0.4 \times 10^{-19} \text{ J}$; $\epsilon_r = 78.5$; $\kappa = 3 \times 10^8 \text{ m}^{-1}$.

When the stern potential ψ_d is big, the total energy encounters an energy barrier, which keeps the two particles repelling from each other and staying stable. However, when the stern potential decreases, the energy barrier decreases and disappears at a critical stern potential.

As the decay length decreases in a solution, the electrostatic energy also decreases. At a constant stern potential, the potential energy also has an energy barrier at small κ value, and the energy barrier decreases with increasing κ value and disappears at the critical coagulation condition. The critical coagulation condition could be obtained with the conditions that at critical coagulation conditions,

$\frac{dU_{total}}{dD} = 0$, and $U_{total} = 0$. In this way, the critical coagulation κ value is known to have a relation with separation distance D as $\kappa D = 2$.

However, in reality the surface charge density is a function of separation distance between the two particles. The assumption of constant surface charge density and constant surface potential boundary conditions constitutes the upper and lower limits of the interaction forces. A realistic case is far complicated than the two ideal cases. But the description is between the two limits.

3.2 Extended DLVO theory

The classical DLVO theory only dominates at long distance. Over the past decades, the researchers tried to explain the molecular interactions with DLVO theory, but their experimental results can not be totally explained by this theory. People measured the surface force with AFM or SFA and always found the deviation from the classical DLVO theory, which provided the evidence of additional forces. The additional forces together with DLVO forces constitute the extended DLVO (EDLVO) theory. The additional forces include the repulsive hydration force⁸⁴⁻⁸⁶ for the hydrophilic surfaces, the attractive hydrophobic forces for the hydrophobic surfaces, the steric repulsion due to special polymer adsorption and bridging forces⁸⁷ for polymer-bearing surfaces, and other forces. The total force can be written as equation:

$$F_{total} = F_{VDW} + F_E + F_{HB} + F_S + F_{HD} + F_B + \dots \quad (3-18)$$

where F_{HB} is hydrophobic force, F_S is steric force, F_{HD} is hydration force and F_B is bridging force. The nature of these non-DLVO forces has not been fully understood, but their interacting range has been determined and some of the empirical expressions have also been derived. It is known that hydration force affects at relatively short range; hydrophobic force is long range and attractive and much stronger than van der Waals force; steric force is at longer range than hydration force but shorter range than electrostatic force; the polymer bridging

force is attractive at long distance and repulsive at short distance and is a very strong force. The qualitative draw of all the EDLVO forces is shown in Figure 3.7.

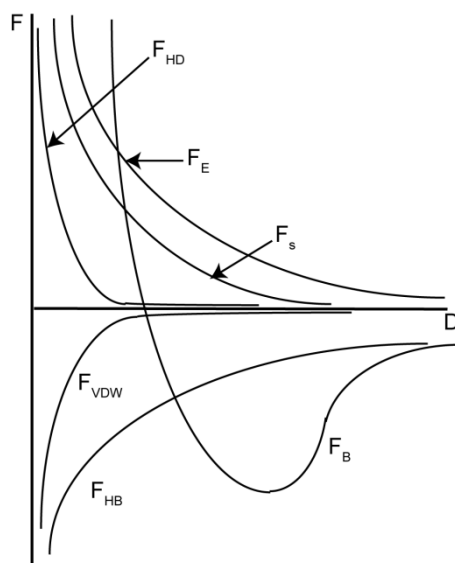


Figure 3.7 A schematic show of EDLVO forces. (From the note book of MAT E633, U of A)

3.2.1 Hydrophobic force

Hydrophobic force was found to exist between hydrophobic surfaces immersed in an aqueous solutions.⁸⁸ It has been measured for various systems over the last several decades.⁸⁹⁻⁹¹ The origin of hydrophobic force has many theories. Some people suggest that it is essentially an entropic force resulting from the entire system's statistical tendency to increase its entropy, rather than from a particular underlying microscopic force. When a hydrophobic surface is immersed in aqueous solutions, the water molecules near the surface reorientate to attain the best configuration of the maximized number of H-bonds, i.e. increase in parallel orientation of water molecule dipole moment⁸³. However, the reorientation of the water molecules around a non-polar surface is entropically unfavourable, so once two hydrophobic surfaces approach each other, the rearrangements of H-bond in the overlapping salvation zones would result in the attraction between the two

surfaces, in order to reduce the entropy. There are also theories supporting the origin of hydrophobic force is other forces such as capillary forces due to cavitations in the vicinity of hydrophobic surfaces⁹², the charge correlations⁹³ and the hydrodynamic correlation between fluctuating liquid-solid interfaces⁹⁴ or the correlation of dipoles associated with molecular domains⁹¹. Although the mechanism of hydrophobic force has not been fully understood, people proposed several empirical relationships over the last years mainly based on the information of direct force measurements. In 1985, Pashley⁹⁰ gave an empirical equation for calculating the hydrophobic force as:

$$\frac{F_{HB}}{R} = C_1 \exp\left(-\frac{H}{D_1}\right) + C_2 \exp\left(-\frac{H}{D_2}\right) \quad (3-19)$$

in which R is the curvature of the mica surfaces; H is the closest distance separating two interacting surfaces, C_1 and C_2 are parameters characterizing the magnitudes of the short and long range hydrophobic forces, respectively; D_1 and D_2 are the decay lengths. Here, the short range refers to hydrophobic force observed at $H < 10$ nm with decay length of 1 – 2 nm. The hydrophobic force was also described by a power law as:

$$\frac{F_{HB}}{R} = -\frac{K}{6D^2} \quad (3-20)$$

where K is a fitting parameter. This equation is in the form of the van der Waals equation but the K value is usually much bigger than Hamaker constant.

3.2.2 Steric force

Steric force exists in systems involving brush-like surfaces, such as polymer or surfactant surfaces. According to the measured steric force, people divide it into different types, such as the osmotic repulsion in good solvent, the osmotic attraction in poor solvent and the attractive bridging effect due to polymer chains simultaneously adsorbed on both surfaces. The theoretical expression of steric force has many forms under different conditions. At low surface coverage, when

there is no overlap of neighbouring chains and each chain interact with opposite surface independent of other chains, the repulsive energy per unit area is:

$$W(D) = 36\Gamma kT \exp\left(-\frac{D}{R_g}\right) \quad (3-21)$$

where Γ is the number of the grafted chains per unit area, D is the distance, R_g is the radii of the particle.

However, at high surface coverage for uncharged polymeric surfaces, de Gennes⁹⁵ assumed a brush-model and derived an expression of the steric force for two parallel plates as:

$$P(D) \cong \frac{kT}{s^3} \left[\left(\frac{2L}{D}\right)^{9/4} - \left(\frac{D}{2L}\right)^{3/4} \right] \quad (3-22)$$

where $P(D)$ is the repulsive pressure between two brush-bearing surfaces closer than $2L$ (L is the length of the polymer brushes), s is the average distance between two grafting points. Using Derjaguin approximation (discussed later), this equation could also be used for the interactions between a plate and a sphere configuration. For two symmetrical surfaces with both covered with polymers, the steric force is derived from equation (3-22) in the form as:

$$\frac{F(D)}{R} = 2\pi \int_D^R P(D') dD' = \frac{16\pi kTL}{35s^3} \left[7 \left(\frac{2L}{D}\right)^{5/4} + 5 \left(\frac{D}{2L}\right)^{7/4} - 12 \right] \quad (3-23)$$

For asymmetric systems (a polymer brush against solid substrate), the equation changes to:

$$\frac{F(D)}{R} = \frac{8\pi kTL}{35s^3} \left[7 \left(\frac{2L}{D}\right)^{5/4} + 5 \left(\frac{D}{2L}\right)^{7/4} - 12 \right] \quad (3-24)$$

In the above, the Derjaguin approximation is mentioned. Derjaguin approximation is a relationship derived by Derjaguin⁸³ and White (1983) to relate the energy per

unit area between two planar surfaces w which are separated by a gap x to the energy between two bodies of any arbitrary shape W which is at a distance D :

$$W(D) = \int_0^\infty w(x) dA_a \quad (3-25)$$

in which A_a is the area of the arbitrary surface. By doing many derivations, the relationship between the interaction force F for a given geometry and the interaction energy U_{p-p} for two parallel plates is written as:

$$F_{s-s} = 2\pi \frac{R_1 R_2}{R_1 + R_2} U_{p-p} \text{ for two spheres with radii } R_1 \text{ and } R_2;$$

$$F_{s-p} = 2\pi R U_{p-p} \text{ for a sphere with radii } R \text{ to a plane};$$

$$\text{and } F_{c-c} = 2\pi \sqrt{R_1 R_2} U_{p-p} \text{ for two cylindrical surfaces with radii } R_1 \text{ and } R_2.$$

Using the equation for two cylindrical surfaces approximation back into equation 3-22, the symmetrical force equation for two identical surfaces will be calculated in equation 3-23.

The steric force exists not only in the uncharged conditions. For the charged surfaces, Picus⁹⁶ developed an expression of steric force as a function of the separation distance for a plate-sphere configuration in the form of:

$$\frac{F_s}{R} = \frac{4\pi k T N_B^2}{1000 N_0 \sum_i z_i M_i s^4} \left(\frac{1}{D} - \frac{1}{2L} \right) \text{ for } D < 2L \quad (3-26)$$

where N_0 is Avogadro number ($6.02 \times 10^{23} \text{ mol}^{-1}$), z_i and M_i are valence and molar concentration of the electrolyte respectively, N_B is the number of monomer units per chain. For two cylindrical surfaces with identical radii R , the expression is same with equation 3-26.

3.2.3 Hydration force and bridging force

The short-range forces between hydrophilic surfaces determine the behaviour of many diverse systems such as soap films⁹⁷, swelling of clays⁸², stability of

colloidal dispersions⁹⁸ and interactions of biological membranes. The experimental measurements identified it as repulsive and decay monotonically with distance out to separations up to ~6 nm. The force is termed as hydration force. When hydrophilic surface is immersed in aqueous solutions, the hydrophilicity of the surface drives the surface to be in contact with water rather than with other hydrophilic surfaces. So when the surfaces approach each other, an additional strong force is needed to remove the water layer from the surface regions, showing a repulsive hydration force. The hydration force was measured with SFA⁹⁹, and this kind of force was observed in silica, lipid and surfactant systems.

The polymer bridging force is a very strong interaction between polymer-covered surfaces. The mechanism of this force is still unclear. The polymer bridging force is used widely in settling. For example, in the oil sands tailing treatment, the polymer is added into the tailing pond. The polymer is expected to cover the clays surface and bring the clay together to accelerate the settling efficiency of the tailings. However, in use of polymer, the amount of polymer should be controlled in a range, since over dosage of polymer could cause the polymer to repel from each other due to steric force.

CHAPTER 4 MATERIALS AND EXPERIMENTAL TECHNIQUES**4.1 Materials**

The model compound C5Pe was received as a gift from Johan Sjöblom as a gift, and the detailed synthesis has been reported elsewhere⁹. C5Pe solution was prepared by dissolving C5Pe in HPLC grade toluene (> 99.9%, Fisher scientific, Canada). The 0.2 mM C5Pe solution was sonicated for 30 mins, left for more than 24 hours and filtered using a 0.2 μm filter before use. Ultrahigh purity KCl (> 99.999%, Aldrich, Canada) was used as the supporting electrolyte while agent grade CaCl_2 (99.9965%, Fisher, Canada) was used as the source of calcium ions. De-ionized water with a resistivity of 18.2 $\text{M}\Omega\cdot\text{m}$, prepared with an Elix 5 followed by a Millipore-UV plus ultra water purification system (Millipore Inc., Canada) was used anywhere the experiments need. HPLC grade heptane (>99.99%, Fisher scientific, Canada) was used as an injection solution in the organic experiments part. Original mica was purchased from S & J Trading (USA), and was cleaved into ~ 2 μm , step-free film and silvered before gluing on the substrate. All the other chemicals are from Fisher Scientific and used as received unless specified.

4.2 Surface forces apparatus (SFA) technique

A SFA (SurForce LLC, Santa Barbara, CA, USA) was used to measure the interaction forces between C5Pe. The working principle, setup and other related features are introduced in detail below.

4.2.1 Multiple beam interference (MBI)

In the case of a basic reflectance and transmittance, if assuming no absorption, as the case shown in the Figure 4.1, the reflected and transmitted light could be calculated in Equation 4-1 & 4-2, respectively. (CHAPTER 7, Optics 505, James C. Wyant)

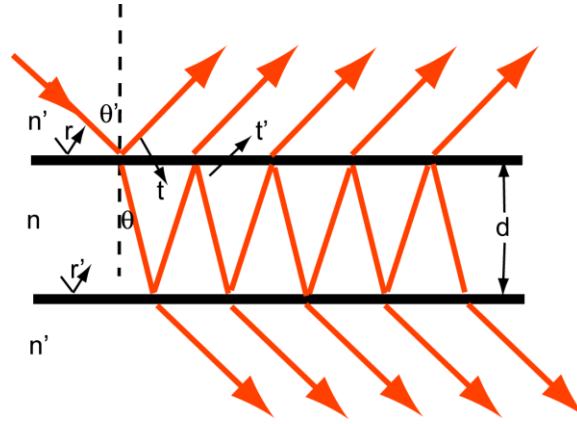


Figure 4.1 A basic light reflectance and transmittance.

$$E_r = E_i(r + tt'r'e^{i\delta} + \dots + tt'r'^{(2p-3)}e^{i(p-1)\delta}) \quad (4-1)$$

$$E_t = E_it't'(1 + r'^e e^{i\delta} + r'^4 e^{i2\delta} + \dots + r'^{2(p-1)} e^{i(p-1)\delta}) \quad (4-2)$$

where E_i , E_r and E_t represent the incident light, reflected light and transmitted light respectively; r (r') and t (t') are the reflected index and transmitted index from the material A to material B (from material B to material A) respectively; δ is the phase due to optical path difference and defined as $\delta = \frac{2\pi}{\lambda_o} 2nd \cos \theta$, p is transmitted times.

If there is no loss in the light propagation, the wave must be reversible, which means $tt' + r^2 = 1$; $tr' + rt = 0$; $tt' = 1 - r^2$ and $r = -r'$. The total transmitted light and reflected light is the incident light, so $R' + T' = 1$. Therefore, we can get $tt' = T'$ and $R' = r^2 = r'^2$. If substituting $r = -r'$ and let $p \rightarrow \infty$ in Equation 4-1,

$$E_r = E_i \left(\frac{\sqrt{r}(1-e^{i\delta})}{1-Re^{i\delta}} \right) \quad (4-3)$$

$$\frac{I_r}{I_i} = \frac{4R \sin^2(\delta/2)}{(1-R)^2 + 4R \sin^2(\delta/2)} \quad (4-4)$$

In the same way,

$$\frac{I_t}{I_i} = \frac{T^2}{(1-R')^2 + 4R \sin^2(\delta/2)} \quad (4-5)$$

Equation 4-4 and 4-5 are known as Airy's formula. Define F as the coefficient of finesse, given by $F = \frac{4R'}{(1-R')^2}$, and then $\frac{I_r}{I_i} = \frac{F \sin^2(\delta/2)}{1 + F \sin^2(\delta/2)}$ and $\frac{I_t}{I_i} = \frac{1}{1 + F \sin^2(\delta/2)}$.

This again shows that the reflected and transmitted lights are complementary. The transmitted light does go to zero for all values of R but goes to 1 only in the limit $R' \rightarrow 1$ and transmitted light goes to 1 for all values of R but goes to zero when $R' \rightarrow 1$. So as $R' \rightarrow 1$, the transmitted light becomes narrow bright fringes on a dark background, and reflected light becomes narrow dark fringes on a bright background. The transmitted and reflectance fringes at different transmission and reflective index are shown in Figure 4.2.

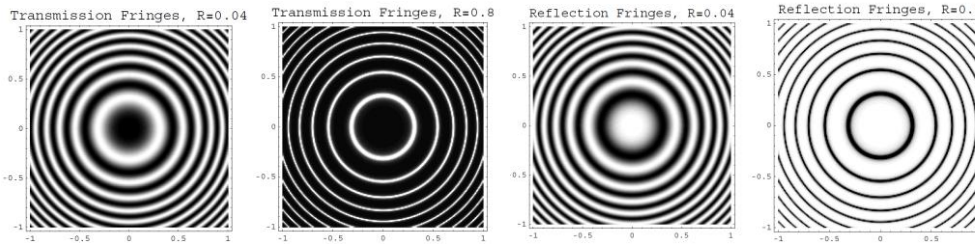


Figure 4.2 Transmission and reflection fringes at different transmission or reflection index.

4.2.2 Film thickness studies using MBI

In the last section, the concern of MBI is discussed. If the incident light is a white light, the MBI fringes will be colourful. In this section, a multiple beam interferometer (Figure 4.3) is combined with a spectrometer to get Fringes of Equal Chromatic Order (FECO), which was used to measure the film thickness. The FECO fringes have been studied extensively by Tolansky⁵¹. We have already

know that $\frac{I_t}{I_i} = \frac{1}{1+F \sin^2(\delta/2)}$, where $\delta = \frac{2\pi}{\lambda_0} 2nd \cos \theta + 2\phi$, and ϕ is the phase change on reflection at each surface.

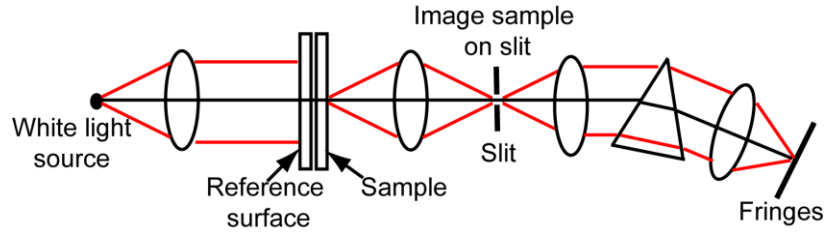


Figure 4.3 A schematic diagram of a FECO interferometer.

If $n = 0$ and $\theta = 0$ for a bright fringe of order n , $\frac{\phi}{\pi} + 2 \frac{d}{\lambda} = n$, where $\frac{d}{\lambda}$ is a constant and $\lambda_n = \frac{2d}{n - \frac{\phi}{\pi}}$. With many coatings, ϕ could be considered independent of λ over a small spectral region used for the analysis (Born & Wolf or Jean Bennett, JOSA 54, P. 612 (1964)). If $\lambda_n = \frac{2d}{n - \frac{\phi}{\pi}}$ is written as $d = (n - \frac{\phi}{\pi}) \frac{\lambda}{2}$, $d_2 - d_1 = (n - \frac{\phi}{\pi}) (\frac{\lambda_{2,n} - \lambda_{1,n}}{2})$ we can see an example shown in Figure 4.4

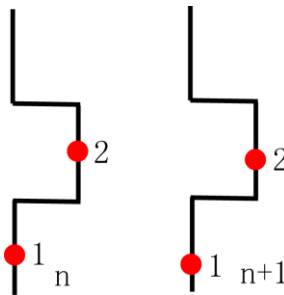


Figure 4.4 An example of thickness difference calculation.

For point 1 and fringe orders n and $n + 1$, $(n - \frac{\phi}{\pi}) \lambda_{1,m} = (n + 1 - \frac{\phi}{\pi}) \lambda_{1,m+1}$, so $(n - \frac{\phi}{\pi}) = \frac{\lambda_{1,n+1}}{\lambda_{1,n} - \lambda_{1,n+1}}$ and $d_2 - d_1 = \frac{\lambda_{1,n+1}}{\lambda_{1,n} - \lambda_{1,n+1}} (\frac{\lambda_{2,n} - \lambda_{1,n}}{2})$. From this equation, we know that we can measure the thickness difference of point 1 and 2 by measuring

their wavelength. This is the basic principle of how we measure the film thickness in SFA.

4.2.3 Force measurement

In SFA 2000, there are two discs loading in the SFA chamber during the measurement, with the upper disc connected to a piezoelectric motor, and the lower disc suspended at the end of a steel cantilever leaf spring with the stiffness of K_s . There are four main controls between the surfaces (Figure 4.5): the coarse and medium control micrometer-driven rod can move up and down in an accuracy of about one micrometer by use of a differential micrometer. The fine control micrometer-driven is moved similarly by a two-way stepping synchronous motor and operate in a different mechanism: the double cantilever steel spring is about thousand times stiffer than the helical spring, so one micrometer movement in the motor driven rod induces only one nanometer movement between the two mica surface. Finally, a piezoelectric crystal tube is connected to the upper disc which expands or contracts longitudinally by ~ 0.7 nm/V. This nonmechanical fine control is used to position the two surfaces in an accuracy of less than 0.1 nm. A voltage ramp generator connected to the piezoelectric tube could offset any purely thermal or mechanical drifts of the two surfaces in a short time during which delicate measurements could be made.

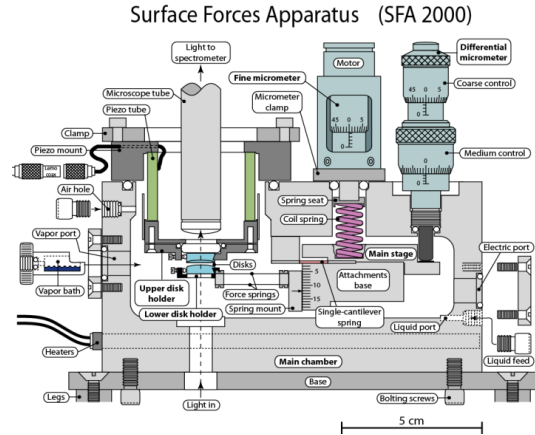


Figure 4.5 The sectional view of SFA 2000.¹⁰⁰

The separation of the two mica surfaces could be measured down to 0.1 nm by the use of MBI as described in the last two sections. During an experiment, the movement of the fringes is continually monitored in a spectrometer and the fringes are used to measure the separation distance between the two surfaces. The refractive index of the liquid medium, the shape and radii of the surfaces and any surface deformation could also be measured¹⁰¹⁻¹⁰³. In a force distance measurement, the separation distance is controlled by suddenly reversing the voltage of the piezoelectric tube, which will drive the upper disc move up or down. The resulting change in the separation between the two discs is measured optically MBI, and then multiplied by the spring stiffness K_s , which gives the force difference, attractive or repulsive, between the initial and final separations. This method could be comprehended with a theoretical basis shown in Figure 2.6. We choose a position on top of the lower surface, where the two surfaces are far away so there is no interaction between them, to be position $x = 0$, and the position of the upper surface is defined as $x = \infty$ so we know that there is a large distance between the two surfaces. As the upper surface moves downwards to the position $x = D_o$, the lower surface also moves downwards to $x = -(D - D_o)$ due to the forces between the two surfaces. In this case the head of the spring moves in a distance $(D - D_o)$. At this time, the separation between the two surface is D , which means at any distance D , the interactions between the two surfaces are balanced

by the restoring force of the spring $F(D) = K (D - D_o)$. When $F(D) > 0$, the force is repulsive. Let's consider another situation when the piezoelectric tube expands by a distance ΔD_o , so that the position of the upper disc is $(D_o - \Delta D_o)$. This leads to a new equilibrium separation at $(D - \Delta D)$. Then we can get the restoring force $F(D - \Delta D) = K (D - \Delta D - D_o + \Delta D_o) = K (\Delta D_o - \Delta D) + F(D)$. This equation shows that if the piezoelectric tube expand by an amount of ΔD_o and causes the separation between the two surfaces changing by ΔD , the force difference between the initial position $F(D)$ and the final position $F(D - \Delta D)$ is $K(\Delta D_o - \Delta D)$. So if $\Delta D_o = \Delta D$, there is no force difference between the initial and final state. Therefore, in order to measure the force $F(D)$ between the two surfaces using the optical technique, the required parameters are:

- 1) the spring stiffness K_s , which could be calibrated within 1% after each experiment by placing small weights at the place where mica surfaces were touching and measuring the deflection by a microscope.
- 2) The distance the piezoelectric crystal expands or contracts, i.e. ΔD_o , when the voltage is applied. This is measured at large separation distance when no forces are detected.

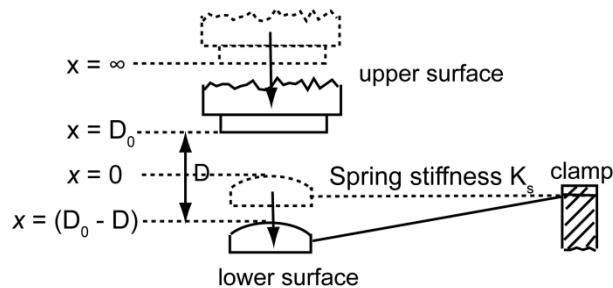


Figure 4.6 Configuration of the two discs loaded in SFA chamber. ⁹⁹

For example, the spring stiffness used in the SFA measurement is 10^2 N/m, and the initial separation between the two surfaces is 100 nm, where there is no separation detected. If the piezoelectric tube expands by 20 nm, and the distance between the two surfaces is 80 nm, there is no interaction between the two

surfaces. But if the distance between the two surfaces at equilibrium is 79 nm, there is an attractive force $F = K_s (\Delta D_o - \Delta D) = 10^2 \times (20 - 21) \times 10^{-9} = 1 \times 10^{-7}$ N.

4.2.4 Other unique functions of SFA 2000

The advantage of SFA 2000 comparing to the old versions is that it has many other functionalities other than measuring the normal forces between the two surfaces. Here a few of its functions are list here:

1) Measuring shear (friction and lubrication) forces: in SFA 2000, the surfaces can be sheared passing each other by using a piezoelectric bimorph slider or a motor-driven micrometer to move the upper surface in a lateral direction (Figure 4.7). In the use of friction device or bimorph seder, two vertical double-cantilever springs and four semiconductors or resistance strain gauges are attached symmetrically to bending arms of the springs. The detailed operation of the shearing force measurement could be found elsewhere¹⁰⁰.

2) Measuring forces in three orthogonal directions (3D or XYZ attachments): The SFA 2000 contains a variety of XYZ translation stages and detectors for generating relative movement of surfaces, and measuring the resulting forces independently in three directions X, Y, Z. Measuring the adhesion, friction and molecular ordering in three dimensions is also possible by moving one of the surfaces in some arbitrary direction in the X-Y plane or the upper surface in the Z direction. In this way, some circular or other type of non-linear motion can be induced. The force corresponding to the upper surface along any spatial direction can also be simultaneously measured.

3) High speed attachment: a rotating high-speed disk is also included in the SFA 2000. It provides much longer range and higher sliding speed than other friction devices. This device requires sophisticated position and adjustment system for the rotating disk consisting of numerous springs and weights. Using this method, reflection FECO appears as dark bands on a bright background. The multi-matrix method could convert the wavelengths to separation distance¹⁰⁴⁻¹⁰⁵.

4) 3D displacement and force sensing probe attachment: A 3D displacement and force sensing attachment is designed to measure forces in any spatial directions suitable for SFA. This attachment enables SFA to scan and measure forces on a probe tip in three orthogonal directions, linearly and simultaneously¹⁰⁶.

There are many other attachments to enable SFA 2000 of different functionalities. For example, a bimorph vibrator attachment allows the top surface to be vibrated vertically using the piezo tube while measuring the amplitude and phase of the vibration induced in the lower surface; the constant-force attachment can be used to measure the weak forces which take long time to reach equilibrium and also the drive surfaces together at constant force; and the variable normal force-measuring springs enable SFA to deal with experiments with different scales and purposes. In conclusion, the SFA technique has been developed more maturely to be used for various purposes. What needs to be mention here is that by incorporation with other techniques, such as x-ray scattering¹⁰⁷, IR spectroscopy, Fluorescence microscopy¹⁰⁸ and AFM¹⁰⁶, SFA could carry out different measurements on the same sample at the same time.

4.2.5 C5Pe film preparation

The C5Pe films were prepared by a drop coating method (Figure 4.7). Several drops of C5Pe solution were dropped on a thin mica sheet which is glued on a cylindrical disk with radius of $R = 2$ cm. The film was allowed to deposit for 10 mins in a sealed chamber with saturated toluene vapour and then washed by pure toluene before loading into the SFA chamber. The C5Pe coated mica was used for force measurements by SFA and topography imaging by AFM.

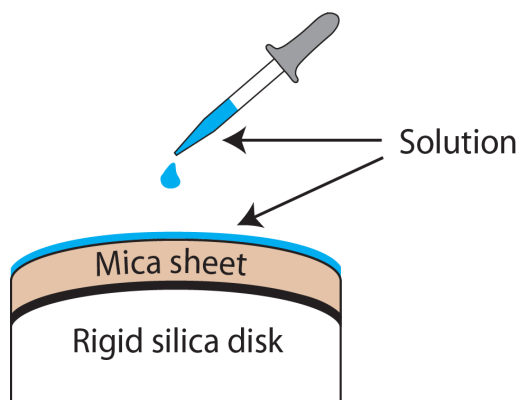


Figure 4.7 Schematic of drop-coating method.

4.2.6 Operation procedure

The schematic of a typical SFA setup is shown in Figure 4.8. Before carrying out the force measurement, the most important part is to get a good thin mica surface. The thin mica sheet is first cleaved from a thick mica plate. Cleavage is initiated by inserting a sharp tweeze into the edge of the plate and carefully peeling away a thin sheet. The freshly cleaved thin sheet is examined in the light of an ordinary light to check if it is sufficiently thin, in which case the interference colors are seen reflected by the surface. The reflected color change abruptly at the steps but remain uniform over the regions of constant thickness. If a large step-free region is found, it may be cut out with a hot platinum wire heated above the melting point of mica by passing a current through it. The mica is then immediately transferred to a large thick sheet of freshly cleaved mica (called the backing sheet), molecular contact should take place at once except at the edges, which was damaged by the melting. It is essential that all the operations be carried out in a dust free cabinet to prevent dust and mica flakes from settling on the fresh surface. When the backing sheet has enough cleaved mica sitting on it, the exposed surfaces of the thin mica are silvered in an evaporator at a pressure of $10^{-5} - 10^{-6}$ mm Hg, to get a uniform silver layer of about 0.5 nm thick. In the experiment, the thin piece of step-free mica sheet (1-5 μm) was glued on a cylindrical silica disk ($R = 2$ cm) with the silvered side down and coated with a layer of C5Pe film. The

two prepared disks were then mounted into the SFA chamber in a cross-cylinder geometry, which roughly corresponds to a sphere of radius R approaching a flat surface locally when the separation of the two surfaces is much smaller than the radius R . The absolute distance of the two surfaces D was monitored in real time and *in situ* by an optical technique called multiple beam interferometry (MBI) using interference fringes of equal chromatic order (FECO) with a distance resolution down to 0.1-0.2 nm. The in-situ force $F(D)$ was then determined as a function of the separation D based on the deflection of the supporting spring. The measured force $F(D)$ can be converted into energy per unit area between two flat surface $W(D)$ by the Derjaguin approximation: $F(D) = 2\pi RW(D)$. When $\partial F(D)/\partial D$ is greater than the spring stiffness, there is a mechanical instability that causes the lower surface to jump either towards or away from the upper surface during approaching or separation process, respectively.

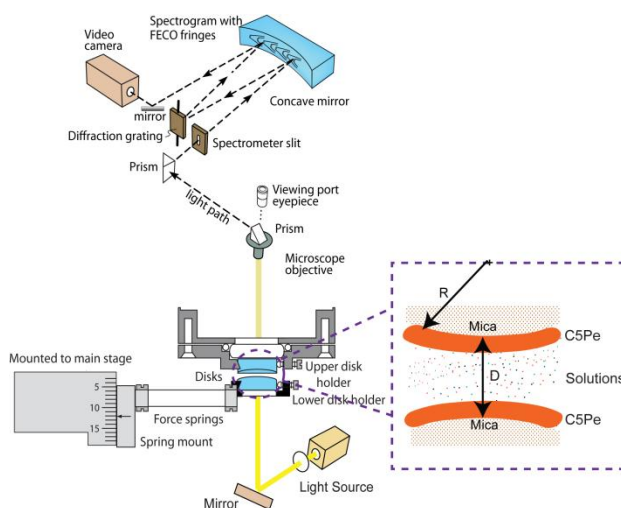


Figure 4.8 Schematic of experimental setup for measuring the molecular interactions of asphaltene model compound C5Pe. (a) SFA experimental setup for measuring the normal forces and (b) a typical experimental configuration used in this thesis.

The two bare mica surfaces are brought into contact first and the fringes were recorded as the reference for the distance calculation. In the objective experiment,

the moving fringes is recorded with defined software and analyzed by MATLAB with a special coded program to get the information of the wavelength. The FECO fringes of two bare mica surfaces and mica surfaces with film coated are shown in Figure 4.9. From the wavelength move ($\Delta\lambda_n, \Delta\lambda_{n-1}$), the distance could be calculated.

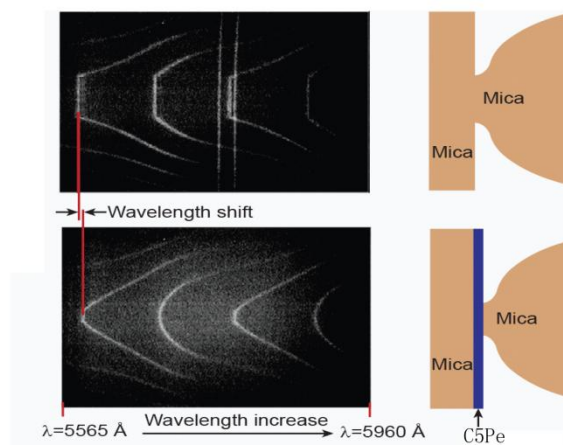


Figure 4.9 FECO fringes of two bare mica surfaces in contact and in separation.

4.2.7 Experiment configurations

To comprehensively understand the interaction force, the interactions of C5Pe in both aqueous solutions and organic solvents are studied in this thesis. The geometry of the two surfaces in the experiments is shown in Figure 4.10 and 4.11, with Figure 4.10 showing the geometry of the experiments in organic solvents and Figure 4.11 showing the geometry of the experiments in aqueous solutions.

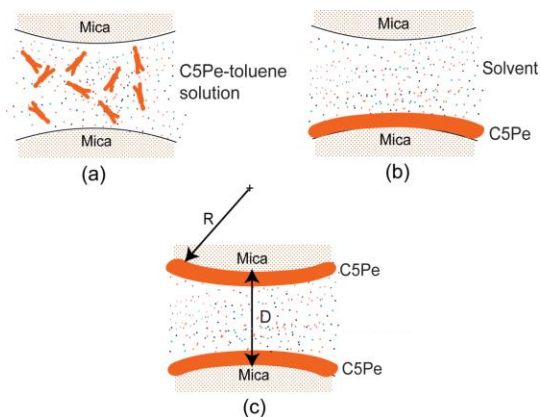


Figure 4.10 Geometry of the experiments in organic solvents. (a) adsorption of C5Pe in toluene; (b) asymmetric experiment with only one side coated with C5Pe; (c) symmetric experiments with both mica surfaces coated with C5Pe.

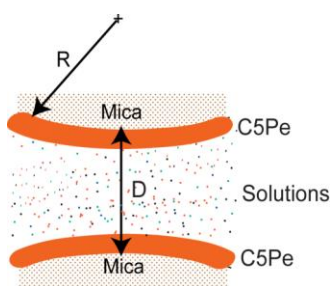


Figure 4.11 Geometry of the experiments in aqueous solutions.

1) Organic solvents

The interactions of C5Pe in toluene and heptane are studied in this thesis. In the symmetric experiments, both the upper and lower mica surfaces are coated with C5Pe films and loaded into the SFA chamber. The organic solvents were injected in the gap between the two surfaces and trapped when the two surfaces approach. When toluene was injected in between, the chamber was sealed and filled with toluene vapour so that the toluene solvent in the gap will not evaporate. The same experiment was carried out for the heptane solvent because toluene and heptane were expected to have huge difference in determining the behaviour of C5Pe. The adsorption of C5Pe in toluene was carried out with two different concentrations.

In the experiment, the saturated (~0.2 mM) or the ten times diluted C5Pe in toluene solution was injected between two bare mica surfaces. The adsorption behaviour with time was studied with time up to 20 hrs.

2) Aqueous solutions

The interaction of C5Pe in aqueous solutions is of great importance in understanding its interfacial behaviour. KCl solutions was chosen as the simple electrolyte because KCl has less dangerous in the metal corrosion at high concentration. The effect of solution pH was carried out at a constant KCl concentration of 1 mM. For the effect of Ca^{2+} , a mixture solution of KCl and CaCl_2 was tuned at different Ca^{2+} concentration but same K^+ concentration, and injected between the two C5Pe surfaces.

4.3 Langmuir trough and LB film deposition

4.3.1 Principles of Langmuir trough and LB film deposition

The principle of surface pressure – area isotherm is actually very easy. It is based on the force balance of a Whihelmy plate at the interface of liquid – air or liquid – liquid. The schematic view of the Langmuir technique is shown in Figure 4.12. According to the force balance theory, all the forces applied on the Whihelmy plate should be balanced in all directions. Assuming the angle between the Whihelmy plate and interface is α , the forces is balanced in X direction due to the symmetric alignment on both contacting side. In the +Y direction, there are pulling force applied by a spring based on which the force is calculated, and the buoyant force applied by subphase (and tophase). In the –Y direction, the self weight of the Wilhelmy plate and surface tension force are summed together to balance the up towards forces. So the detected force, which is force applied by the measured system, could be expressed in this way: [force applied on the Wilhelmy plate] = [weight of the Wilhelmy plate] + [surface tension force] – [buoyant force], i.e.

$$F_A = m_W g + 2 (t_p + w_p) \gamma \cos\alpha - \rho_l V_p g, \quad (4-5)$$

Where F_A is the forces applied by the measured system; m_W is the mass of the Wilhelmy plate; t_p and w_p are the thickness and width of the plate respectively; γ is the surface tension of the liquid (liquid – air system) or interface (liquid – liquid system); ρ_l is the density of the liquid; V_p is the volume of the proportion of plate immersed in liquid. However, the weight of the plate can be determined beforehand and set to zero on the electrobalance, and the effect of the buoyancy can be removed by extrapolating the force back to zero depth of immersion. Thus, the only remaining component of the force is the surface tension force. Therefore, $F_A = 2 (t_p + w_p) \gamma \cos\alpha$. If assuming a perfect wetting of the plate occurs ($\alpha = 0$), the surface tension could be calculated as $\gamma = F_A / 2 (t_p + w_p)$.¹⁰⁹ When a surfactant (or other surface active chemicals) is added to form a surface layer or interfacial layer, the surface tension will change, and the change is defined as π , i.e. $\pi = \gamma_o - \gamma$, where π is the surface pressure; γ is the surface tension of subphase with surface (interfacial layer) layer and γ_o is the surface tension of pure subphase. In the measurement, the surface pressure against the compression area was measured to study the interfacial properties of a surfactant.

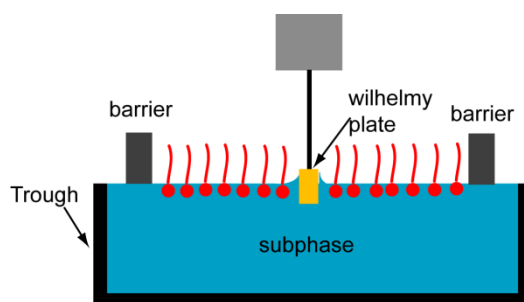


Figure 4.12 Schematic view of Langmuir technique.

The Langmuir technique can be combined with a dipper arm to deposit a film on to a solid substrate (silicon in this thesis), which is referred to LB deposition (Figure 4.13). The deposition could be successful due to the unique properties of surfactants, which can stay at the surface or the interface orderly with their

hydrophilic group extending into air or the oil phase, and hydrophilic group extending in the aqueous phase. The substrate is dipped into the subphase before spreading a layer to make sure of an intact layer. In this way, a monolayer or multilayer is possible to be obtained. To get a multilayer, the substrate only needs to be dipped several times, in which case the process is controlled to automatically carry out.

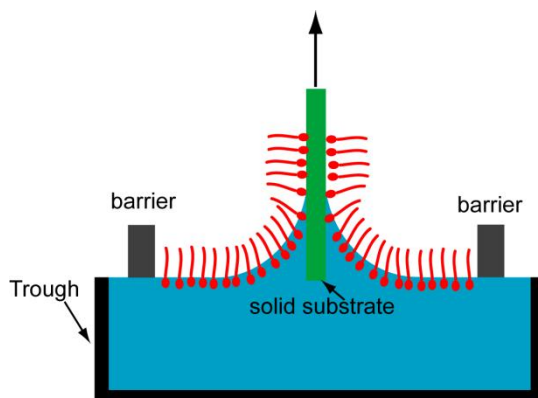


Figure 4.13 Deposition of a monolayer onto a substrate.

4.3.2 Technique of Langmuir trough and LB film deposition

A KSV Langmuir interfacial minitrough (KSV Instruments, Finland) is used in this thesis. The interfacial trough has an area of 17,010 mm². The trough and two symmetric barriers are made of Derlin. The trough has two compartments: a lower compartment for a heavier phase and an upper compartment for a lighter phase. There are several holes in the two barriers, which enable the lighter phase to flow freely during compressing. The trough is cleaned by rinsing with Acetone, ethanol, HPLC grade toluene and wiped with acetone-soaked Texwipe prior to each run. The subphase is further cleaned by removing its surface layer with a pipet connected to a vacuum system until the surface pressure is smaller than 0.5 mN/m upon full compression.

To study the C5Pe layer characteristics, a 50 μ L C5Pe in toluene solution (0.2 mM) was spread dropwise at the air-water interface by a Hamilton precision

microsyringe. In this process, the Langmuir trough was cleaned with the procedure stated above and 100 mL ultrapure clean water at its natural pH (~5.6) was used as the subphase. 50 μL C5Pe in toluene solution was poured dropwise on the water surface and 10 mins was allowed for the incubation before 100 mL optima toluene (topphase) was poured over the aqueous phase. The system was left 30 mins for equilibrium before compression was carried out at a speed of 5 mm/min. The compression cycle was conducted for 3 times continuously in sequence to study the reversibility of C5Pe aggregate. The surface pressure is constantly monitored with a Wilhelmy plate and plotted as a function of the trough area. If the molecular weight of the surfactant is known, the mean molecular area is usually used as the x-axis. A typical surface pressure (SP) – area isotherm is shown in Figure 4.14. This isotherm includes all the phase and phase transition, such as gaseous phase when the surfactants are far away from each other; liquid phase when the surface pressure increases and solid phase when no more compression is possible. Depending on the compressibility of the film, the layer can behave as liquid expanded or a liquid condensed state sometimes.

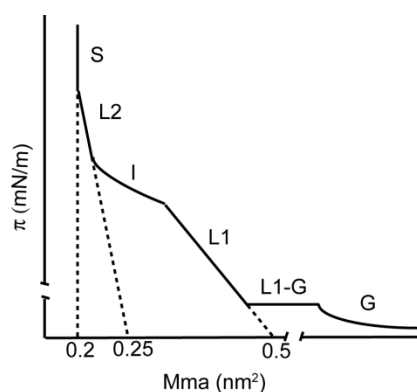


Figure 4.14 A SP - area isotherm including different phase and phase transitions.¹¹⁰

To prepare a monolayer of C5Pe at toluene – water interface, the LB deposition method was used. A clean silicon substrate (see next section for clean procedure) was vertically dipped in the aqueous phase before spreading the C5Pe film. The

left procedures are similar to LB isotherm except for the compression. For the LB deposition, the film is deposited at a constant surface pressure. So a compression to reach the target surface pressure is required before the deposition starts. The speed and cycle number was set before the experiment started. In this thesis, a monolayer is needed, so only a one way deposition was carried out.

4.3.3 Silicon wafer cleaning (Piranha cleaning)

Silicon wafer is usually cleaned with Piranha solution, which is a mixture of sulphuric acid and hydrogen peroxide. In this thesis, a volume ration of 1:1 96% H_2SO_4 and 30% H_2O_2 was used as the piranha solution. For the cleaning process, there is a standard operation procedure which could be found from Prof. Robert White's posting online¹¹¹. To be brief, the silicon samples were left in an empty beaker before pouring H_2O_2 and H_2SO_4 in sequence. The solution will heat up and start to bubble. Wait until the bubbling stopped, which usually takes one day, and transfer the samples to a clean beaker. The samples were rinsed with ultrapure water 10 – 20 times and stored in ultrapure water prior to each use. The cleaned samples need to be used in 48 hours in case it will get dirty again after a long time.

4.4 Atomic force microscope (AFM) imaging

In 1981, the first scanning tunnelling microscope (STM) was developed at IBM Zurich by Gerd Binnig and Heinrich Rohrer. STM is capable of imaging conductors at the Angstrom resolution. Their contribution was recognized with a Nobel Prize for physics in 1986 and in the same year they reported a kin – AFM device, which can be used to image the surfaces of both conductor and non-conductor materials.

4.4.1 Fundamental principle of AFM imaging

A thorough discussion of AFM is given in a monograph by D. Sarid¹¹². To be brief, the fundamental of AFM imaging could be understood in the way described below. In AFM, the elastic deformation of the spring caused by the force between

the tip and surface is monitored. The displacement can be measured by well-developed devices such as a laser beam down to the resolution of $10^{-4} - 10^{-6}$ angstroms. This level of sensitivity certainly is able to capture the topography of surface. A typical AFM consists mainly of a piezo scanner, a cantilever substrate with for cantilevers, a split photodiode and a laser source. A piezo scanner is used to scan and position the sample fixed on a sample substrate, relative to the tip on a cantilever spring at a nanometer resolution in three dimensions. The force between the sample and tip causes the cantilever to move up and down, and the deflection of the cantilever is detected with a position sensitive laser beam that is focused on the upper surface of the cantilever spring above the tip position and reflected to the split photodiodes through a mirror. A relation between the cantilever deflection and sample position could be obtained via a computer data acquisition system by employing various feedback options. In the AFM imaging, the force is kept at a small constant value. When the tip scans the surface, it will follow the surface contours to keep the force between the tip and the surface at a constant value. There are two modes of AFM imaging: contact mode and tapping mode. In the contact mode, the tip contacts the sample, so it is more suitable to image the hard material. In the tapping mode, the cantilever oscillates at its resonant frequency, and excited by a piezo stack. When the cantilever oscillates vertically, the laser beam is deflected in a regular pattern over a photodiode array, generating a sinusoidal electric signal. In the process of the imaging, the piezo stack keeps exciting the cantilever substrate with a constant energy and the tip is deflected in its encounter with the surface. The deflected beam reveals the information about the sample surface character. In the tapping mode, the tip does not contact the sample, so it could be used to image the soft materials. C5Pe is a soft polymer, so tapping mode is used in this thesis to do the imaging.

4.4.2 AFM imaging

Morphology of C5Pe layer coated on mica was characterized by an Agilent 5500 AFM (Agilent Technologies, Inc., Chandler, AZ) operated under acoustic AC

mode in air. Silica cantilevers (RTESP, Veeco, Santa Barbara, CA) with a nominal resonance frequency of 200-400 kHz were used for imaging. During the imaging, the amplitude setpoint (A_s) was set at a value of 98% of the free amplitude (A_0). At this ratio of A_s/A_0 , the tapping force between the cantilever tip and the sample surface is small enough to avoid damaging the sample. The AFM image of the LB deposited C5Pe film is also characterized in the tapping mode. The resonance frequencies of a silicon cantilever were obtained by “auto tuning” in the AFM software. Integral and proportional gains were set according to the imaging surface. A scan rate of 1Hz or 0.5 Hz was used for the imaging.

4.5 Other techniques

4.5.1 Contact angle measurement

To study the hydrophilicity (hydrophobicity) of the C5Pe surfaces (drop-coated surfaces, surfaces immersed in toluene, heptane and aqueous solutions) are measured with a Krüss drop shape analysis system (DSA 10-MK2). A sessile drop of ultra pure water was placed on the film and the contact angle was measured immediately through the water phase.

4.5.2 Ellipsometer

C5Pe film was deposited on clean silicon water by means of drop-coating method. The film preparation is the same with film preparation on mica. The thickness of the dried C5Pe film was measured using a Gaertner multiangle Ellipsometer, assuming negligible absorption at the wavelength of the incident laser (633 nm). The reflective index was assumed to be 1.6964. Multiple samples deposited in the same way with at least six positions on each sample were measured for the thickness. The accuracy of thickness measurement by the ellipsometer used is $\pm 0.1\text{nm}$.

CHAPTER 5 INTERACTIONS OF C5Pe IN ORGANIC SOLVENTS

Studies on the molecular interaction mechanisms of asphaltenes in organic solvent have not reached a widely accepted conclusion, mainly due to poor definition of asphaltene molecules and lack of accurate information on molecular structure. In this study C5Pe of polyaromatic core with proper molecular weight and hetero atoms in its structure was used as a model compound of asphaltenes in an attempt to understand interaction mechanisms of molecular aggregation in organic solvents. A surface forces apparatus (SFA) was used to directly measure the molecular interactions of C5Pe in toluene and heptane. For the interactions between two model clay (mica) surfaces across a C5Pe-in-toluene solution, the repulsion observed between the adsorbed C5Pe molecules was shown to be of a steric origin. The force-distance profiles at short separation distances under high compression force during approaching were well fitted with the Alexander-de Gennes (AdG) scaling theory while the weaker repulsive forces at lower compression force regime over longer separation distances can be also fitted with the AdG model using an independent set of fitting parameters, indicating the presence of possible secondary brush structures of the C5Pe molecules in toluene. For interactions of casted C5Pe films (C5Pe vs. mica, and C5Pe vs. C5Pe), no significant adhesion was detected in toluene while strong adhesion was measured in heptane. The comparison of the results obtained with the model compound C5Pe and native asphaltenes shows that C5Pe behaves quantitatively different from the real asphaltenes in the context of contact angle and interaction force profiles. However, there are qualitative similarities in terms of intermolecular forces, indicating that the polar components in real asphaltene molecules play an important role in determining their interfacial activities.

5.1 Introduction

It is commonly believed that asphaltenes play a critical role in stabilizing the W/O emulsions in crude oil processing or bitumen production.^{2-4,113} However, as stated previously, the exact composition, structure of the subfractions of asphaltenes and

active components and the mechanism of asphaltene behaviour still remain unclear and under investigation. Several factors have been considered to determine the removal efficiency of emulsified water from W/O emulsions, including the size of emulsified water droplets, viscosity of continuous oil phase¹¹⁴, density difference between the oil and aqueous phases¹¹⁵, solids content at oil-water interfaces¹¹⁶⁻¹¹⁷ and energy input¹¹⁸⁻¹²⁰. To avoid the probably last-for-ever issue, several asphaltene model compounds were synthesized and the surface/interfacial properties and film properties were investigated. And the results demonstrate that model compounds resemble the surface active behaviour of asphaltenes and that only the fraction with hydrophilic polar groups are responsible for stabilizing W/O emulsion, concordant with the recent study revealing that only a small fraction of asphaltenes is responsible for the formation of interfacial films.

The objective of this study is to investigate the similarity and disparity between an asphaltene model compound C5Pe and real asphaltene molecules in the context of interaction force profiles, molecular aggregation/adsorption at mica-solvent interfaces. The chemical structure of C5Pe is shown in Figure 1.1. It consists of four aromatic rings fused together with three cyclic rings containing heteroatoms of O and N. A pentyl carboxylic acid is attached to one end of the fused rings through the nitrogen atom, while a hexyl-heptyl double chain is connected to the other end of the fused rings, also through the other nitrogen atom. The molecular weight (689 Da.) of C5Pe is within the molecular weight range of asphaltenes. The adsorption mechanism of C5Pe to clay surface (mica) and interactions between two C5Pe films in both toluene and heptane were measured using a surface forces apparatus (SFA). The results obtained with C5Pe were compared with that obtained under similar experimental conditions using asphaltenes extracted from Athabasca bitumen (Alberta, Canada). The information obtained from asphaltene model compounds system is of great importance for elucidating the mechanism of asphaltene-caused problems in petroleum industry, confirming that studying on model systems with well-defined molecular structures rather than

real complex systems is a viable approach for understanding the molecular mechanism of asphaltene aggregation in heavy oil processing.

5.2 Characterization of C5Pe film

5.2.1 AFM imaging

The AFM images of a bare mica surface and an adsorbed C5Pe film are shown in Figure 5.1. As expected, freshly cleaved mica was a flat, featureless surface with a root-mean-square (RMS) roughness of 0.2 nm (Figure 5.1a). The deposited C5Pe film on mica in Figure 5.1b appeared to be not uniform, with elongated holes distributed evenly across the film plane, which had a RMS roughness of ~0.3 nm. Previous studies have shown that a layer of asphaltene film strongly attached to hydrophilic substrates (e.g., mica or silica) even after rinsing with toluene.^{71,95} Considering the adsorbed film of C5Pe on mica being thoroughly washed with toluene, the results here indicate a similar binding of C5Pe as asphaltenes to mica. Both AFM images (Figure 5.1b) and SFA measurement (discussed later) confirmed the successful deposition of a layer of C5Pe on mica by the adsorption method.

To further test the film stability, the deposited C5Pe film on mica was soaked in fresh toluene for half an hour. The film was then dried and imaged by AFM in air. Unlike asphaltene films we studied recently⁷², there was no obvious conformational rearrangement or “molecular swelling” when C5Pe film was soaked in toluene for ~30 min, as shown by AFM image in Figure 5.1c. The AFM images before and after soaking in toluene showed similar surface features and roughness of ~0.3 nm. The film thickness measurement by ellipsometry showed a film thickness of 5.8 and 5.5 nm for unsoaked and soaked C5Pe films, respectively. The above results indicate that the C5Pe molecules could stay firmly on mica surface even after re-exposing to organic solvents such as toluene.

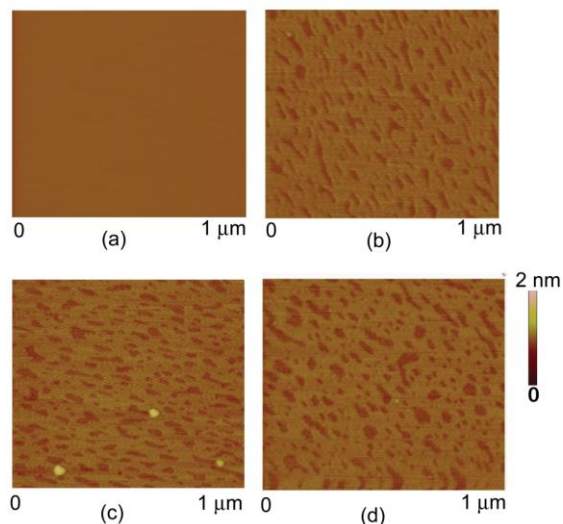


Figure 5.1 AFM images of (a) bare mica surface; (b) C5Pe adsorbed on mica surface; (c) C5Pe adsorbed on mica surface after immersion in toluene for 0.5 hour; (d) C5Pe adsorbed on mica surface after immersion in heptane for 0.5 hour.

5.2.2 Langmuir trough, LB film deposition and contact angle measurement

The contact angle of water on the deposited C5Pe surface was measured to be $35 \pm 3^\circ$. In comparison to the contact angle values above 80° of deposited asphaltene films²¹, the contact angle on C5Pe indicates that the C5Pe molecules were not uniformly adsorbed and packed as a highly ordered monolayer on mica with a substantial fraction of polar carboxylic terminal groups facing away from the mica to lead to much less hydrophobic film surfaces. Recent molecular dynamics simulations¹²¹ confirmed molecular stacking or aggregation of C5Pe in toluene at these concentrations. This configuration was also confirmed at the oil-water interface by means of the Langmuir-Blodgett (LB) technique. Figure 5.2a shows the typical interfacial pressure-area isotherms of C5Pe at toluene-water interfaces. For comparison an interfacial isotherm of asphaltene at toluene-water interface was also shown in the inset of Figure 5.2a. The results indicate that C5Pe did not form as stable films as asphaltenes at the water-toluene interface, as evidenced by

a low interfacial pressure of 22 mN/m in comparison to 30 mN/m for asphaltenes.⁵³

It is important to note that the interfacial pressure of the C5Pe film in the second compression became lower at the same mean area per C5Pe molecule than the first compression, while for asphaltenes there was very little hysteresis between the first two compressions, evidencing again C5Pe can not form stable films like asphaltenes. Interestingly, there was no hysteresis between the second and third interfacial isotherms of C5Pe. These results collectively indicate the formation of C5Pe aggregates during the first compression shown by a significant hysteresis between the first and second interfacial isotherms, and the molecular aggregation was irreversible as shown by a negligible hysteresis between the second and third isotherms obtained with a time interval of 3 hours. The aggregates were directly visualized by AFM on the LB-deposited C5Pe film as shown in Figure 5.2b. In this case, the C5Pe film was deposited by LB technique at a constant interfacial pressure of 5 mN/m with a pulling speed of 1 mm/min during the first compression. It is evident that C5Pe did not form a uniform monolayer at the toluene-water interface. Instead, small aggregates (domains) of ~50 nm diameter were seen to be evenly distributed throughout the film.

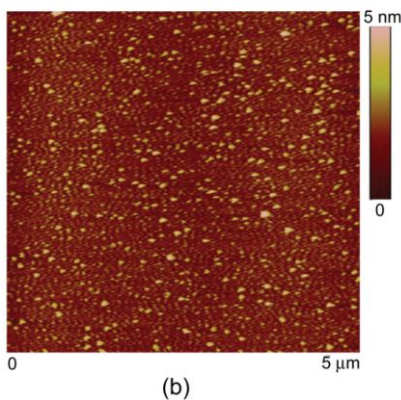
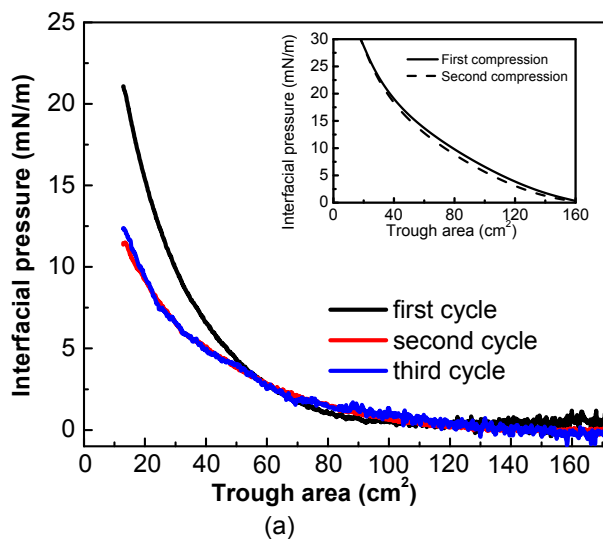


Figure 5.2 (a) Interfacial pressure-area isotherms of C5Pe film at toluene-water interface obtained with an interfacial Langmuir trough. The second cycle of the compression was carried out immediately after the first compression. The third cycle was carried out 3 hours after the second compression. Inset is the interfacial pressure-area isotherm of asphaltene film at toluene-water interface under similar experimental conditions from a previous work by Zhang et al.⁵³ for comparison. In this case the second compression was carried out right after the first compression. (b) AFM image of the C5Pe film deposited with LB method at an interfacial pressure of 5 mN/m with a pulling speed of 1 mm/min during the first cycle with a transfer ratio of 1.15.

5.3 Adsorption kinetics

5.3.1 High concentration adsorption

The 0.002 wt% and 0.02 wt% C5Pe in toluene solutions were injected between two closely placed mica surfaces in the SFA chamber saturated with toluene vapour to study the adsorption of C5Pe on a model clay surface (mica). For a typical force measurement, the normal force-distance (F vs. D) profile was obtained by an initial approach of two surfaces to a “hard wall” distance followed by separation of the two surfaces. Note that the “hard wall” distance in this study is defined as the mica-mica separation distance or thickness of confined C5Pe films, which shows a negligible change with increasing the normal load or pressure.¹²²⁻¹²³ The approach and separation force-distance profiles for two mica surfaces interacting in 0.02 wt% C5Pe in toluene solutions are shown in Figure 5.3. Figure 5.3a shows quite similar interaction force-distance profiles during the approaching of two mica surfaces in 0.02 wt% C5Pe solution for the first four hours of adsorption. The hard wall distances shift slightly from 15 to 19 nm, which translates to a thickness of C5Pe film adsorbed on each mica surface to be around 7.5-9.5 nm. This thickness value is slightly larger than the film thickness of 5.8 nm measured for adsorbed C5Pe films by ellipsometry, indicating a limited swelling or protrusion of the C5Pe molecules adsorbed. As the adsorption time increases to 20 hours, the hard wall distance shifts to ~38 nm, while the range of repulsive force during approaching also increases from ~5 to ~10 nm. The great shift of hard wall distance to 38 nm indicates a slow build-up of C5Pe on mica surfaces to form nanoaggregates. Interestingly, this hard wall distance translates to C5Pe layer thickness of 19 nm on each mica surfaces which is in excellent agreement with film thickness of 18.2 nm measured by ellipsometry on C5Pe films formed by adsorption on silicon wafer in C5Pe solution of the same concentration for overnight. The force-distance profiles during the separation processes in Figure 5.3b show weak adhesions ($F_{ad}/R \sim 1$ mN/m) for adsorption time below 4 hours. It is interesting to note that the adsorbed C5Pe layers were stretched for

about 3-4 nm before the two surfaces jumped apart, indicating a limited interdigitation of C5Pe molecules/aggregates from two interacting surfaces upon compression.

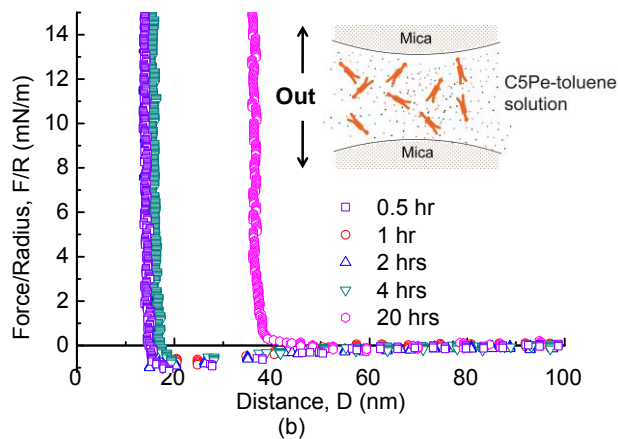
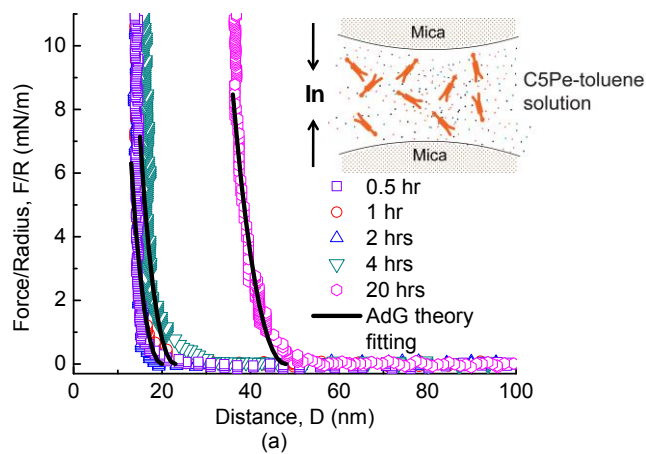


Figure 5.3 Force-distance profiles of two mica surfaces interacting in 0.02 wt% C5Pe-toluene solution at different time intervals: (a) approaching plots and fitting curves by Alexander-de Gennes (AdG) theory; (b) retracting plots following the approaching in (a).

5.3.2 Adhesion

Adhesion was detected during the separation processes for the first several hours adsorption as shown in Figure 5.3b. However, the adhesion disappeared after ~20 hours adsorption and only pure repulsive force was measured. It is suggested that the adhesion measured during the initial stage of adsorption was due to possible hydrogen bonding among the polar groups –COOH of C5Pe molecules as well as van der Waals interactions. The disappearance of the adhesion at longer adsorption times was attributed to the conformational rearrangement and aggregation of the C5Pe molecules, which was shown by AFM imaging in Figure 5.4 and increased contact angle from 35° to $53 \pm 5^\circ$.

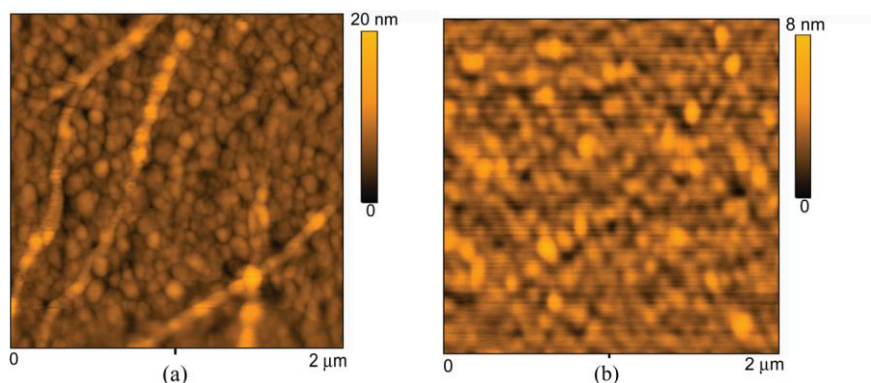


Figure 5.4 AFM images of C5Pe surfaces prepared by immersing the mica surface for 20 hours in a C5Pe-toluene solution of (a) 0.02 wt% and (b) 0.002 wt%.

5.3.3 Data fitting and nature of the surface forces

The repulsive forces during the approach of the two mica surfaces mainly came from the steric repulsive interactions between the adsorbed C5Pe molecules. The polyaromatic rings with aliphatic hydrocarbon chains of adsorbed C5Pe molecules/nano-aggregates tended to be extended in toluene and repel each other. The aggregation and adsorption of C5Pe molecules were found to be similar to asphaltenes. The Alexander-de Gennes (AdG) scaling theory^{79,95,124} for the steric

repulsion between two interacting brush layers is applied here to fit the force-distance profiles in Figure 5.3a.

The fitted values of L and s are summarized in Table 5.1. The good fitness of the measured force profiles with the AdG theory indicates that although C5Pe is not a polymer, the adsorbed C5Pe layers on mica surfaces do bare some similarities to polymer brushes in terms of surface interactions. The fitted curve gives a film thickness L of 24 nm for C5Pe films adsorbed after overnight soaking. From the hard wall of the force curve, the film thickness is ~19 nm, while the ellipsometry measurement gives a value of 18.2 nm for the films adsorbed on silicon wafer overnight from C5Pe solutions of the same concentration as the above SFA measurement. The thickness values obtained by ellipsometry and SFA as summarized in Table 5.2 are in excellent agreement with each other. The fitted mean distances s between grafting sites are very close to each other in Table 5.2, which are also close to the s values obtained for asphaltenes under similar experimental condition⁷², indicating a similar adsorption pattern of C5Pe and asphaltenes from toluene on mica.

It is noted from Figure 5.3a that the AdG scaling theory fits the force-distance profiles well at short distances under high compression. However, at longer distances under lower compression, a significant deviation is observed. It appears that there is a weaker repulsive force over longer separation distance which might be due to protrusion of flexible chains on C5Pe aggregates in the films, as schematically shown in the inset of Figure 5.5. Such model is not considered in the AdG theory which is applicable to mono-dispersed brushes. Nevertheless, the lower compression regime can also be fitted with the AdG model using an independent set of fitting parameters as shown by the dash line in Figure 5.5. The measured force-distance profiles between two adsorbed C5Pe films in toluene can therefore be explained as follows. The weak repulsion at large separation distances appears to be the result of steric repulsion between the secondary brushes of flexible aliphatic chains on C5Pe aggregate core, while the repulsion at

shorter separation distance under higher compression is the results of compressing the core of C5Pe molecular aggregates. The schematic of the proposed core-brush configuration is shown in the inset of Figure 5.5. The fitted parameters of s and L for the force-distance curve obtained for selected adsorption time are listed in Table 5.3.

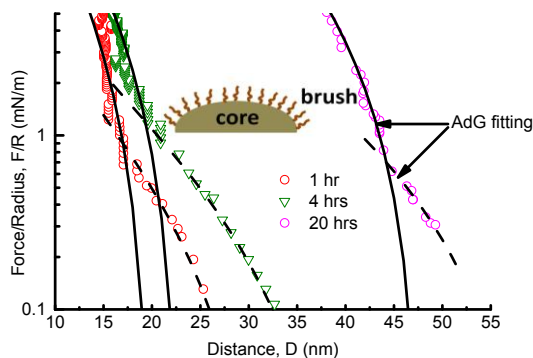


Figure 5.5 Experimentally measured repulsion forces and best fitted curves using the Alexander-de Gennes (AdG) theory. Open squares are the measured forces; solid lines are the fitting force curves at high compression regime and dash lines are the fitting force curves at low compression regime. Inset schematically shows a proposed core-brush configuration of the absorbed C5Pe aggregates.

Table 5.1 Fitting parameters using Alexander-de Gennes theory (corresponding to Figure 5.3a).

Adsorption time	≤ 2 hrs	4 hrs	20 hrs
L (nm)	10	11.5	24
s (nm)	2.8	2.8	2.6

Table 5.2 Film thickness (nm) obtained by different methods (corresponding to Figure 5.3).

Adsorption time	Ellipsometer measurement	Hard wall distance	Fitting value
≤ 4 hrs	5.8-5.5	7-11	10-12
20 hrs	18.2	19	24

Table 5.3 Fitting parameters using Alexander-de Gennes theory at high and low compression regimes (corresponding to Figure 5.5).

	1 hr of adsorption		4 hrs of adsorption		20 hrs of adsorption	
	high loading	low loading	high loading	low loading	high loading	low loading
L (nm)	10	16	11.5	20	24	30
s (nm)	2.8	8.1	2.8	8.7	2.6	6.7

5.3.4 Low concentration adsorption

The adsorption behaviour of C5Pe on mica in a diluted (0.002 wt%) solution was also investigated. As shown in Figure 5.6a, there is no significant difference in both force profiles and the hard wall distances with adsorption time up to 20 hours. However the adhesion disappeared after overnight immersion as shown in Figure 5.6. AFM imaging of C5Pe film adsorbed overnight on mica in Figure 5.4b

revealed a similar surface morphology to the films formed at higher C5Pe concentrations as shown in Figure 5.4, which was responsible for the disappearance of the adhesion forces although the hard wall thickness in these two cases were different. The observed differences indicate an important role of C5Pe concentration in toluene in determining the adsorption kinetics and molecular aggregation from C5Pe solutions.

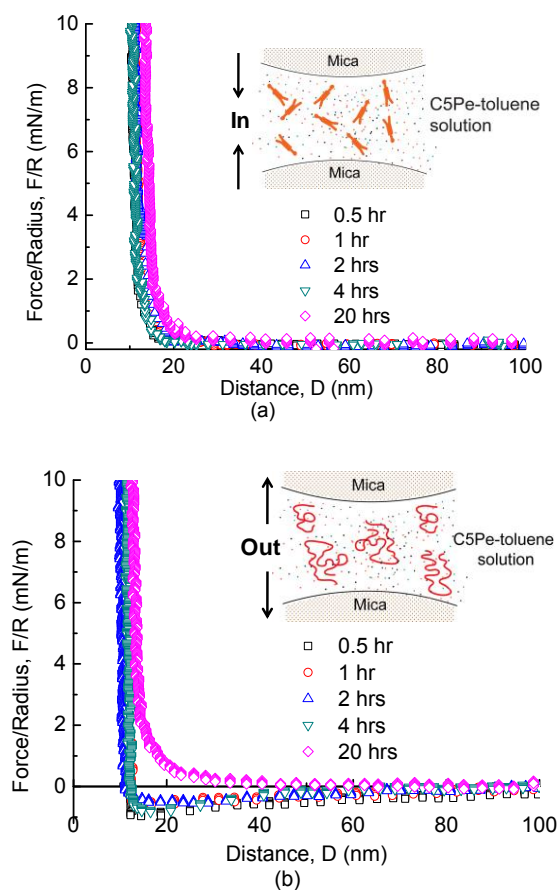


Figure 5.3 Force-distance profiles of two mica surfaces interacting in 0.002 wt% C5Pe-toluene solution at different time intervals during (a) approaching and (b) retracting following the approaching in (a).

5.3.5 Comparison with real asphaltenes

For comparison, the force-distance profiles for two mica surfaces interacting in a 0.01 wt% asphaltene-toluene solution with different adsorption times are shown in Figure 5.7. The comparison of the results obtained with asphaltenes and C5Pe shows that the asphaltenes and C5Pe behave similarly in terms of adsorption behaviour to clay (mica) surfaces. Both the native asphaltenes and C5Pe model compound built up a layer on mica quickly (within 0.5 hour), and the layer then continued to grow slowly with time on the mica surface. The force-distance profiles on separation for both asphaltenes and C5Pe showed that the adhesion, observed during the initial stage of adsorption, decreased with increasing the adsorption time and eventually disappeared. Both C5Pe and asphaltenes were noted to have similar hard wall distance of 12-15 nm within the first half-hour adsorption. However, the C5Pe layer did not continue to grow significantly within the first few hours, while the asphaltene layer grew more quickly than C5Pe. After 2 hours of adsorption, the hard wall distance of the asphaltenes became much larger than that of C5Pe. After 20 hours adsorption, the hard wall distance for asphaltenes grew to ~60 nm in comparison to ~38 nm for C5Pe, suggesting a much stronger aggregation of asphaltene molecules than C5Pe, most probably due to more complex nature of asphaltene molecules.

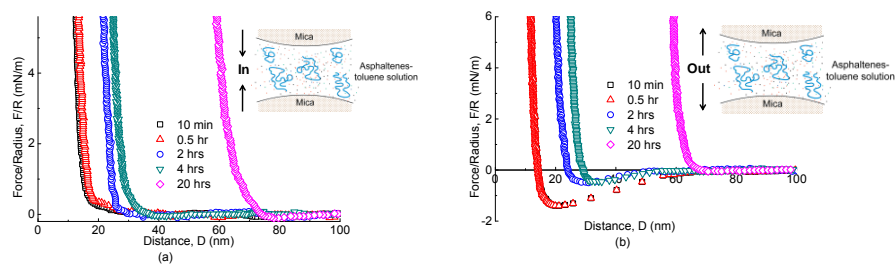


Figure 5.4 Force-distance profiles of two mica surfaces interacting in 0.01 wt% asphaltene-toluene solution at different time intervals during (a) approaching and (b) retracting following the approaching in (a).

5.4 Interactions in toluene and heptane

5.4.1 In toluene

Figure 5.8a shows the interaction forces between a C5Pe film adsorbed on mica and a bare mica (asymmetric configuration) or between two C5Pe surfaces (symmetric configuration) in toluene. The hard wall distance of the asymmetric case was found to be about half of the symmetric case. Weak adhesion ($F_{ad}/R \sim -0.5$ mN/m) was measured during the separation for the asymmetric case, which was due to the affinity of C5Pe to the opposing mica surface. For both symmetric and asymmetric cases, there was a hysteresis between the approaching and separating force-distance profiles, even though there was no adhesion for the symmetrical case. The observed hysteresis indicates an irreversible deformation of C5Pe films upon compression during the approaching. The absence of adhesion between two C5Pe films in symmetrical case indicates the absence of interdigitation or bridging of between C5Pe molecules across the two surfaces. These results on the interactions of C5Pe films in toluene were very similar to the results of asphaltenes reported recently.⁷²

5.4.2 In heptane

Heptane is a paraffinic and apolar solvent, which is considered as a poor solvent for the polyaromatic and polar C5Pe molecule. Previous study confirmed that the model compound C5Pe cannot be dissolved in heptane¹²⁵. As shown in Figure 5.8b, the hard wall distance of the asymmetric case was estimated to be about half of the symmetric configuration as anticipated. Strong adhesion forces were measured for both the asymmetric and symmetric configurations interacting in heptane, with $F_{ad}/R \sim -32$ and -30 mN/m, respectively. In our recent SFA study on asphaltenes, adhesion ($F_{ad}/R \sim -3$ mN/m) was measured between two asphaltene surfaces in heptane. The adhesion became slightly weaker after 30 min immersion. These findings indicate that some of the asphaltene components have limited swelling in heptane, leading to limited conformational rearrangement and

aggregation of asphaltene molecules.⁷² The adhesion forces measured for both C5Pe and asphaltenes in heptane were mainly attributed to van der Waals attraction between C5Pe or asphaltene surfaces across the poor solvent heptane, while the weaker adhesion forces measured between asphaltene films than C5Pe films were probably caused by more rigid and rougher asphaltene films than C5Pe films in heptane. The complex nature of asphaltenes have led to limited solubility and swelling of asphaltenes in heptane, which increases the steric effect and thus lowers the adhesion. Contrary to asphaltenes, C5Pe is completely insoluble in heptane, indicating the absence of swelling or molecular rearrangement even after longer time incubation. The measured smaller hard wall distance of ~ 4.6 nm in heptane than that of ~ 6 nm in toluene for the asymmetric configuration supports non-swelling hypothesis of C5Pe in heptane. The direct AFM imaging of a C5Pe film shown in Figure 5.1d confirms a negligible change in morphology of C5Pe films after immersed in heptane for half an hour.

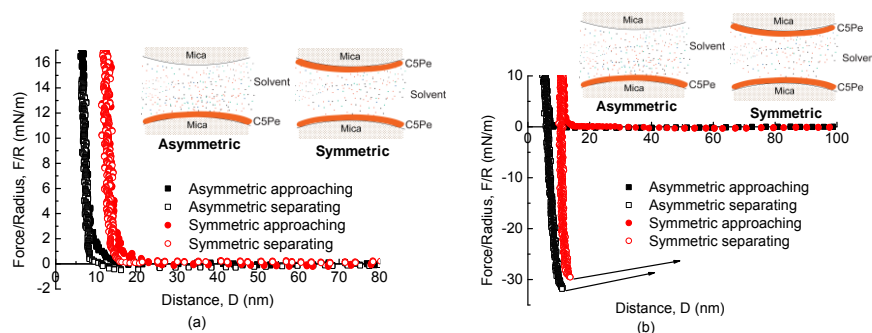


Figure 5.5 Force-distance profiles between two C5Pe films (symmetric configuration) and between a C5Pe film and a bare mica surface (asymmetric configuration) in (a) toluene and (b) heptane.

5.6 Summary of chapter

The interaction force of an asphaltene model compound C5Pe in organic solvents is presented in this chapter. The results are also compared with real asphaltenes

and show some similarities and dissimilarities. The general conclusions derived from the measurements are in the following.

- Organic solvents significantly affect the molecular interaction and aggregation behaviour of C5Pe model compound.
- For the interactions of two mica surfaces across C5Pe solutions, the repulsion measured showed a steric origin resulting from the adsorbed C5Pe molecules.
- The repulsive force-distance profiles measured during approaching were well fitted with the Alexander-de Gennes scaling theory over a short and long separation distance regimes using two independent sets of fitting parameters, indicating the core-brush configuration of C5Pe molecular aggregates.
- For the interactions of C5Pe films (in asymmetric or symmetric configurations), no significant adhesion was detected in good solvent toluene, while strong adhesion was measured in heptane.
- The comparison of results between the asphaltene and model compound C5Pe shows that C5Pe behaves similarly as asphaltenes in terms of intermolecular forces in organic solvents, emphasizing the importance of the polar components in real asphaltenes for their interfacial activities and aggregation behaviour.
- However, there is a distinct difference quantitatively between C5Pe and nature asphaltene molecules that C5Pe aggregates at a much slower rate and shows a negligible swelling in toluene as compared to asphaltenes.
- It is evident that using a single model compound is unlikely to mimic quantitatively the aggregation of asphaltenes in a given solvent.
- A mixture of several well-designed asphaltene model compounds in combination with maltene molecules could probably provide a more accurate representation of real asphaltenes and hence successfully mimic

the molecular aggregation of asphaltenes and their role in stabilizing water-in-oil emulsions.

- The direct force-distance measurement in this study provides an insight into mechanisms of molecular interaction and interfacial behaviour of asphaltene model compound C5Pe in different organic solvents.

CHAPTER 6 INTERACTIONS OF C5Pe IN AQUEOUS SOLUTIONS

Studies on the molecular interaction mechanisms of polyaromatic surfactants in stabilizing W/O or O/W emulsions are of great practical and fundamental importance. In this study, a polyaromatic surfactant C5Pe, used as an asphaltene model compound with well-defined molecular structure containing corresponding hetero atoms, was employed in an attempt to understand its molecular interaction mechanisms in aqueous solutions. A surface forces apparatus (SFA) was used to directly measure the molecular interactions of C5Pe. Solution pH, salt concentration and Ca^{2+} addition showed a strong impact on the interactions between two C5Pe surfaces. The repulsion observed between the two adsorbed C5Pe molecular layers was shown to have a steric origin. The force-distance profiles at short separation distance and high compression regime were well fitted with the Alexander-de Gennes (AdG) model. At high pH ($> \text{pKa}$), the repulsive forces measured over a long separation distance and low compression regime were shown to where deviate from the AdG model but could be fitted with the Derjaguin-Landau-Verwey-Overbeek (DLVO) theory, indicating an electrostatic origin of the observed repulsion due to ionization of $-\text{COOH}$ groups. The adhesion between two C5Pe surfaces was shown to decrease sharply with increasing solution pH and salt concentration, being attributed to the decrease of surface hydrophobicity and hydrophobic attraction. Addition of Ca^{2+} ions was able to induce the formation of large aggregates on C5Pe films due to the strong bonding of Ca^{2+} with $-\text{COOH}$ groups, leading to a longer-range steric interaction. Our results provide a new insight into the fundamental molecular interactions of polyaromatic surfactants at oil-water interfaces and in complex aqueous solutions.

6.1 Introduction

Surfactants or amphiphiles, are widely used as cleaning, wetting, dispersing, foaming and anti-foaming agents in numerous practical applications of heterogeneous systems including detergents, paints, inks, cosmetics, firefighting, food processing, materials and minerals processing, petroleum processing and

production, formulation of agriculture products, etc. Surfactants are usually organic compounds containing both hydrophilic heads and hydrophobic tails.¹²⁶ Therefore, a surfactant molecule will migrate to water surface where its tail extends out of the bulk water phase, either into the air, or into the oil phase. As a consequence the surface tension of a liquid or the interfacial tension of two immiscible liquids is reduced in comparison with pure liquids. The buildup of monolayers at W/O interfaces has immense importance in stabilization of emulsion systems.¹²⁷⁻¹²⁹

The formation and stabilization of emulsions are important in many industrial applications and processes. For example, the oil-in-water emulsions are commonly encountered in food industry, such as homogenized milk, mayonnaise and cream in espresso.¹³⁰⁻¹³¹ In medicine, microemulsions are used to deliver vaccines and kill microbes.¹³² In these cases, stable emulsions are intentionally formulated. In other cases, demulsification by coalescence of oil or water droplets is more desirable. For instance, in a water-based extraction process (WBEP) of oil sands, O/W and W/O emulsions are inevitably generated during bitumen flotation and bitumen froth cleaning, respectively. The presence of water containing dissolved salts (e.g., Cl⁻) in the form of W/O emulsions can lead to corrosion of downstream equipment for bitumen upgrading.⁷² On the other hand, the formation of tiny bitumen droplets in the form of bitumen-in-water emulsions leads to reduced recovery of bitumen and causes many challenging issues in tailings treatment.^{72,113} The presence of natural amphiphilic chemicals, e.g. polyaromatic surfactants (mainly asphaltenes) at the water-oil interface has a significant influence on the stability of these undesirable emulsions in oil sands industry.^{133,2-4,134}

The objective of this study is to elucidate the molecular interaction mechanisms of a polyaromatic surfactants, C5Pe in aqueous solutions. C5Pe consists of four aromatic rings fused together with three cyclic rings containing heteroatoms O and N. One end of the fused rings is attached with a pentyl carboxylic acid via the

nitrogen atom, and the other end is connected to a hexyl-heptyl double chain also through a nitrogen atom. As C5Pe has a $-\text{COOH}$ terminal group, the solution conditions such as pH, salinity and Ca^{2+} addition are expected to show significant impact on the molecular forces and interfacial behaviour of C5Pe. The results obtained from C5Pe provide a new insight into the molecular interaction mechanisms and interfacial properties of polyaromatic surfactants in various oil-water mixture systems and petroleum industry.

6.2 Characterization of C5Pe film

AFM was applied to characterize the surface properties of C5Pe film deposited on mica. The AFM images of bare mica surface and drop-coated C5Pe film are shown in Figure 6.1. As expected, freshly cleaved mica prior to film deposition is a featureless, flat surface with a root-mean-square (RMS) roughness of 0.2 nm (Figure 6.1a). The deposited C5Pe compound film has a RMS roughness of 0.5 nm. To study the effect of aqueous solutions on the configuration of C5Pe on mica surface, the drop-coated C5Pe film was immersed in 10 mM KCl solution at pH 2 for 10 min and dried in air in a dust-free laminar flow hood for AFM imaging. Figure 6.1c shows the AFM image of the immersed C5Pe film with a RMS roughness of 1.3 nm, which is higher than the un-immersed C5Pe film. It should be noted that small aggregates of C5Pe were formed on the film upon exposure to aqueous solution, which was due to the molecular conformation rearrangement of C5Pe. During the film preparation, C5Pe was adsorbed onto hydrophilic mica with most of the hydrophobic tails preferentially facing toluene/air. After the film was exposed to an aqueous solution, some of the hydrophilic head groups tended to expose to the aqueous phase. However, due to the large hydrophobic group and small hydrophilic head group, the C5Pe molecules were not able to form a uniform monolayer or bilayer, instead, in a form of micelle-like aggregates after exposure to aqueous solutions. In this way, the hydrophobic groups tend to stay inside the aggregate and the hydrophilic -

COOH groups expose to both the aqueous solutions and mica surface, as shown in the schematic in Figure 6.2.

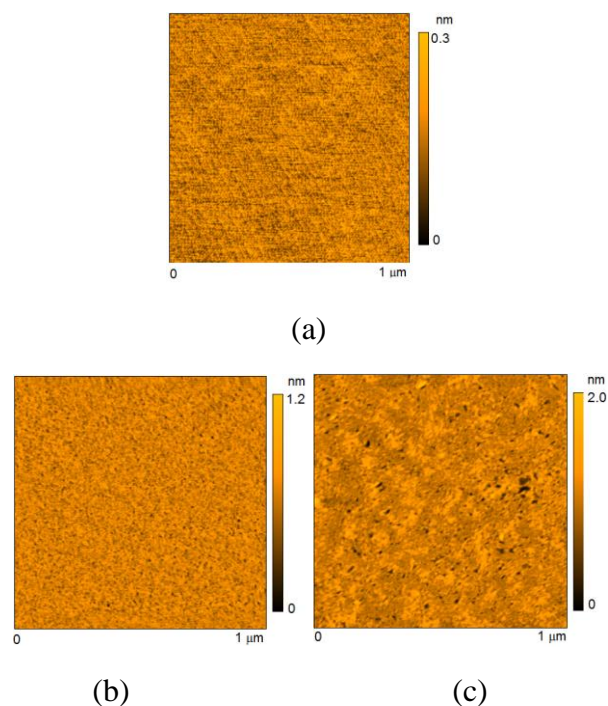


Figure 6.1 AFM images of (a) bare mica surface, (b) C5Pe adsorbed on mica, and (c) C5Pe adsorbed on mica after immersing in pH 2, 10 mM KCl solution for 10 min.

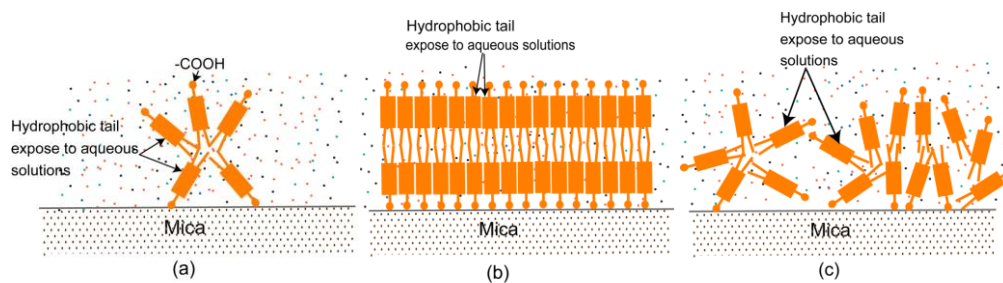


Figure 6.2 Proposed schematic of C5Pe aggregates on mica surface: (a) micelle-like aggregates, (b) an ordered bilayer structure and (c) complex aggregates combining micelle-like and “multi-layer” aggregation.

6.3 Surface force analysis

6.3.1 A typical force measurement

Figure 6.3a shows a force-distance profile when two C5Pe surfaces approach each other in 1 mM KCl solution and pH 2. The hard wall distance is ~ 5.8 nm (note the “hard wall” distance in this study is defined as the mica-mica separation distance or thickness of confined C5Pe which barely changed with increasing the normal load or pressure). A repulsive force was first measured between the two surfaces at distance $D > 9$ nm, which was followed by a jump-in at $D \sim 9$ nm, leading to the hard wall separation distance.

6.3.2 Adhesion

Figure 6.3b shows the force-distance profile obtained when the two C5Pe surfaces were separated after being kept in contact for 1 min following the approaching process in Figure 6.4a. A strong adhesion $F_{ad}/R \sim 15$ mN/m was measured, which was mainly due to the attractive hydrophobic interaction between the hydrophobic domains on the interacting films. Interestingly, the two surfaces were stretched for about 6 nm before detachment (jump apart) as shown in Figure 5b, which indicates each film was stretched ~ 3 nm. The extended length of the C5Pe molecule can be approximated estimated as 2.7 nm based on the bond lengths of C-C (SP³-SP³), C-N, C-O, C-C (benzene) 0.15 nm, 0.14 nm, 0.14 nm, 0.14 nm respectively and the bond angle 109.5°, 180°, 180°, and 120° respectively¹³⁵⁻¹³⁶. The actual molecular length of C5Pe should be smaller than 2.7nm. The stretching associated the separation shown in Figure 5b confirms that C5Pe molecules aggregate on mica surface upon exposure to aqueous environment, as also visualized by AFM. The above force measurement indicates the molecular interactions of C5Pe in aqueous solution can be largely affected by the aggregation of the polyaromatic molecules, due to π - π interactions among aromatic rings, hydrophobic interactions and van der Waals interactions.

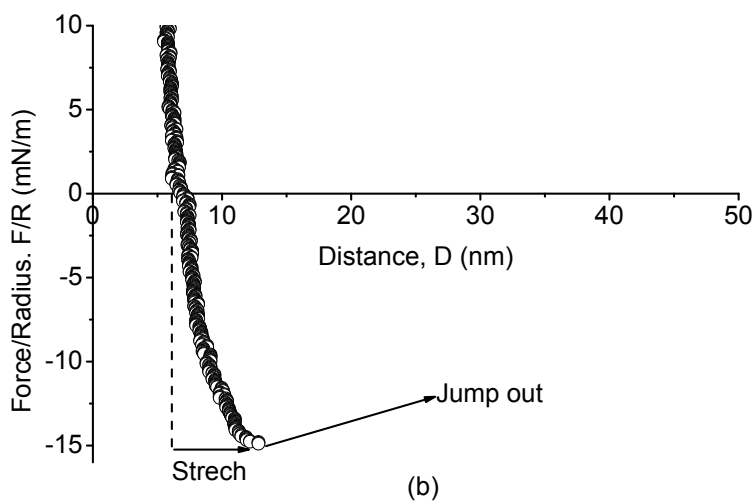
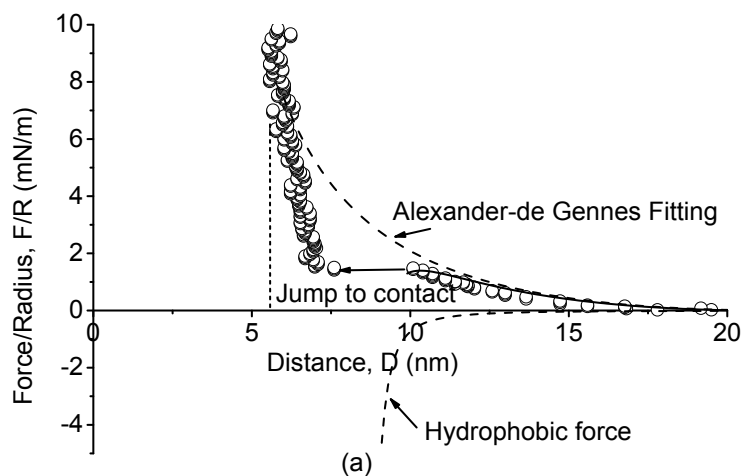


Figure 6.3 Force-distance profiles of two C5Pe surfaces interacting in 0.1 mM KCl solution at pH 2: (a) approaching force curve; (b) retracting force curve following the approaching in (a). Open squares are the measure force profile; solid line is the fitting curve by combining AdG equation with a fitted L of 10 nm and fitted s of 6.6 nm and hydrophobic force with a fitted K of 1.0×10^{-20} J; and dash lines are fitting curves by AdG equation and hydrophobic force individually.

6.3.3 Data fitting and nature of the interaction forces

The pKa value of C5Pe was reported to around 4–5,¹³⁷ and C5Pe is hardly ionized at pH 2, which suggests electrostatic force would not play a critical role in the repulsive surface forces measured. It was reported recently that the steric interactions between two asphaltene layers or two C5Pe layers in organic solvents could be described by the Alexander-de Gennes (AdG) model for polymer brush layers.^{8,23} While two C5Pe layers can not be considered as two polymeric brushes due to the small molecular weight and water is not a good solvent for C5Pe, the C5Pe aggregates and their interesting conformation may lead to steric interactions between the two surfaces in aqueous solution and bear some brush properties which could be described by the Alexander-de Gennes (AdG) model. In the AdG model, as two surfaces approach each other, at some distance the films start to overlap, and the increased local density of molecular segments lead to an increase in osmotic pressure and repulsive interaction energy, and the repulsive pressure between two planar surfaces is given by equation 6-1,⁹⁵

$$P(D) \cong \frac{kT}{s^3} \left[\left(\frac{2L}{D} \right)^{9/4} - \left(\frac{D}{2L} \right)^{3/4} \right] \quad \text{for } D < 2L, \quad (6-1)$$

where $P(D)$ is the repulsive pressure between the two C5Pe films (N/m^2), k is Boltzmann constant ($\text{m}^2\text{Kg/s}^2/\text{K}$), T is temperature (K), s is the average space (m) between two “grafting” points of the molecules and L is brush layer thickness (m). For the geometry of two crossed cylindrical surfaces of radius R , the force-distance relation $F(D)$ is given by integrating the Equation 1 using the Derjaguin approximation⁸⁹ and shown in equation 6-2.

$$\frac{F(D)}{R} = \frac{8\pi kTL}{35s^3} \left[7 \left(\frac{2L}{D} \right)^{5/4} + 5 \left(\frac{D}{2L} \right)^{7/4} - 12 \right] \quad \text{for } D < 2L. \quad (6-2)$$

As shown in Figure 6.3a, the repulsive force at $D > 9$ nm can be well fitted with the AdG equation with fitted L and s of 10 nm and 6.6 nm respectively. However, the jump-in motion at $D \sim 9$ nm must be due to some strong attractive force and cannot be predicted by the steric interaction based on the AdG equation, which was most likely due to the hydrophobic forces between the two C5Pe films. C5Pe is constituted by a small hydrophilic head group (-COOH) and a long hydrophobic tail. Geometrically, it is almost impossible that the hydrophilic head group could fully shield and prevent the large hydrophobic groups exposing to water even in the most hydrophilic configuration shown in Figure 6.2b. Thus the hydrophobic tails exposing to the aqueous solution can form local hydrophobic domains and induce hydrophobic forces between the two C5Pe films.⁷⁹ The hydrophobic surface forces F_{HB} can be approximately described by an empirical equation shown in equation 6-3, where K is a fitted value (J), representing the strength of hydrophobic interaction (similar to the Hamaker constant for van der Waals forces), and D_0 is the fitted hard wall distance of the measured force-distance profiles.³⁹

$$\frac{F_{HB}}{R} = -\frac{K}{6(D-D_0)^2} \quad (6-3)$$

As shown in Figure 6.3a, the force-distance curve and the jump-in could be well fitted by including the hydrophobic force with fitted K and D_0 of 1×10^{-20} J and 6.8 nm respectively. Figure 6.3b shows the force-distance profile obtained when the two C5Pe surfaces were separated after being kept in contact for 1 min following the approaching process in Figure 6.3a. A strong adhesion $F_{ad}/R \sim 15$ mN/m was measured, which was mainly due to the attractive hydrophobic interaction between the hydrophobic domains on the interacting films. Interestingly, the two surfaces were stretched for about 6 nm before detachment (jump apart) as shown in Figure 6.3b, which indicates each film was stretched ~ 3 nm. The extended length of the C5Pe molecule can be approximated estimated as 2.7 nm based on the bond lengths of C-C (SP^3 - SP^3), C-N, C-O, C-C (benzene) 0.15 nm, 0.14 nm, 0.14 nm, 0.14 nm respectively and the bond angle 109.5° , 180° ,

180°, and 120° respectively¹³⁵⁻¹³⁶. The actual molecular length of C5Pe should be smaller than 2.7nm. The stretching associated the separation shown in Figure 5b confirms that C5Pe molecules aggregate on mica surface upon exposure to aqueous environment, as also visualized by AFM. The above force measurement indicates the molecular interactions of C5Pe in aqueous solution can be largely affected by the aggregation of the polyaromatic molecules, due to π - π interactions among aromatic rings, hydrophobic interactions and van der Waals interactions. It is expected that the solution conditions can also largely impact the molecular interactions of C5Pe, and the effects of pH, salinity and presence of Ca^{2+} are detailed as follows.

6.4 Effect of pH

The interactions between two C5Pe surfaces in 1 mM KCl solutions as a function of pH were determined by the SFA. Figure 6.4 shows the force-distance profiles for two C5Pe surfaces approaching in 1 mM KCl at pH = 2, 4 and 6, and a strong impact of pH on the interactions of C5Pe was observed. At pH 2, repulsive forces were measured at $D > 9$ nm followed by a jump-in at $D \sim 9$ nm. As pH was increased to 4, only pure repulsive forces and no jump-in were observed. When pH was further increased to 6, the repulsive force becomes stronger and longer-ranged than that at pH 4. The disappearance of adhesive jump-in at higher pH was due to the decreased hydrophobicity with increasing pH. The pKa of C5Pe is about 4-5, and the ionization of -COOH is negligible at pH 2, thus the hydrophobic force is relatively stronger leading to the adhesive jump-in during the approach of the two surfaces. At pH 4, part of -COOH groups were ionized into -COO^- , which decreases the hydrophobicity of C5Pe surface. At pH 6, much more -COOH groups were ionized into -COO^- . The increased -COO^- dramatically decrease the hydrophobicity of the surfaces, resulting in a sharp decrease of the hydrophobic force and disappearance of the adhesive jump-in.

Figure 6.5 shows the logarithmic force-distance profiles at pH 4 and 6, which is evident that the AdG equation fits the force-distance profiles well at short distance

and relatively high compression regime, but deviate at longer separation distance and low compression regime. The forces predicted by AdG model at longer distance are smaller than the measured forces, indicating the presence of other repulsive forces at longer distance, which could be attributed to the long-range electrostatic forces from the negatively charged C5Pe surfaces at pH 4 and 6 due to the ionization of $-\text{COO}^-$ groups.

The classic Derjaguin, Landau, Verwey and Overbeek (DLVO) theory describes the force between two charged surfaces interacting in an aqueous medium. The total interaction force (F_{total}) is the summation of van de Waals force (F_V) and electrostatic force (F_E),⁸³ as shown in equation 6-4.

$$F_{total} = F_V + F_E \quad (6-4)$$

Van de Waals force between two crossed cylindrical surfaces with radius R is given in equation 6-5, where A_{cwc} is Hamaker constant for C5Pe/Water/C5Pe and $A_{cwc} = 2.8 \times 10^{-21}$ J.⁷⁵

$$\frac{F_V}{R} = -\frac{A_{cwc}}{6D^2} \quad (6-5)$$

Electrostatic force for two identical charged particles can be calculated by numerically solving the Poisson-Boltzmann equation 6-6 under constant surface charge boundary conditions:²⁰ at $x = 0$, $\frac{d\psi}{dx} \Big|_{x=0} = \text{constant}$, and at $x = \infty$, $\psi = 0$ in the form of equation 6-7.

$$\epsilon \epsilon_0 \frac{d^2\psi}{dx^2} = -e \sum_i z_i n_{i\infty} \exp\left(-\frac{z_i e \psi}{kT}\right) \quad (6-6)$$

$$\frac{F_E}{R} = -2\pi \left[kT n_{i\infty} \sum_i \left(1 - \exp\left(-\frac{z_i e \psi}{kT}\right) \right) - \frac{\epsilon \epsilon_0}{2} \left(\frac{d\psi}{dx} \right)^2 \right] \quad (6-7)$$

where ϵ is dielectric constant of aqueous solution and ϵ_0 is vacuum permittivity ($\text{C}^2/\text{N}/\text{m}^2$), e is elementary charge (C), Z_i is electrolyte valence, $n_{i\infty}$ is the

concentration of bulk solution (mol/L), k is Boltzmann constant and T is temperature ($T = 298$ K). The reverse decay length κ is defined in equation 6-8 as:

$$\kappa = \left(\frac{e^2}{\epsilon k T} \sum_i n_{i0} z_i^2 \right)^{\frac{1}{2}} \quad (6-8)$$

During the fitting, the surface potential Ψ and decay length κ^{-1} were set as adjustable parameters. The dash lines shown in Figure 6.5 are the fitted curve using the above DLVO model with $\Psi = -32$ mV, $\kappa^{-1} = 9.8$ nm and $\Psi = -60$ mV, $\kappa^{-1} = 9.8$ nm at pH 4 and pH 6 respectively.⁷⁵ The fitted decay length is close to the theoretical decay length ($\kappa^{-1} = 10.4$ nm) for 1 mM KCl calculated by equation 6-8. Combining the DLVO forces at longer separation and steric force at shorter distance, the overall force-distance profiles can be well fitted as shown in Figure 6.5, which is evident that the electrostatic force dominates at longer distance and low compression regime while steric force plays a more important role at shorter separation distance and high compression regime.

The adhesion force measured during the separation processes following the approaching in solutions of different pH were shown in the inset of Figure 6.4. Strong adhesion $F_{ad}/R \sim 15$ mN/m was observed for the separation in 1 mM KCl at pH = 2, and the adhesion disappeared at pH 4 and 6 due to the dramatically decreased hydrophobic force and increased electrostatic force.

The molecular interactions of C5Pe were also measured at pH 8 and 10 with 1 mM KCl. The force-distance curves were similar to that at pH 6 and no adhesion was measured, which indicates that the head groups of C5Pe were completely ionized at pH 6 or higher, and the hydrophobic interaction between the two surfaces could be considered negligible.

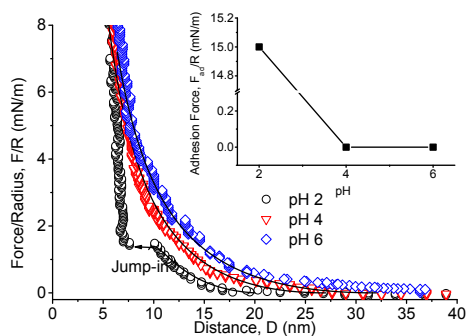


Figure 6.4 Force-distance profiles of two C5Pe surfaces interacting in 0.1 mM KCl solution at different pH during approaching. Solid lines are fitted curves using the AdG model with the fitted values: (I) pH 2, $L = 10\text{nm}$, $s = 6.6\text{ nm}$; (II) pH 4, $L = 13.5\text{ nm}$, $s = 7.3\text{ nm}$; (III) pH 6, $L = 16\text{ nm}$, $s = 8.1\text{ nm}$. Inset is the adhesion measured during the separation.

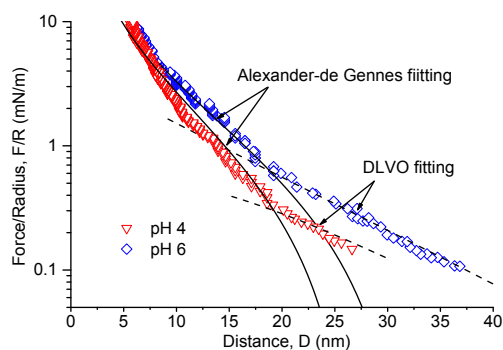


Figure 6.5 Force-distance profiles of two C5Pe surfaces interacting in 0.1 mM KCl solution at pH 4 and pH 6. solid lines are the fitted curves by AdG equation at short separation distance and high compression regime, and dash lines are the fitted curves using the DLVO theory at long separation distance and low compression regime with Hamaker constant $A_{CWC} = 2.8 \times 10^{-21}\text{ J}$, and with fitted decay lengths and surface potentials of (I) pH 4, $\Psi = -32\text{ mV}$, $\kappa^{-1} = 9.8\text{ nm}$; (II) pH 6, $\Psi = -60\text{ mV}$, $\kappa^{-1} = 9.8\text{ nm}$.

6.5 Effect of salinity

6.5.1 At pH above pKa

Ionic strength plays an important role in the interaction of charged particles or emulsions in aqueous solution by affecting their interfacial properties and electric double layer. The interaction forces between two C5Pe surfaces as a function of KCl concentrations at pH 6 were measured and the force-distance curves during the approaching processes are shown in Figures 6.6. As the KCl concentration increased from 1 mM to 100 mM, the range of the repulsive forces before reaching the hard wall separation was clearly shorter, which was due to the compression of the electric double layer at higher salt concentrations. All the force-distance curves can be well fitted by combining the AdG equation at shorter distance and by DLVO model at longer distance. At $[KCl] = 1$ mM and 10 mM, the fitted decay length $\kappa^{-1} = 9.8$ nm and 3.2 nm were in good agreement with the theoretical values $\kappa^{-1} = 10.4$ nm, 3.3 nm given by equation 6-8 respectively, and the fitted surface potential decreased from -60 mV to -20 mV because of the compression of electric double layer. At high salt concentration $[KCl] = 100$ mM, the electric double layer was much suppressed ($\kappa^{-1} \sim 1$ nm), and electrostatic contribution was negligible and steric interaction dominated.

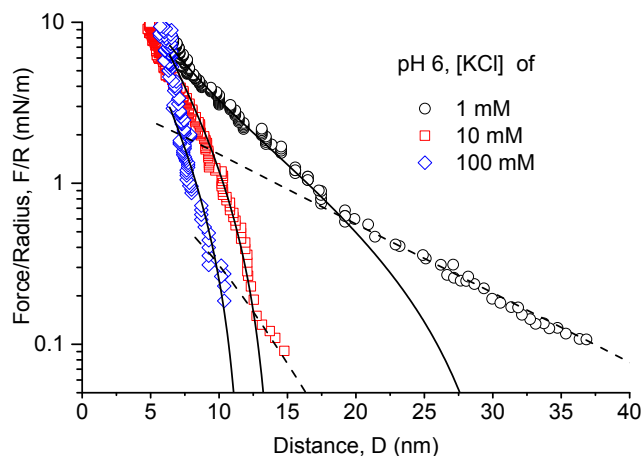


Figure 6.6 Force-distance profiles of two C5Pe surfaces interacting in pH 6 of different KCl concentrations during approaching. Solid lines are fitted curves using AdG equation with fitted parameters as (I) for [KCl] = 1 mM, $L = 16$ nm, $s = 8.1$ nm, (II) for [KCl] = 10 mM, $L = 7.1$ nm, $s = 3.8$ nm, and (III) for [KCl] = 100 mM, $L = 6$ nm, $s = 3.9$ nm; dash lines are the fitted curves using DLVO theory with Hamaker constant $A_{CWC} = 2.8 \times 10^{-21}$ J and with fitted decay lengths and surface potentials as (I) for [KCl] = 1mM, $\Psi = -60$ mV, $\kappa^{-1} = 9.8$ nm.; (II) for [KCl] = 10 mM, $\Psi = -20$ mV, $\kappa^{-1} = 3.3$ nm. In 100 mM KCl solution, the DLVO force is negligible comparing to the strong steric force.

6.5.2 At pH below pKa

At pH 2, C5Pe molecule is slightly ionized and the ionic strength is not expected to have significant influence on the surface interaction by affecting the electric double layer. Figure 6.7a shows the force curves of two C5Pe surfaces in different KCl concentrations of 1 to 100 mM at pH 2. It is evident that the range of the repulsive forces at pH 2 (Figure 6.7a) is clearly shorter than that at pH 6 (Figure 6.6), which is due to the much weaker electrostatic interaction at pH 2. The force range also slightly decreases with increasing the KCl concentration from 1 to 100 mM, as shown in Figure 6.7a. The force curves were fitted with the AdG equation

by including hydrophobic force. The fitted film thickness L were 10, 7 and 5 nm, and the corresponding s were 6.6, 4.3 and 3.7 nm for the C5Pe films in KCl concentration of 1, 10 and 100 mM, respectively. The hydrophobic strength K decreased from 1.0×10^{-20} to 0.4×10^{-20} J with increasing the KCl concentrations from 1 mM to 10 mM, leading to a weaker hydrophobic force, and the hydrophobic force became negligible in 100 mM KCl at pH 2. As shown in the inset of Figure 6.7a, the adhesion measured during the separation were $F_{ad}/R = 15$, 7 and 0 mN/m in 1, 10 and 100 mM KCl respectively.

According to the configuration of adsorbed C5Pe film in Figure 6.2c, the hydrophobic force between two C5Pe surfaces originates from the hydrophobic groups exposed to the water, which is closely related to the separation distance between the hydrophilic head groups of C5Pe. Figure 6.7b schematically shows the impact of ionic strength on the conformation of the C5Pe aggregates. Under high salt condition, the electric double layer and charges of the head groups are more compressed leading to a relatively smaller separation distance between -COOH groups than that in low salt condition, reducing the contact of hydrophobic groups of C5Pe with water and decreasing the hydrophobic force between two C5Pe surfaces sequentially, which is consistent with the impact of KCl concentration on the force-distance profiles shown in Figure 6.7a. The above results show that high salinity decreases the hydrophobic force of two C5Pe surfaces, and also provide significant implication on the stability of O/W emulsions with polyaromatic surfactants such as C5Pe present at the oil/water interface: O/W emulsions could be more difficult to aggregate at low salt condition due to longer-ranged repulsive force but more difficult to break up once they “stick” together.

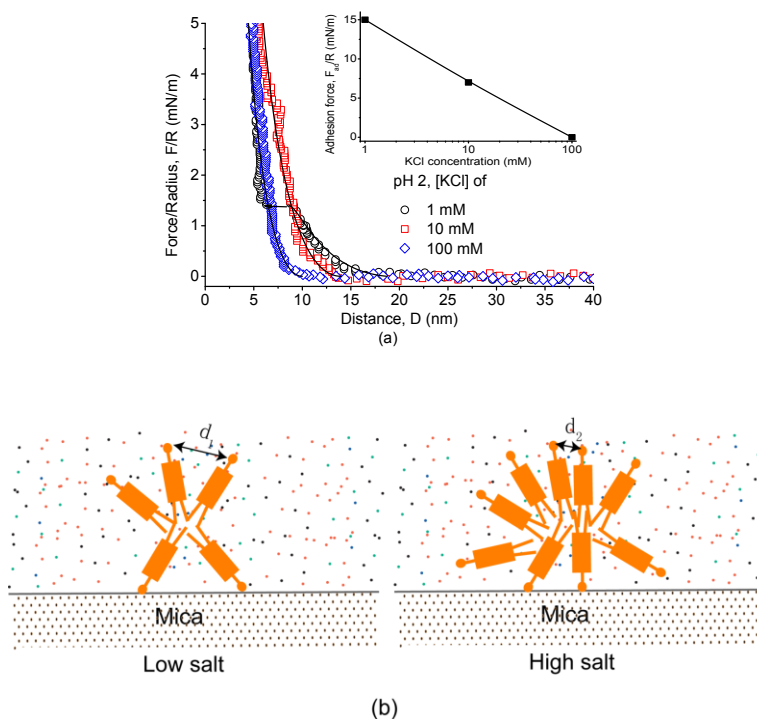
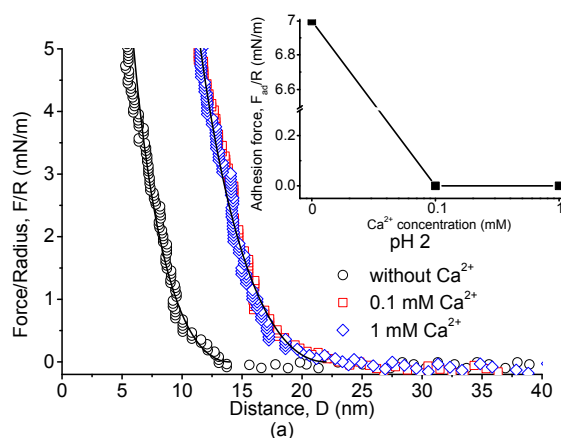


Figure 6.7 (a) Force-distance profiles of two C5Pe surfaces interacting in aqueous solutions of pH 2 of different KCl concentrations during approaching. Solid lines are fitted curves using the AdG equation with fitted layer thickness and averaging spacing as (I) for $[KCl] = 1$ mM, $L = 10$ nm, $s = 6.6$ nm; (II) for $[KCl] = 10$ mM, $L = 7$ nm, $s = 4.3$ nm; (III) for $[KCl] = 100$ mM, $L = 5$ nm, $s = 3.7$ nm. Inset is the adhesion measured during the separation of two C5Pe surfaces. (b) Proposed conformation change of C5Pe molecules and aggregates under low and high KCl concentrations.

6.6 Effect of Ca^{2+}

Figure 6.8a shows the approaching force-distance profiles of two C5Pe surfaces in the presence of 0, 0.1 and 1 mM of Ca^{2+} in 10 mM KCl at pH 2. With Ca^{2+} addition, the hard wall distance was dramatically increased from ~ 6 nm to ~ 12 nm, and the adhesion force disappeared as shown in the inset of Figure 6.8a. The increased hard wall distance and disappearance of the adhesion were due to the

conformation change and aggregation of C5Pe induced by Ca^{2+} ions through the strong bonding with the $-\text{COOH}$ head groups. One Ca^{2+} ion is able to interact with two $-\text{COOH}$ groups which could bridge two small C5Pe aggregates into a large aggregate as shown in the schematic of Figure 6.8b, leading to a significantly increased hard wall distance. Similar impact of Ca^{2+} on the interaction of C5Pe surfaces was observed at higher pH as shown in Figure 6.9 for two C5Pe surfaces in the presence of 0 and 1 mM Ca^{2+} in 100 mM KCl at pH 6. Figure 6.10 shows the topography and phase AFM images of C5Pe film after immersed in 10 mM KCl + 0.1 mM CaCl_2 solution for 10 min. Comparing to the C5Pe film immersed only in KCl solution (Figure 6.2), the Ca^{2+} treated C5Pe film forms much bigger aggregates. The RMS roughness of the Ca^{2+} treated C5Pe surface is 3.6 nm, higher than the surface only treated with KCl (RMS ~ 1.3 nm). It is evident that the AFM images confirmed the proposed Ca^{2+} induced aggregation mechanism.



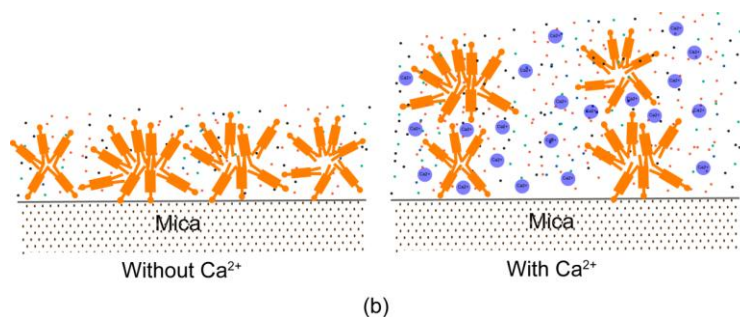


Figure 6.8 (a) Force-distance profiles of two C5Pe surfaces interacting in 10 mM KCl solutions at pH 2 in the presence of different amount of Ca^{2+} ions. Solid lines are fitted curves using the AdG equation with fitted layer thickness and averaging spacing as (I) without Ca^{2+} , $L = 7$ nm, $s = 4.3$ nm; (II) with addition of 0.1 and 1 mM Ca^{2+} , $L = 11$ nm, $s = 4.2$ nm. (b) Proposed conformation change of C5Pe molecules and aggregates in the presence Ca^{2+} .

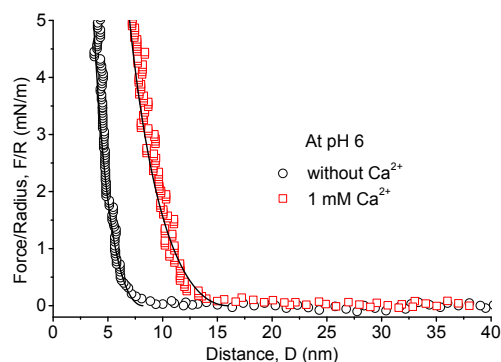


Figure 6.9 Force-distance profiles of two C5Pe surfaces interacting in 100 mM KCl solutions at pH 6 in the presence of different amount of Ca^{2+} . Solid lines are fitted curves using AdG equation with the fitted parameters as (I) without Ca^{2+} , $L = 4$ nm, $s = 3.5$ nm; (II) with 1 mM Ca^{2+} addition, $L = 8$ nm, $s = 4.4$ nm.

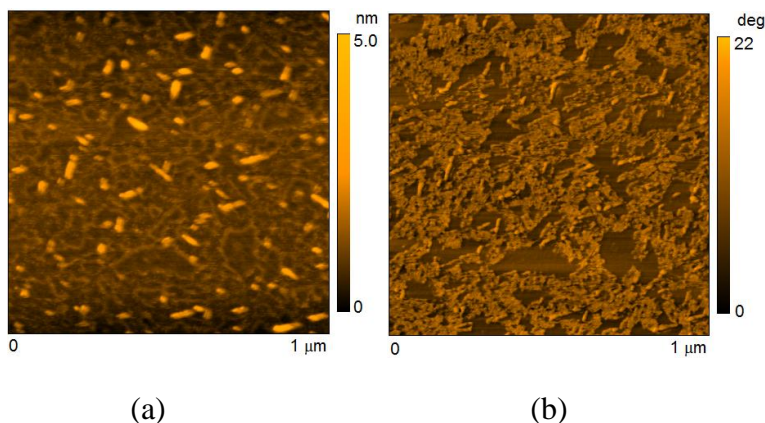


Figure 6.10 AFM images of a C5Pe film coated mica after immersing in aqueous solution of pH 2 with 10 mM KCl + 0.1 mM CaCl₂ for 10 min: (a) topography and (b) phase images.

6.5 Summary of chapter

The interaction force of polyaromatic surfactants is of great importance in understanding the mechanism of emulsion stabilization. The interaction between C5Pe surfaces is measured by SFA in aqueous solutions, and the following are the general conclusions.

- The interaction between C5Pe surfaces were largely affected by solution pH. With increasing solution pH, the range of repulsive force increased. At low pH, an obvious strong jump-in motion is detected, while the jump-in motion disappears at high pH. The adhesion disappears at high pH due to the decrease of hydrophobic force and increase of electrostatic force.
- High salt concentration compressed the electrostatic double layer and decreased the hydrophobicity of C5Pe surfaces, also leading to an adhesion reduction.
- A small amount of Ca²⁺ ions in the aqueous solution were able to induce large aggregation of C5Pe through the strong bonding to –COOH groups, resulting in much-longer ranged steric repulsion and dramatically increased hard wall distance.

- The repulsion observed between the adsorbed C5Pe molecules was shown to have a steric origin. The force-distance profiles at short separation distance and high compression regime were well fitted with the Alexander-de Gennes (AdG) model. At high pH ($> pK_a$), the repulsive forces measured over long separation distance and low compression regime were shown to be electrostatic interaction due to the ionization of $-COOH$ groups, where deviated from the AdG model but could be fitted with the Derjaguin-Landau-Verwey-Overbeek (DLVO) theory.
- Our results obtained from C5Pe provide new insight into the basic molecular interaction mechanisms and interfacial properties of polyaromatic surfactants in various oil-water mixture systems and petroleum industry.

CHAPTER 7 SUMMARY**7.1 General conclusions**

This thesis focuses on the interaction forces of an asphaltene model compound C5Pe in organic solvents and aqueous solutions, to help elucidate the molecular interaction mechanism and interfacial activities of asphaltene-type molecules in O/W and W/O emulsions. The study led to the following conclusions:

1. Surface forces apparatus (SFA), incorporating with other techniques including AFM, contact angle measurement and Langmuir–Blodgett trough, has been shown to be a powerful approach to study the molecular interaction mechanism of interfacial active chemicals at the molecular level and stabilization mechanisms of O/W and W/O emulsions.
2. The adsorption of an asphaltene model compound C5Pe onto a model clay (mica) and the interaction forces between the adsorbed C5Pe films in different organic solvents (toluene and heptane) showed that organic solvents significantly affect the molecular interaction and aggregation behaviour of C5Pe model compound.
3. In organic solvents, the force-distance profiles at short separation distances under high compression during approaching were well fitted with the Alexander-de Gennes (AdG) scaling theory while the lower compression regime over longer separation distances deviate could be also fitted with the AdG model using an independent set of fitting parameters, indicating the presence of possible secondary brush structures of the C5Pe molecules in toluene.
4. In aqueous solutions, the molecular interactions of C5Pe were largely affected by the solution pH, salt concentration and addition of Ca^{2+} . The repulsion observed between the C5Pe molecules adsorbed on mica was shown to have a steric origin. The force-distance profiles at short separation distance and high compression regime were well fitted with the Alexander-de Gennes (AdG) model. At high pH ($> \text{pKa}$), the repulsive forces measured

over long separation distance and low compression regime were shown to be electrostatic interaction due to the ionization of $-\text{COOH}$ groups, which deviated from the AdG model but could be fitted with the Derjaguin-Landau-Verwey-Overbeek (DLVO) theory.

5. The comparison of the results obtained with the model compound C5Pe and native asphaltenes shows that C5Pe behaves quantitatively different from the real asphaltenes in the context of contact angle and interaction force profiles. However, there are qualitative similarities in terms of intermolecular forces, indicating that the polar components in real asphaltene molecules play an important role in determining their interfacial activities.
6. It is evident that using a single model compound is unlikely to mimic quantitatively the aggregation of asphaltenes in a given solvent. Nevertheless, a mixture of several well-designed asphaltene model compounds in combination with maltene molecules could probably provide a more accurate representation of real asphaltenes and hence successfully mimic the molecular aggregation of asphaltenes and their role in stabilizing water-in-oil emulsions.

7.2 Suggestions for future work

There are a number of areas in which this research can be continued. In this thesis, the C5Pe film is coated on mica surfaces by drop coating method. It would be interesting to get a uniform LB film if possible and study the interaction forces of C5Pe with this LB film and compare with the results from the drop-coated film.

The study in this thesis shows that C5Pe, as an asphaltene model compound, qualitatively mimic the asphaltene properties in the context of interaction forces and aggregation/adsorption behaviour. Yet, the quantitative differences indicate that using a single model compound is unlikely to mimic the aggregation of asphaltenes in a given solvent. In the future, a mixture of several well-designed asphaltene model compounds in combination with maltene molecules could probably provide a more accurate representation of real asphaltenes and hence

successfully mimic the molecular aggregation of asphaltenes and their role in stabilizing water-in-oil emulsions.

The effect of Ca^{2+} was evidenced to have strong bonding effect on C5Pe molecules in this thesis. A study of investigating the effect of Ca^{2+} on asphaltene molecules by surface force measurement and QCM-D would be of interest since Ca^{2+} is of great importance in oil sands processing.

Investigating the molecular interaction mechanism and interfacial activities of asphaltene type molecules in W/O and O/W emulsions by measuring the surface force is still an indirect way to study emulsions. A direct way could be carried out on real O/W emulsions stabilized by asphaltene model compounds. The effect of pH, salinity and Ca^{2+} can also be studied.

REFERENCES

- (1) Clarke, T.P.; Google Patents: **1980**.
- (2) Gafonova, O.V.; Yarranton, H.W. *Journal of Colloid and Interface Science* **2001**, *241*, 469-478.
- (3) Yang, X.; Hamza, H.; Czarnecki, J. *Energy & Fuels* **2004**, *18*, 770-777.
- (4) Yarranton, H.W.; Hussein, H.; Masliyah, J.H. *Journal of Colloid and Interface Science* **2000**, *228*, 52-63.
- (5) Buenrostro-Gonzalez, E.; Groenzin, H.; Lira-Galeana, C.; Mullins, O.C. *Energy & Fuels* **2001**, *15*, 972-978.
- (6) Poteau, S.; Argillier, J.F.; Langevin, D.; Pincet, F.; Perez, E. *Energy & Fuels* **2005**, *19*, 1337-1341.
- (7) Schneider, M.H.; Andrews, A.B.; Mitra-Kirtley, S.; Mullins, O.C. *Energy & Fuels* **2007**, *21*, 2875-2882.
- (8) Zhang, L.Y.; Breen, P.; Xu, Z.; Masliyah, J.H. *Energy & Fuels* **2007**, *21*, 274-285.
- (9) Nordgard, E.L.; Sjoblom, J. *Journal of Dispersion Science and Technology* **2008**, *29*, 1114-1122.
- (10) Groenzin, H.; Mullins, O.C. *Energy & Fuels* **2000**, *14*, 677-684.
- (11) Fossen, M.; Kallevik, H.; Knudsen, K.D.; Sjöblom, J. *Energy & Fuels* **2007**, *21*, 1030-1037.
- (12) Fossen, M.; Sjoblom, J.; Kallevik, H.; Jakobsson, J. *Journal of Dispersion Science and Technology* **2007**, *28*, 193-197.
- (13) Aston, D.E.; Berg, J.C. *Journal of Colloid and Interface Science* **2001**, *235*, 162-169.
- (14) Hartley, P.G.; Grieser, F.; Mulvaney, P.; Stevens, G.W. *Langmuir* **1999**, *15*, 7282-7289.
- (15) Mulvaney, P.; Perera, JM; Biggs, S.; Grieser, F.; Stevens, GW *Journal of Colloid and Interface Science* **1996**, *183*, 614-616.
- (16) Snyder, B.A.; Aston, D.E.; Berg, J.C. *Langmuir* **1997**, *13*, 590-593.
- (17) Nordgård, E.L.; Landsem, E.; Sjo blom, J. *Langmuir* **2008**, *24*, 8742-8751.

- (18) Nordg rd, E.L.; S rland, G.; Sjoblom, J. *Langmuir* **2009**, *26*, 2352-2360.
- (19) Speight, J.G. *The Chemistry and Technology of Petroleum*; CRC, **2007**; Vol. 114.
- (20) Sundman, O.; Nordg rd, E.L.; Grimes, B.; Sjoblom, J. *Langmuir* **2010**, *26*, 1619-1629.
- (21) Wang, S.; Liu, J.; Zhang, L.; Masliyah, J.; Xu, Z. *Langmuir* **2009**, *26*, 183-190.
- (22) Kirkwood, KM; Ebert, S.; Foght, JM; Fedorak, PM; Gray, MR *Journal of Applied Microbiology* **2005**, *99*, 1444-1454.
- (23) Wattana, P.; Fogler, H.S.; Yen, A.; Garc a, M.D.C.; Carbognani, L. *Energy & Fuels* **2005**, *19*, 101-110.
- (24) Merdrignac, I.; Espinat, D. *Oil & Gas Science and Technology* **2007**, *62*, 7-32.
- (25) Kaminski, T.J.; Fogler, H.S.; Wolf, N.; Wattana, P.; Mairal, A. *Energy & Fuels* **2000**, *14*, 25-30.
- (26) Andreatta, G.; Bostrom, N.; Mullins, O.C. *Langmuir* **2005**, *21*, 2728-2736.
- (27) Yarranton, H.W.; Alboudwarej, H.; Jakher, R. *Industrial & Engineering Chemistry Research* **2000**, *39*, 2916-2924.
- (28) Yarranton, H.W.; Masliyah, J.H. *AIChE Journal* **1996**, *42*, 3533-3543.
- (29) Pomerantz, A.E.; Hammond, M.R.; Morrow, A.L.; Mullins, O.C.; Zare, R.N. *Journal of the American Chemical Society* **2008**, *130*, 7216-7217.
- (30) Kuznicki, T.; Masliyah, J.H.; Bhattacharjee, S. *Energy & Fuels* **2008**, *22*, 2379-2389.
- (31) Rogel, E. *Langmuir* **2002**, *18*, 1928-1937.
- (32) Gawrys, K.L.; Spiecker, P.M.; Kilpatrick, P.K. *Petroleum Science and Technology* **2003**, *21*, 461-490.
- (33) Sheremata, J.M.; Gray, M.R.; Dettman, H.D.; McCaffrey, W.C. *Energy & Fuels* **2004**, *18*, 1377-1384.
- (34) Hannisdal, A.; Ese, M.H.; Hemmingsen, P.V.; Sjoblom, J. *Colloids and Surfaces A: Physicochemical and Engineering Aspects* **2006**, *276*, 45-58.

- (35) Hannisdal, A.; Hemmingsen, P.V.; Sjöblom, J. *Industrial & Engineering Chemistry Research* **2005**, *44*, 1349-1357.
- (36) Sheu, E.Y. *Journal of Physics: Condensed Matter* **1996**, *8*, A125.
- (37) Acevedo, S.; Ranaudo, MA; Pereira, JC; Castillo, J.; Fernández, A.; Pérez, P.; Caetano, M. *Fuel* **1999**, *78*, 997-1003.
- (38) Bouhadda, Y.; Bendedouch, D.; Sheu, E.; Krallafa, A. *Energy & Fuels* **2000**, *14*, 845-853.
- (39) Andersen, S.I.; Christensen, S.D. *Energy & Fuels* **2000**, *14*, 38-42.
- (40) Andersen, S.I.; del Rio, J.M.; Khvostitchenko, D.; Shakir, S.; Lira-Galeana, C. *Langmuir* **2001**, *17*, 307-313.
- (41) Ese, M.H.; Galet, L.; Clause, D.; Sjöblom, J. *Journal of Colloid and Interface Science* **1999**, *220*, 293-301.
- (42) Czarnecki, J.; Moran, K. *Energy & Fuels* **2005**, *19*, 2074-2079.
- (43) Graham, B.F.; May, E.F.; Trengove, R.D. *Energy & Fuels* **2008**, *22*, 1093-1099.
- (44) Wu, X. *Energy & Fuels* **2003**, *17*, 179-190.
- (45) Islam, MR *Asphaltenes and Asphalts* **1994**, *1*, 249-298.
- (46) Leontaritis, K.J.; Ali Mansoori, G. *Journal of Petroleum Science and Engineering* **1988**, *1*, 229-239.
- (47) Tuttle, R. *Journal of Petroleum Technology* **1983**, *35*, 1192-1196.
- (48) Buenrostro Gonzalez, E.; Lira Galeana, C.; Gil Villegas, A.; Wu, J. *AIChE Journal* **2004**, *50*, 2552-2570.
- (49) Mullins, O. *SPE Journal* **2008**, *13*, 48-57.
- (50) Stachowiak, C.; Viguié J.R.; Jean-Pierre, E.; Rogalski, M. *Langmuir* **2005**, *21*, 4824-4829.
- (51) Takanohashi, T.; Sato, S.; Saito, I.; Tanaka, R. *Energy & Fuels* **2003**, *17*, 135-139.
- (52) Zhang, L.Y.; Lawrence, S.; Xu, Z.; Masliyah, J.H. *Journal of Colloid and Interface science* **2003**, *264*, 128-140.

- (53) Zhang, L.Y.; Lopetinsky, R.; Xu, Z.; Masliyah, J.H. *Energy & Fuels* **2005**, *19*, 1330-1336.
- (54) Zhang, L.Y.; Xu, Z.; Masliyah, J.H. *Langmuir* **2003**, *19*, 9730-9741.
- (55) Zhang, L.Y.; Xu, Z.; Masliyah, J.H. *Industrial & Engineering Chemistry Research* **2005**, *44*, 1160-1174.
- (56) Acevedo, S.; Escobar, G.; Gutiérrez, L.B.; Rivas, H.; Gutiérrez, X. *Colloids and Surfaces A: Physicochemical and Engineering Aspects* **1993**, *71*, 65-71.
- (57) Lawrence, S.; Zhang, L.Y.; Xu, Z.; Masliyah, J. *The Canadian Journal of Chemical Engineering* **2004**, *82*, 821-828.
- (58) Ese, M.H.; Yang, X.; Sjöblom, J. *Colloid & Polymer Science* **1998**, *276*, 800-809.
- (59) Alvarez, G.; Jestin, J.; Argillier, JF; Langevin, D. *Langmuir* **2009**, *25*, 3985-3990.
- (60) Jestin, J.; Simon, S.; Zupancic, L.; Barré L. *Langmuir* **2007**, *23*, 10471-10478.
- (61) Czarnecki, J. *Energy & Fuels* **2008**, *23*, 1253-1257.
- (62) Singh, S.; McLean, JD; Kilpatrick, PK *Journal of Dispersion Science and Technology* **1999**, *20*, 279-294.
- (63) Lobato, MD; Pedrosa, JM; Hortal, AR; Martinez-Haya, B.; Lebron-Aguilar, R.; Lago, S. *Colloids and Surfaces A: Physicochemical and Engineering Aspects* **2007**, *298*, 72-79.
- (64) Andreatta, G.; Goncalves, C.C.; Buffin, G.; Bostrom, N.; Quintella, C.M.; Arteaga-Larios, F.; Pérez, E.; Mullins, O.C. *Energy & Fuels* **2005**, *19*, 1282-1289.
- (65) Roux, J.N.; Broseta, D.; Demé B. *Langmuir* **2001**, *17*, 5085-5092.
- (66) Rogel, E.; Leon, O.; Torres, G.; Espidel, J. *Fuel* **2000**, *79*, 1389-1394.
- (67) Long, J.; Xu, Z.; Masliyah, J.H. *Langmuir* **2007**, *23*, 6182-6190.
- (68) Mitchell, D.L.; Speight, J.G. *Fuel* **1973**, *52*, 149-152.
- (69) Porte, G.; Zhou, H.; Lazzeri, V. *Langmuir* **2003**, *19*, 40-47.

- (70) Buckley, JS; Hirasaki, GJ; Liu, Y.; Von Drasek, S.; Wang, J.X.; Gill, BS *Petroleum Science and Technology* **1998**, *16*, 251-286.
- (71) Wang, S.; Liu, J.; Zhang, L.; Xu, Z.; Masliyah, J. *Energy & Fuels* **2008**, *23*, 862-869.
- (72) Natarajan, A.; Xie, J.; Wang, S.; Liu, Q.; Masliyah, J.; Zeng, H.; Xu, Z. *The Journal of Physical Chemistry C*. **2011**.
- (73) Liu, J.; Xu, Z.; Masliyah, J. *The Canadian Journal of Chemical Engineering* **2004**, *82*, 655-666.
- (74) Liu, J.; Xu, Z.; Masliyah, J. *Colloids and Surfaces A: Physicochemical and Engineering Aspects* **2005**, *260*, 217-228.
- (75) Liu, J.; Zhang, L.; Xu, Z.; Masliyah, J. *Langmuir* **2006**, *22*, 1485-1492.
- (76) Akbarzadeh, K.; Bressler, D.C.; Wang, J.; Gawrys, K.L.; Gray, M.R.; Kilpatrick, P.K.; Yarranton, H.W. *Energy & Fuels* **2005**, *19*, 1268-1271.
- (77) Gray, M.R.; Tykwinski, R.R.; Stryker, J.M.; Tan, X. *Energy & Fuels* **2011**.
- (78) McNaught, A.D.; Wilkinson, A. *IUPAC Compendium of Chemical Terminology*; Blackwell Scientific Publications, **1997**; Vol. 2.
- (79) Israelachvili, J.N. *Intermolecular and Surface Forces*, **2011**.
- (80) Hamaker, HC *Physica* **1937**, *4*, 1058-1072.
- (81) Lee, S.; Sigmund, W.M. *Colloids and Surfaces A: Physicochemical and Engineering Aspects* **2002**, *204*, 43-50.
- (82) von Helmholtz, H.; Hittorf, J.W.; Waals, J.D. *Physical Memoirs Selected and Translated from Foreign Sources*; Taylor and Francis, **1888**.
- (83) Israelachvili, J.N. **1992**.
- (84) Butt, H.J. *Biophysical Journal* **1991**, *60*, 1438-1444.
- (85) McIntosh, TJ; Simon, SA *Biochemistry* **1986**, *25*, 4058-4066.
- (86) Rau, DC; Lee, B.; Parsegian, VA *Proceedings of the National Academy of Sciences* **1984**, *81*, 2621.
- (87) Huang, H.; Ruckenstein, E. *Advances in Colloid and Interface Science* **2004**, *112*, 37-47.

- (88) Ben-Naim, A. *Ben-Naim (1980) Hydrophobic Interactions*; Plenum Press (New York), **1980**.
- (89) Derjaguin, BV; Churaev, NV *Journal of Colloid and Interface Science* **1974**, *49*, 249-255.
- (90) Pashley, R.M.; McGuiggan, P.M.; Ninham, B.W.; Evans, D.F. *Science* **1985**, *229*, 1088.
- (91) Rabinovich, Y.I.; Yoon, R.H. *Langmuir* **1994**, *10*, 1903-1909.
- (92) Christenson, H.K.; Claesson, P.M.; Pashley, R.M. *Journal of Chemical Sciences* **1987**, *98*, 379-389.
- (93) Podgornik, R. *The Journal of Chemical Physics* **1989**, *91*, 5840.
- (94) Ruckenstein, E.; Churaev, N. *Journal of Colloid and Interface Science* **1991**, *147*, 535-538.
- (95) De Gennes, PG *Advances in Colloid and Interface Science* **1987**, *27*, 189-209.
- (96) Pincus, P. *Macromolecules* **1991**, *24*, 2912-2919.
- (97) Clunie, JS; Goodman, JF; Symons, PC **1967**.
- (98) Israelachvili, J.N.; Pashley, R.M. **1983**.
- (99) Israelachvili, J.N.; Adams, G.E. *J. Chem. Soc., Faraday Trans. 1* **1978**, *74*, 975-1001.
- (100) Israelachvili, J.; Min, Y.; Akbulut, M.; Alig, A.; Carver, G.; Greene, W.; Kristiansen, K.; Meyer, E.; Pesika, N.; Rosenberg, K. *Reports on Progress in Physics* **2010**, *73*, 036601.
- (101) Israelachvili, JN; Adams, GE *Nature* **1976**, *262*, 774-776.
- (102) Israelachvili, JN; Tabor, D. *Proceedings of the Royal Society of London. A. Mathematical and Physical Sciences* **1972**, *331*, 19.
- (103) Tabor, D.; Winterton, RHS *Proceedings of the Royal Society of London. A. Mathematical and Physical Sciences* **1969**, *312*, 435.
- (104) Connor, J.N.; Horn, R.G. *Review of Scientific Instruments* **2003**, *74*, 4601.
- (105) Heuberger, M.; Luengo, G.; Israelachvili, J. *Langmuir* **1997**, *13*, 3839-3848.

- (106) Kristiansen, K.; McGuiggan, P.; Carver, G.; Meinhart, C.; Israelachvili, J. *Langmuir* **2008**, *24*, 1541-1549.
- (107) Idziak, S.H.J.; Safinya, C.R.; Hill, R.S.; Kraiser, K.E.; Ruths, M.; Warriner, H.E.; Steinberg, S.; Liang, K.S.; Israelachvili, J.N. *Science* **1994**, *264*, 1915.
- (108) Mukhopadhyay, A.; Zhao, J.; Bae, S.C.; Granick, S. *Review of Scientific Instruments* **2003**, *74*, 3067.
- (109) Erbil, H.Y. *Surface Chemistry of Solid and Liquid Interfaces*; Wiley-Blackwell, **2006**.
- (110) Nordgaard, E.L. *PhD thesis*.
- (111) http://engineering.tufts.edu/microfab/index_files/SOP/PiranhaClean_SOP.pdf.
- (112) Sarid, D. *Scanning Force Microscopy: With Applications to Electric, Magnetic, and Atomic Forces*; Oxford University Press, USA, **1994**; Vol. 5.
- (113) Schramm, L.L. *Emulsions: (Fundamentals and Applications in the Petroleum Industry)*; American Chemical Society, **1992**.
- (114) Hemmingsen, P.V.; Silset, A.; Hannisdal, A.; Sjöblom, J. *Journal of Dispersion Science and Technology* **2005**, *26*, 615-627.
- (115) Hiemenz, P.C.; Rajagopalan, R. *Principles of Colloid and Surface Chemistry*; CRC, **1997**; Vol. 14.
- (116) Chandra, W.; Dabros, T.; Hamza, H.A. *Energy & Fuels* **2007**, *21*, 912-919.
- (117) Gu, G.; Zhou, Z.; Xu, Z.; Masliyah, J.H. *Colloids and Surfaces A: Physicochemical and Engineering Aspects* **2003**, *215*, 141-153.
- (118) Liu, E.H.; McGrath, K.M. *Colloids and Surfaces A: Physicochemical and Engineering Aspects* **2005**, *262*, 101-112.
- (119) McClements, D.J.; Decker, E.A.; Park, Y.; Weiss, J. *Critical Reviews in Food Science and Nutrition* **2009**, *49*, 577-606.
- (120) Vankova, N.; Tcholakova, S.; Denkov, N.D.; Ivanov, I.B.; Vulchev, V.D.; Danner, T. *Journal of Colloid and Interface Science* **2007**, *312*, 363-380.

- (121) Teklebrhan, R. B.; Ge, L.; Bhattacharjee, S.; Xu, Z.; Sjoblom, J. *in preparation* **2011**.
- (122) Zhao, B.; Pesika, N.; Rosenberg, K.; Tian, Y.; Zeng, H.; McGuiggan, P.; Autumn, K.; Israelachvili, J. *Langmuir* **2008**, *24*, 1517-1524.
- (123) Zeng, H.; Tian, Y.; Anderson, T.H.; Tirrell, M.; Israelachvili, J.N. *Langmuir* **2008**, *24*, 1173-1182.
- (124) Akbulut, M.; Alig, A.R.G.; Min, Y.; Belman, N.; Reynolds, M.; Golan, Y.; Israelachvili, J. *Langmuir* **2007**, *23*, 3961-3969.
- (125) Rosen, M.J.; Wiley, J. *Surfactants and Interfacial Phenomena*; Wiley Online Library, **2004**; Vol. 464.
- (126) Wang, J.; van der Tuuk Opedal, N.; Lu, Q.; Xu, Z.; Zeng, H.; Sjoblom, J. *Energy & Fuel* in print.
- (127) Becher, P. *New York* **1957**.
- (128) McCutcheon, JW *1968 annual, John W. McCutcheon, Inc., Morristown, NJ* **1968**.
- (129) Zettlemyer, AC *Journal of the American Chemical Society* **1958**, *80*, 3806-3806.
- (130) Kralova, I.; Sjöblom, J. *Surfactants Used in Food Industry: A Review*; Taylor & Francis, **2009**; Vol. 30.
- (131) Xu, W.; Nikolov, A.; Wasan, D.T.; Gonsalves, A.; Borwankar, R.P. *Journal of Food Science* **1998**, *63*, 183-188.
- (132) Reed, S.G.; Bertholet, S.; Coler, R.N.; Friede, M. *Trends in Immunology* **2009**, *30*, 23-32.
- (133) Salager, J.L. *Laboratory of Formulation, Interfaces, Rheology and Processes. Universidad de los andes. Facultad de ingenieria. Mérida, Venezuela* **2002**.
- (134) Schramm, L.L. *Surfactants: Fundamentals and Applications in the Petroleum Industry*; Cambridge Univ Pr, **2000**.
- (135) da Silva, M.A.S.; Pinheiro, S.O.; Francisco, T.S.; da Silva, F.O.N.; Batista, A.A.; Ellena, J.; Carvalho, I.M.M. *J. Braz. Chem. Soc* **2010**, *21*, 1754-1759.

-
- (136) Lide, D.R. *CRC Handbook of Chemistry and Physics: A Ready-reference Book of Chemical and Physical Data*; CRC Pr I Llc, **2004**.
- (137) Brückner, R. *Advanced Organic Chemistry: Reaction Mechanisms*; Academic press, **2002**.